Reduced vegetation uptake during the extreme 2023 drought turns the Amazon into a weak carbon source

Santiago Botía[1], Cléo Quaresma Dias-Junior[2], Shujiro Komiya[3], Auke van der Woude[4], Myriam Terristi[1], Remco de Kok[4], Gerbrand Koren[5], Hella van Asperen[1], Sam P. Jones[1], Flávio Augusto Farias D'Oliveira[2], Ulrich Weber[6], Edson Marques-Filho[7], Ivan Mauricio Cely Toro[8], Alessandro Araújo[9], Jost Lavric[10], David Walter[11], Xiaojun Li[12], Jean-Pierre Wigneron[13], Benjamin Stocker[14], Jeffeson Goncalves de Souza[15], Michael O'Sullivan[16], Stephen Sitch[15], Philippe Ciais[17], Frederic Chevallier[18], Wei Li[19], Ingrid Theodora Luijkx[4], Wouter Peters[4], Carlos A. Quesada[20], Sönke Zaehle[3], Susan Trumbore[3], and Ana Bastos[21]

[1]Max-Planck-Institut fur Biogeochemie
[2]Federal Institute of Pará (IFPA)
[3]Max Planck Institute for Biogeochemistry
[4]Wageningen University
[5]Utrecht University
[6]Max-Planck Institute for Biogeochemistry
[7]Universidade Federal da Bahia
[8]Universidade de Sao Paulo
[9]Embrapa Amazonia Oriental
[10]Acoem GmbH
[11]Max-Planck-Institut für Chemie
[12]Institut national de recherche pour l'agriculture l'alimentation et l'environnement
[13]INRAE
[14]Universitat Bern
[15]University of Exeter
[16]College of Engineering, Mathematics and Physical Sciences
[17]Laboratory for Climate Sciences and the Environment (LSCE)
[18]Laboratoire des Sciences du Climat et de l'Environnement (LSCE)
[19]Tsinghua University
[20]Instituto Nacional de Pesquisas da Amazônia
[21]Leipzig University

January 22, 2025

Abstract

In 2023, the biogeographic Amazon experienced temperature anomalies of 1.5°C above the 1991-2020 average from September to November. These conditions were driven by high sea surface temperature in the Atlantic and Pacific oceans, together with reduced moisture advection from the Atlantic, causing large vapor pressure and water deficits in the second semester of 2023. Here, we evaluate the response of the Amazon carbon cycle to this extreme event across different spatial scales. We combined atmospheric CO2 mole fractions and eddy covariance flux data from the Amazon Tall Tower Observatory (ATTO), near-real-

time simulations by Dynamic Global Vegetation Models (DGVMs), an atmospheric inversion, and remote sensing data. We find that in 2023 the Amazon region was, including fires, a net carbon source of 0.01 to 0.17 PgC. Fire emissions (0.15 [0.13-0.17] PgC) were within typical variability of the 2003-2023 period, thus we attribute the weak carbon source to reduced vegetation uptake during the dry season. A stronger-than-normal vegetation uptake early in the year (January to April), consistent across data streams and spatial scales, mitigated the total carbon losses by the end of the year. We find a shift from carbon sink to source in May and a peak source in October. Our findings show a reduced vegetation carbon uptake over the Amazon region, leading to a weak carbon source that contributed 30% of the net carbon loss in the tropical land in 2023.

Reduced vegetation uptake during the extreme 2023 drought turns the Amazon into a weak carbon source

S. Botía[1], C. Q. Dias-Junior[2], S. Komiya[3], A. M. van der Woude[4], M. Terristi[5,9], R.J. de Kok[4,8], G. Koren[7], H. van Asperen[3], S. P. Jones[3], F.A.F. D'Oliveira[2], U. Weber[9], E. P. Marques-Filho[10], I.M. Cely[11], A. Araujo[12], J. V. Lavric[13], D. Walter[14], X. Li[15], J.P. Wigneron[15], B. D. Stocker[6,21], J. Gonçalves de Souza[16], M. O'Sullivan[16], S. Sitch[16], P. Ciais[17], F. Chevallier[17], W. Li[18], I. Luijkx[4], W. Peters[4,19], C. A. Quesada[20], S. Zaehle[1], S. Trumbore[3], and A. Bastos[5,9]

[1]Biogeochemical Signals Department, Max Planck Institute for Biogeochemistry, Jena, Germany

[2]Departamento de Física, Instituto Federal de Educação, Ciência e Tecnologia do Pará, Belém, Brazil

[3]Biogeochemical Processes Department, Max Planck Institute for Biogeochemistry, Jena, Germany

[4]Wageningen University, Meteorology & Air Quality Dept, Wageningen, The Netherlands

[5]Institute for Earth System Science and Remote Sensing, Leipzig University

[6]Institute of Geography, University of Bern, Hallerstrasse 12, 3012 Bern, Switzerland

[7]Copernicus Institute of Sustainable Development, Utrecht University, Utrecht, The Netherlands

[8]ICOS ERIC, Carbon Portal, Geocentrum II, Sölvegatan 12, SE-22362, Lund, Sweden

[9]Biogeochemical Integration Department, Max Planck Institute for Biogeochemistry, Jena, Germany

[10]Departamento de Física, Universidade Federal da Bahia, Salvador, Brazil

[11]Atmospheric Physics Laboratory, University of São Paulo, São Paulo, Brazil

[12]Embrapa Amazônia Oriental, Belém, Pará, Brazil

[13]Acoem GmbH, Hallbergmoos, Germany

[14]Multiphase Chemistry Department, Max Planck Institute for Chemistry, Mainz, Germany

[15]INRAE, UMR1391 ISPA, 33140 Villenave d'Ornon, France

[16]Faculty of Environment, Science and Economy, University of Exeter, Exeter, UK.

[17]LSCE/IPSL, CEA-CNRS-UVSQ, Université Paris-Saclay, 91191 Gif-sur-Yvette, France

[18]Department of Earth System Science, Ministry of Education Key Laboratory for Earth System Modeling, Institute for Global Change Studies, Tsinghua University, Beijing, China

[19]University of Groningen, Centre for Isotope Research, Nijenborgh 6, Groningen, The Netherlands

[20]Instituto Nacional de Pesquisas da Amazônia (INPA), Manaus, Brazil

[21]Oeschger Centre for Climate Change Research, University of Bern, Bern, Switzerland

Corresponding author: Santiago Botía (sbotia@bgc-jena.mpg.de)

Key Points:

- Drought turned the biogeographic Amazon in 2023 to a weak carbon source, with magnitude similar to the drought of 2015 but less than 2016.
- Seasonal development of net carbon exchange in 2023 was marked by early uptake that partly compensated the carbon source of the dry season.
- The 2023 fire season in the Amazon was extended until November, though annual fire emissions were close to the long-term average.

Abstract

In 2023, the biogeographic Amazon experienced temperature anomalies of 1.5°C above the 1991-2020 average from September to November. These conditions were driven by high sea surface temperature in the Atlantic and Pacific oceans, together with reduced moisture advection from the Atlantic, causing large vapor pressure and water deficits in the second semester of 2023. Here, we evaluate the response of the Amazon carbon cycle to this extreme event across different spatial scales. We combined atmospheric CO_2 mole fractions and eddy covariance flux data from the Amazon Tall Tower Observatory (ATTO), near-real-time simulations by Dynamic Global Vegetation Models (DGVMs), an atmospheric inversion, and remote sensing data. We find that in 2023 the Amazon region was, including fires, a net carbon source of 0.01 to 0.17 PgC. Fire emissions (0.15 [0.13-0.17] PgC) were within typical variability of the 2003-2023 period, thus we attribute the weak carbon source to reduced vegetation uptake during the dry season. A stronger-than-normal vegetation uptake early in the year (January to April), consistent across data streams and spatial scales, mitigated the total carbon losses by the end of the year. We find a shift from carbon sink to source in May and a peak source in October. Our findings show a reduced vegetation carbon uptake over the Amazon region, leading to a weak carbon source that contributed 30% of the net carbon loss in the tropical land in 2023.

Plain Language Summary

The Amazon rainforest is a fundamental component in the Earth system as it stores large amounts of carbon in standing biomass. In 2023, unusually high temperatures (1.5°C above typical levels from 1991-2020) and dryness were recorded in the region from September to November. These conditions were caused by less moisture from the Atlantic ocean and warmer water temperatures in the Atlantic and Pacific oceans, which led to low humidity and drought across the Amazon region in the second half of 2023. We studied how these extreme conditions affected the Amazon's ability to absorb and store carbon. Using CO_2 measurements from the Amazon Tall Tower Observatory (ATTO), along with computer simulations and satellite data, we observed that the Amazon became a source of carbon emissions in 2023, releasing between 0.01 and 0.17 billion tons of carbon, rather than absorbing it. Carbon emissions from fires were 0.15 billion tons, which was within normal levels for the last two decades (2003-2023). We therefore attribute the anomalous carbon release in 2023 mostly to weakened vegetation uptake, rather than increased losses from fires. The seasonal development diagnosed by computer models suggest that vegetation absorbed more carbon than usual from January to April, helping offset emissions, but this shifted in May when the Amazon began releasing more carbon, with the highest emissions in October. Our results suggest that the Amazon's reduced carbon absorption accounted for 30% of the net carbon source across the tropical land in 2023.

1 Introduction

The global atmospheric CO_2 growth rate in 2023 was 2.79 +- 0.08 ppm (Ke et al., 2024; Lan, Tans, et al., 2024), the third largest since 2000 and fourth since 1959. The average growth rate for the 2010-2020 decade was close to 2.5 ppm (https://gml.noaa.gov/ccgg/trends/gl_gr.html, last accessed Dec 12, 2024), so this large anomaly, can not be solely explained by an increase of 1.3% in anthropogenic emissions from 2022 to 2023 (Friedlingstein et al., 2024), suggesting a reduction in the global carbon sinks (Ke et al., 2024). Tropical land plays an important role in determining the mean magnitude of the land carbon sink (Schimel et al., 2015), which is controlled by a balance between net carbon sources resulting from deforestation and carbon sinks where uptake surpasses carbon losses in less disturbed forest vegetation. Net release of carbon in the tropical land has been associated with positive phases of El Niño Southern Oscillation events (Gloor et al., 2018; J. Liu et al., 2017; Palmer et al., 2019; Rödenbeck et al., 2018), which in turn is linked to positive surface temperature anomalies globally (Trenberth et al., 2002) and in tropical forests (Jimenez et al., 2018).

Globally, the year 2023 was the first one in which daily global mean temperatures were continuously 1^{o}C above the 1850-1900 reference period, marking an unprecedented record. In about 50% of the days, most of them in the second half of the year, daily global mean temperatures reached values 1.5^{o}C above the 1850-1900 reference period, and from April to December global surface ocean temperatures registered record values (Copernicus, 2024). Associated with these record warming conditions, extreme events were observed both over land and ocean, including major heatwaves and droughts across many regions. For example, in Canada, extreme temperatures combined with low humidity led to unprecedented wildfires which contributed to ca. 25% of total tree cover loss that year (MacCarthy et al., 2024) and released over 0.6 PgC, more than the national fossil fuel emissions (Byrne et al., 2024). In the Amazon basin, historical drought and heat conditions were registered in 2023, with temperatures in October greater than 3^{o}C above the 1981-2020 average, and the Port of Manaus reaching the lowest water levels since records began in 1902 (Espinoza et al., 2024).

These extreme conditions have been linked to a transition from La-Niña conditions in 2022-23 to El-Niño from mid 2023, combined with widespread anomalous warming over the oceans worldwide (Espinoza et al., 2024). Previous droughts in the Amazon region, such as the ones in 2005 and 2010, and those associated with El-Niño conditions like in 2015-16, have resulted in reduced net carbon uptake by the Amazon forest, due to decreased productivity despite a slight increase in greenness (Bastos et al., 2018; Erik et al., 2018; J. Liu et al., 2017; J. Yang et al., 2018), reduced tree growth (Phillips et al., 2009; Feldpausch et al., 2016; H. Yang et al., 2022) and increased mortality (Hartmann et al., 2022; Powers et al., 2020). Hot and dry conditions tend to be associated with high fire activity and increased tree mortality (Brando et

al., 2014) resulting in persistent impacts that compound with human-driven disturbances, and can accelerate forest degradation (Berenguer et al., 2021; Fawcett et al., 2023; Lapola et al., 2023). Furthermore, in previous droughts in 2010 and 2015/2016, intensified fire emissions in the south and east of the Amazon have shifted the region from a carbon sink to a source (Basso et al., 2023; Gatti et al., 2014; Rosan et al., 2024; van der Laan-Luijkx et al., 2015; Alden et al., 2016; Gloor et al, 2018). However, regional differences in drought severity (Aragão et al., 2018; Lapola et al., 2023; Phillips et al., 2009) and thus resistance and resilience to drought (S. Chen et al., 2024) and fires (Berenguer et al., 2018; Esquivel-Muelbert et al., 2020), together with long-term rainfall trends, make impacts of each drought unique (Anderson et al., 2018).

Here, we examine the impacts of the 2023 extreme heat and drought conditions on the Amazon carbon cycle by combining multiple sources of information on ecosystem productivity, changes in biomass growth, fire activity and resulting net carbon fluxes. The combination of different types of surface and atmospheric measurements together with satellite observations of vegetation condition, aboveground biomass and fire activity, as well as atmospheric inversions and dynamical global model simulations, enables a distillation of robust patterns and the linking of atmospheric drivers with continental-to-regional-scale impacts on the land carbon balance. We first study the development of the 2023 drought by analyzing the seasonal evolution of the large-scale atmospheric circulation anomalies over tropical South America, and compare these with previous events such as the El-Niño in 2015/16. Then we analyze the spatiotemporal patterns of the most relevant climatic drivers of vegetation dynamics over the Amazon basin and the evolution of fire activity, contrasting when possible with previous events. We compare net land-atmosphere carbon exchanges, gross primary productivity, and ecosystem respiration from global vegetation models and an atmospheric inversion, analyzing their agreement and differences in magnitude and seasonality during the 2023 extreme event. As a benchmark, we compare the large-scale patterns with in-situ measurements of carbon fluxes and atmospheric CO_2 at the Amazon Tall Tower Observatory (ATTO), which is located in the central Brazilian Amazon in a well preserved location and is one of the few sites in the region providing carbon cycle in-situ data. By combining these multiple lines of evidence, our study aims to provide a robust assessment of the carbon cycle impacts of the 2023 extreme drought in the Amazon, and their relevance in the context of the global carbon cycle anomalies in 2023 (Friedlingstein et al., 2024; Ke et al., 2024).

2 Materials and Methods

2.1 Data sources and carbon cycle flux terms at regional scale

We used ERA5 reanalysis data (Hersbach et al., 2020) and ERA5-Land (Muñoz-Sabater et al., 2021) to analyze climatic drivers and anomalies over the Amazon. Monthly anomalies for sea surface temperature (SST), winds, geopotential height, and water vapor flux were computed

relative to 2000–2023 (Figure 1, Text S1). Potential cumulative water deficit (PCWD) was derived from precipitation and potential evapotranspiration (PET) following Stocker et al., (2023) and vapor pressure deficit (VPD) was calculated using 2m air temperature and relative humidity from ERA5-Land, with anomalies also referenced to 2000–2023. We refer the reader to Text S1 for more details on the reanalysis data.

To calculate the carbon cycle components (see Figure 1 and Text S2 and S3 for more details) we use four land surface models (bottom-up approach): Simple Biosphere model Version 4 (SiB4, Haynes et al., 2019), ORCHIDEE-MICT (Guimberteau et al., 2018; Krinner et al., 2005) , O-CN (hereafter referred to as OCN, Zaehle et al., 2010) and JULES (Clark et al., 2011). Three of the land surface models are Dynamic Global Vegetation Models (DGVMs) and one is a process-based model (SiB4), but for practical reasons we will refer to DGVMs throughout the text. As the top-down approach we use one satellite-driven atmospheric inversion (OCO2-Inv) that has a high resolution globally (1 x 1 degree) and is driven by the OCO-2 satellite atmospheric CO_2 concentration data. The remote sensing data (Figure 1, Text S4), like fire counts and emissions, GPP proxies (Sun Induced Fluorescence - SIF and Near Infrared of Vegetation - NIRv) and the Aboveground Carbon (AGC) based on L-band derived Vegetation Optical Depth (L-VOD) are all described in Text S4.

We define the carbon cycle components as the net flux over land (F_{land}) which results from the Net Biome Exchange (NBE) and the anthropogenic emissions (F_{ff}) from fossil fuels.

$$F_{land} = NBE + F_{ff}$$

NBE is composed by the Net Ecosystem Exchange (NEE) and fire emissions, including deforestation and degradation (F_{fire}) .

$$NBE = NEE + F_{fire}$$

And finally, NEE is given by the difference between terrestrial ecosystem respiration (TER) and photosynthesis (GPP). A negative sign (-) in F_{land}, NBE and NEE indicates a net uptake of carbon over land, whereas a positive (+) sign denotes a net source of carbon over land.

$$NEE = TER - GPP$$

To obtain the bottom-up NBE, we use the ensemble mean of the DGVMs and the mean F_{fire} between GFAS (Kaiser et al., 2012) and GFED4s (van der Werf et al., 2017). The top-down approach NBE is obtained using the OCO2-Inv and by subtracting F_{fire} from NBE, we obtain NEE. In Figure 1, we provide a summary of the data streams used to calculate the bottom-up and top-down NBE and NEE, together with the data used as proxies in this study.

The uncertainty of the F_{fire} is reported in terms of the min-max range [min-max], between GFAS and GFED4s. For the flux components (GPP, TER, NEE and NBE) calculated with the DGVMs we use the standard deviation of the model ensemble mean. For the OCO2-Inv we do not report uncertainty for 2023, but we note that as the global uncertainty (1-σ) for a single year is 3 PgC year^{-1}, the posterior uncertainty for the biogeographic Amazon will be less given the smaller domain and the data constraint, likely within 0.3-0.5 PgC year^{-1}. The inter-annual variability (IAV) is also reported explicitly and is calculated as the standard deviation of the multi-year mean for a given data source (e.g. $\overline{NEE}$ +- IAV). For the DGVMs, the multiyear mean is calculated from the ensemble mean of each individual year.

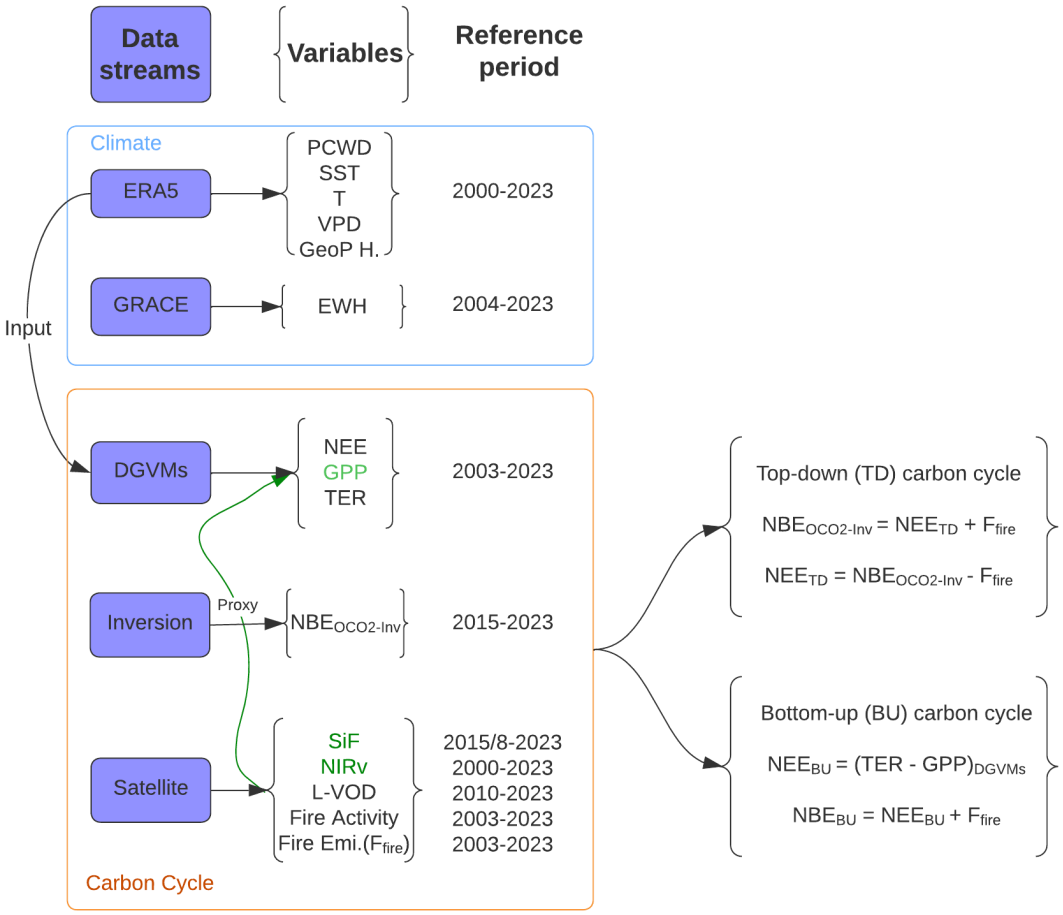

Figure 1. Data streams for climate and carbon cycle cycle components used to obtain the carbon budget for the biogeographic Amazon based on top-down and bottom-up approaches. Note that for SIF, as we describe in Text S4 we are using two products with different reference periods. The green highlight shows that SiF and NIRv are used as GPP proxies.

2.2 Local Measurements of carbon and climate variables

We use several data streams measured at the ATTO site (-2.1441, -58.999, https://www.attoproject.org/). In-situ continuous CO_2 mole fractions covering the period from

2014 to 2023 were used. The ATTO site and most of the measurement systems have been described by Andreae et al., (2015) and the footprint of the CO_2 mole fractions were characterized by Botía et al., (2022) and added in Figure S1. The half-hourly eddy covariance (EC) data was measured with a 3D sonic anemometer (CSAT3, Campbell Scientific Inc., Logan, UT, USA) and an open-path infrared gas analyzer (LI-7500A, Li-COR Inc., Lincoln, NE, USA), both mounted at 81 m above ground level on the ATTO 80 m Instant tower. The filtered high-quality and half-hourly turbulent EC-CO_2 fluxes were used for further data analysis: net ecosystem exchange (EC-NEE) calculation, gap-filling and EC-NEE partitioning to Gross Primary Productivity (GPP) and Ecosystem Respiration (R_{eco}). The complete details on the processing, partitioning, data quality assessment and calibration of the eddy covariance data and the CO_2 mole fraction datasets can be found in Text S5.

3 Results

3.1 Regional climate anomalies

In 2023, large PCWD (Figure 2) were found in the beginning of the year for the areas surrounding the Amazon, but remained low through the first semester within the biogeographic Amazon (hereafter Amazon). PCWD remained particularly low in the southern and eastern sectors of the Amazon forest, while other parts experienced relatively higher water deficits. By July, an increasing PCWD started to develop primarily in the southern sector of the Amazon, intensifying and expanding into central Amazonia. The progressive increase of PCWD is associated with high pressure anomalies between 5-20^{o}S (Figures S2-S3) and a weakening of the trade winds that persisted from June until October 2023 (Figures S7-S8). The persistence of high-pressure anomalies south of the equator in the second half of 2023 further induced a northward shift of the ITCZ (Figure S4) that suppressed regional convection and rainfall (Figure S4, S5) over the Amazon.

The weakened winds coming from the east and northeast flow contributed to reduced moisture transport from the Atlantic Ocean into the Amazon region; such wind anomalies were more pronounced from March to August (Figures S10). This led to the intensification of PCWD, potentially reinforcing anomalous anticyclonic circulation, especially in the eastern and central Amazon. The anomalous circulation patterns from May to December 2023 were likely induced by the above-average sea surface temperatures (SSTs) registered in both the Pacific and Atlantic Oceans (Figure 2). In the eastern Pacific, strong positive SST anomalies developed from April to November, consistent with the predominance of El Niño conditions (Espinoza et al., 2024), as in 2010 and 2015/16 (Marengo et al., 2011; Jiménez-Muñoz et al., 2016). The coincidence of warming in both ocean basins is particularly noteworthy, as it likely amplified the drought effects beyond what would be expected from a typical El Niño event alone.

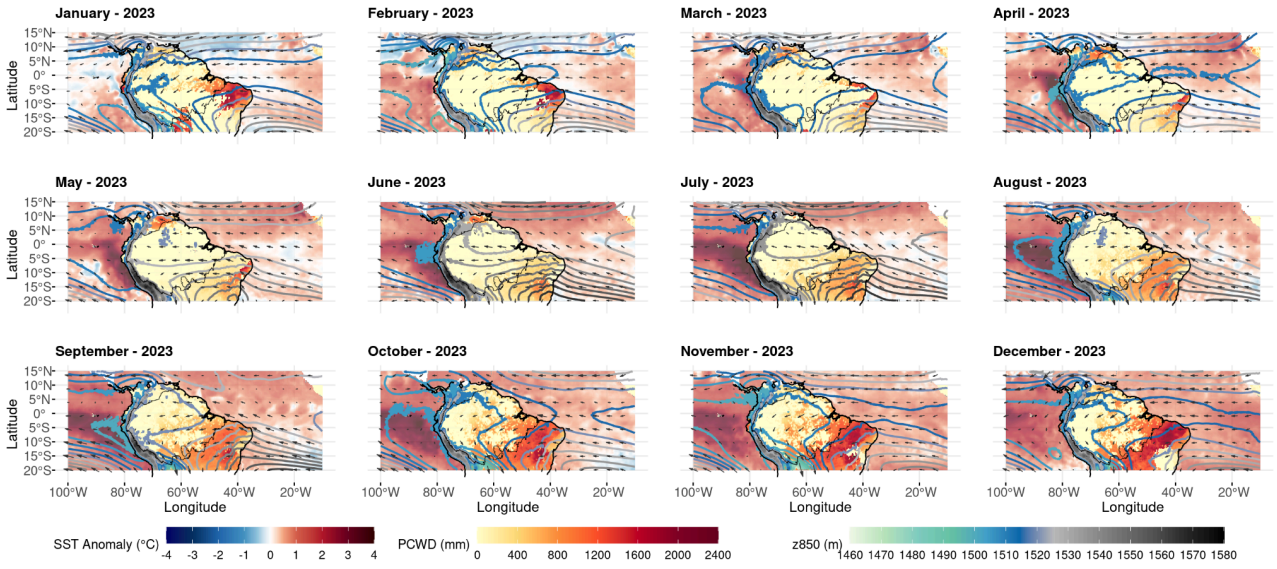

Figure 2. Regional climate analysis for 2023. Sea Surface Temperature (SST, plotted over sea surface), Cumulative water deficit (PCWD, plotted over continental surface), geopotential height contours at 850hPa (plotted as colored contour lines) and wind fields at 850hPa (black arrows). All variables were calculated using ERA5 reanalysis data, and the monthly anomalies were calculated relative to 2000-2023 baseline.

To better understand the 2023 event we compare the large-scale anomalies in climatic drivers in 2023 with those in 2015, the previous El Niño event in the origin year. Compared to 2015, the 2023 drought extended deeper into the Amazon, as shown by positive differences in PCWD emerging from September to December (Figure S9) and by the precipitation anomalies (Figures S5-S6). The exacerbated warming in 2023 is also evident in SST anomalies in 2023 compared to 2015 (Figure S9), which were consistently higher in 2023 than 2015 for most of the year in both the Atlantic and the Pacific oceans. Over the eastern Pacific, 2023 was colder than 2015 from September until December, consistent with it being a weaker El-Niño.

PCWD differences between 2023 and 2015 are partly driven by differences in VPD between those years and linked to 2023 having recorded record air temperatures and VPD over the last 24 years (Figure 3). Moreover, the seasonal evolution of temperature and VPD anomalies were concentrated in the second half of 2023 (Figure 3a,b,c,d), presenting a peak in October (Figure 3f,g). In addition, the equivalent water height from GRACE, was the lowest in this century in the Amazon basin (Figure 3e). Therefore, our results show that other mechanisms additional to El Niño in 2023, like the anomalous sea surface temperature in the Atlantic ocean, contributed to stronger drought conditions over most of the Amazon than in 2015, and are consistent with the attribution of the extreme drought conditions in 2023 to climate change by the World Weather Attribution project (WWA, 2024).

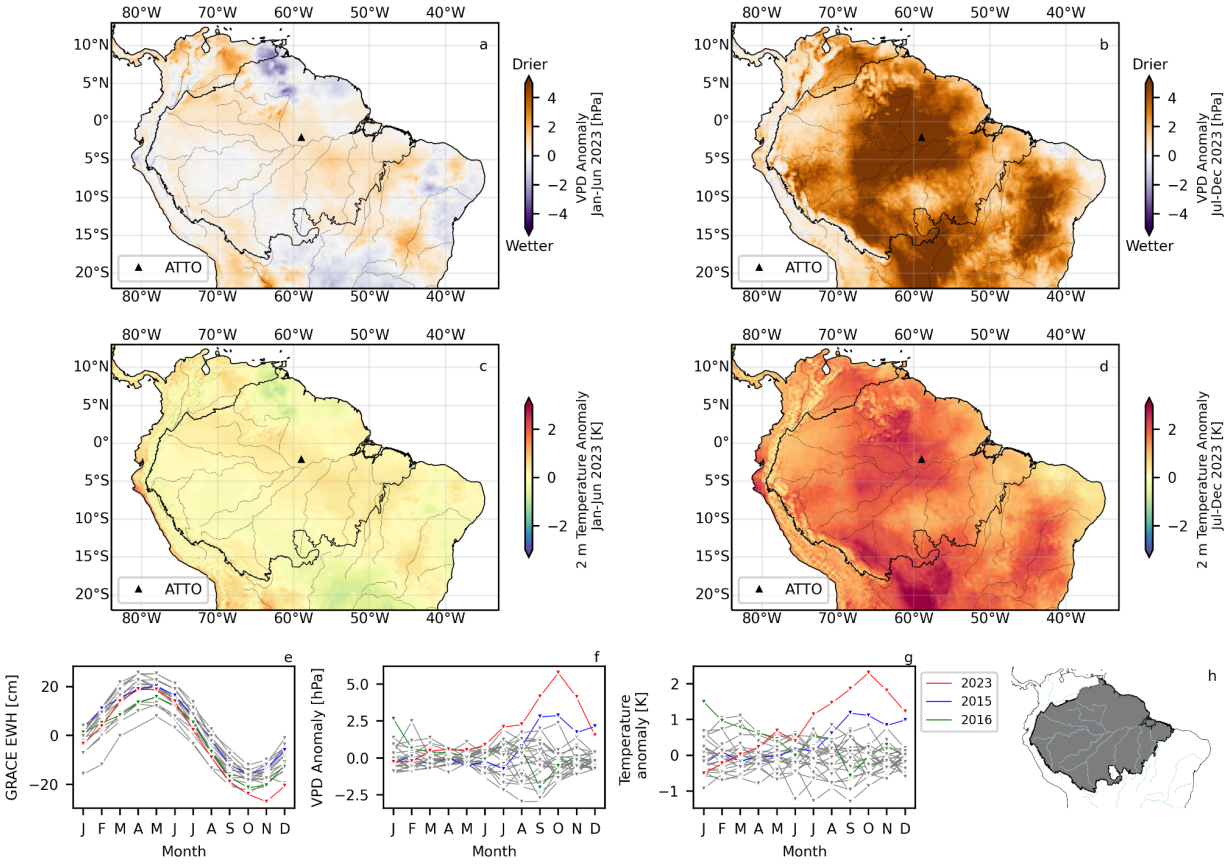

Figure 3. Regional scale climate anomalies for tropical South America. The spatial anomalies of VPD for both semesters in 2023 (a,b) and the same for the 2m temperature (c,d) were calculated using ERA5 land data (Hersbach et al., 2020). The seasonal evolution of the Equivalent Water Height (EWH) anomalies for the Amazon basin (e) were taken from the Gravity Recovery and Climate Experiment (GRACE) (available at: https://grace.jpl.nasa.gov/data-analysis-tool/. Last access: July 17, 2024). The seasonal evolution of VPD (f) and 2m temperature (g) anomalies are shown for the shaded area in (h) that corresponds to the biogeographic Amazon. The anomalies are based on a reference time period from 2000 to 2023.

3.2 Seasonal evolution and spatial distribution of carbon cycle components

Seasonal F_{fire} anomalies

The fire season in 2023 was extended well into November, different from normal years when the fire season offset is in October (Figure 4b,d). This extended fire season was driven by a north-to-south shift, but not necessarily leading to anomalous fire activity and carbon emissions (Figure 4b,c,d,e). Fires were largely concentrated in the Arc of Deforestation, along the southern border of the Amazon (between 70-60ºW and 15ºS), but also further north in the state of Pará and along the main branch of the Amazon river (Figure 4a). The highest fire counts and emissions were in October and November (Figure 4b,d). On average, the fire activity is dominated by fires occurring south of 5ºS, with an increasing contribution in October and November (Figure 4f,g). In 2023, from July to September the relative contribution of fires north of 5ºS was 10% larger than the long-term mean (2003-2023), consistent with the study of Jiménez et al., (2024). Later (November and December), the fire counts in the south (below 5ºS) were doubled relative to the 2003-2023 mean. Note that these spatial patterns are consistent with the development of the PCWD in the second half of 2023 (Figure 2). Furthermore, ATTO carbon monoxide data shows larger than average enhancements of CO, especially in September and October, confirming the larger than average contribution of fires north of 5ºS (Figure S11).

Even though there was an extended fire season, total fire emissions in 2023 (0.15 [0.13-0.17] PgC $year^{-1}$, see Figure 4c) were the same as the long-term (2003-2023) average between the two fire products (0.15 [0.13-0.16] PgC $year^{-1}$) with an interannual variability of +- 0.07 PgC $year^{-1}$. Individually, over the entire record (2003-2023, Figure S12), GFED4s emissions and its inter-annual variability (0.16 +- 0.08 PgC $year^{-1}$) are on average larger than GFAS (0.13 +- 0.07 PgC $year^{-1}$). Our estimate for the biogeographic Amazon in 2023 is similar to 2015 and 2016 (0.13 and 0.14 PgC $year^{-1}$), consistent with the total fire counts in 2023 (~180,000), which were marginally higher than 2015 (~163,000) and 2016 (~145,000). Given these findings, we conclude that fires were within the long-term variability and had a close-to-normal contribution to the NBE in 2023.

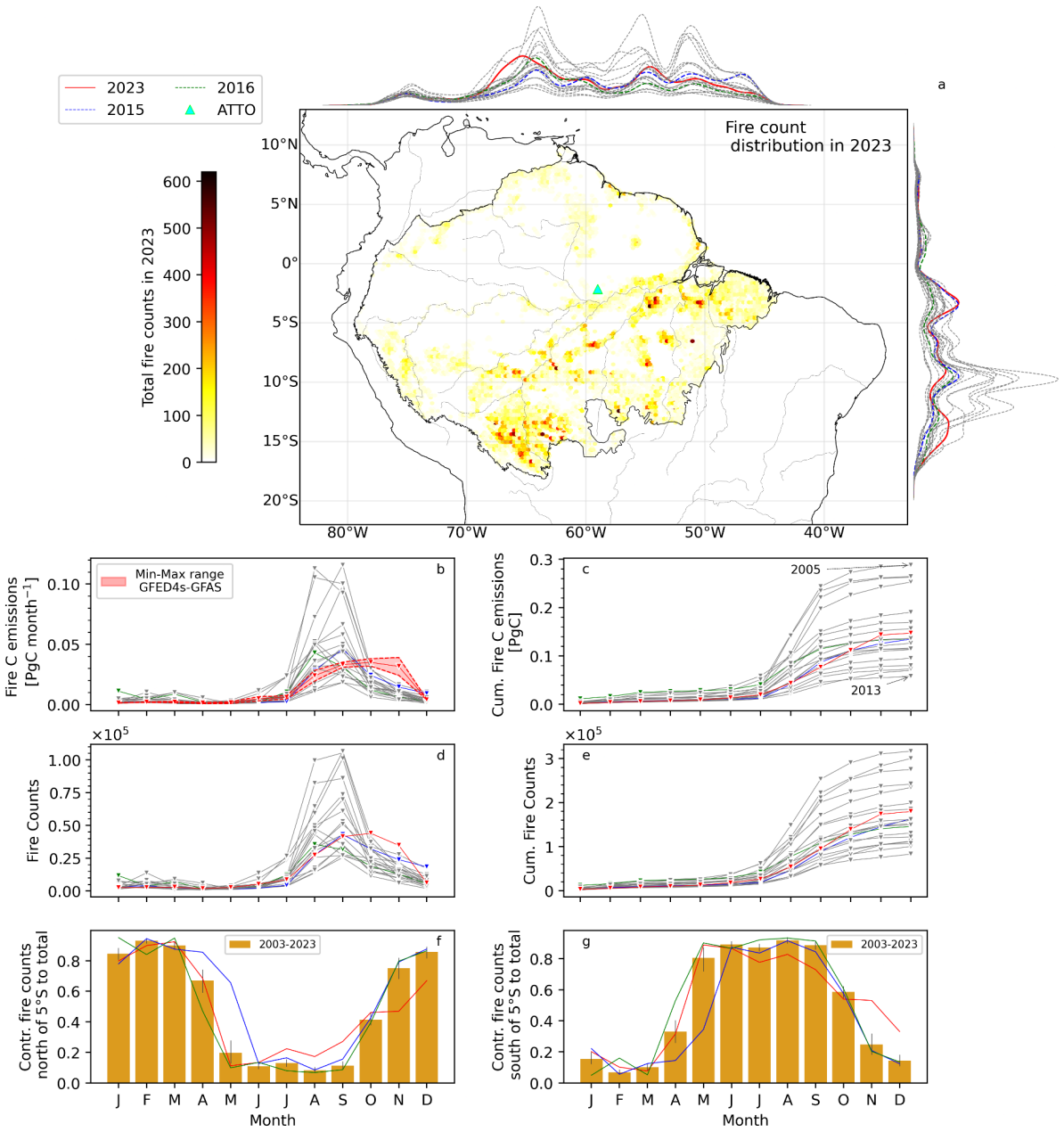

Figure 4. Fire counts and carbon emissions from fire in the biogeographic Amazon. Spatial distribution of total Fire counts in 2023 (a) with the latitudinal and longitudinal marginal distributions on y and x. We calculated the mean fire carbon emissions based on the GFED4s (van der Werf et al., 2017) and GFAS (Kaiser et al., 2012) products for each month from 2003 to 2023 (b). The red shading in (b) indicates the maximum and minimum fire emission between GFED4s and GFAS for the months in 2023. The cumulative fire carbon emissions are shown in (c). The seasonal evolution of fire counts (d) and cumulative fire counts from 2003 to 2023 (e). The relative contribution (%) of fire counts north (f) and south (g) of the latitude 5ºS to the total fire counts per month for 2023 and the mean for 2003 to 2023.

Spatial distribution of NEE, NBE and Fires

In 2023, the spatial patterns of vegetation carbon sources and sinks (NEE), as simulated by DGVMs, show high consistency, with at least three out of four models agreeing on the sign of NEE (Figure 5a). According to these models, vegetation acted as a carbon source south of the main branch of the Amazon River and northeast of ATTO. The source regions south of the Amazon River (e.g., between 70°W–60°W) overlap with fire emissions (Figure 5b), whereas this overlap is not observed in the northeast near ATTO. Spatial patterns of NEE partially align with the temperature and VPD anomalies shown in Figure 3 and with PCWD in Figure 2, particularly in the central, southern, and eastern Amazon. Conversely, regions in the north and northwest, where DGVMs simulate vegetation uptake, do not show significant VPD or temperature anomalies, nor large PCWD throughout the year. Therefore, DGVMs and fire data suggest that vegetation carbon sources were enhanced by fire activity in the south of the Amazon but not in the northeast.

The spatial distribution of NBE in the DGVMs and the OCO2-Inv is broadly consistent in an east-west sink-to-source gradient in the Amazon (Figure 5c,d). The OCO2-Inv indicates a net uptake of carbon concentrated over the west (west of 70°W), but the DGVMs simulate the uptake in the northwest. While DGVMs simulate larger carbon sources than the OCO2-Inv in the south of the Amazon where most of the fires are located, the OCO2-Inv shows a large source northeast of ATTO. Note that northeast of ATTO, fire emissions were low suggesting that the positive NBE (carbon sources) is mainly driven by vegetation. The differences between NEE and NBE in Figure 5a versus 4c,d are indicative of fire emissions in the regions where NBE > NEE, but only where fire emissions overlap. On the other hand, in the grid cells in which NEE (Figure 5 a) is close to NBE (Figure 5 d), the role of the vegetation in the sink or source of carbon is more relevant than fires. Based on this, we found a carbon source (+NEE) due to reduced vegetation uptake in the north of the main branch of the Amazon river and northeast of ATTO.

Seasonal evolution of NEE, NBE and GPP, TER

We compared the calculated seasonal evolution of the gross and net carbon fluxes over the whole basin in 2023 with the long-term mean, both for DGVMs (2003-2023) and the OCO2-Inv (2015-2023) (Figure 6). We use different reference periods as the OCO2-Inv is limited to the OCO2 data coverage. DGVMs simulate positive (slightly above 1σ) TER and GPP anomalies in the beginning of 2023, which result in equally strong negative NEE (increased uptake) until May (Figure 6 a,b,c). Starting in August, DGVMs indicate a steep decline in GPP, shifting from moderately positive values in August to extremely low (<-2σ) levels from September to December. This decline is accompanied by a consistent but less pronounced decrease in TER, with the most significant negative anomalies (also below -2σ) in November. As a result, the NEE over the Amazon shifts from negative (carbon uptake) to positive (carbon source) in September, remaining positive through the end of the year (Figure 6c). Adding fire,

the NBE from DGVMs shows a similar trajectory, with more evident contributions from fire since July onwards (Figure 6d). Note that the anomalies given by the DGVMs are based on a reference period between 2003 and 2023 and represent the largest simulated decline in gross fluxes and net sources (NEE and NBE) during the dry season in the current century.

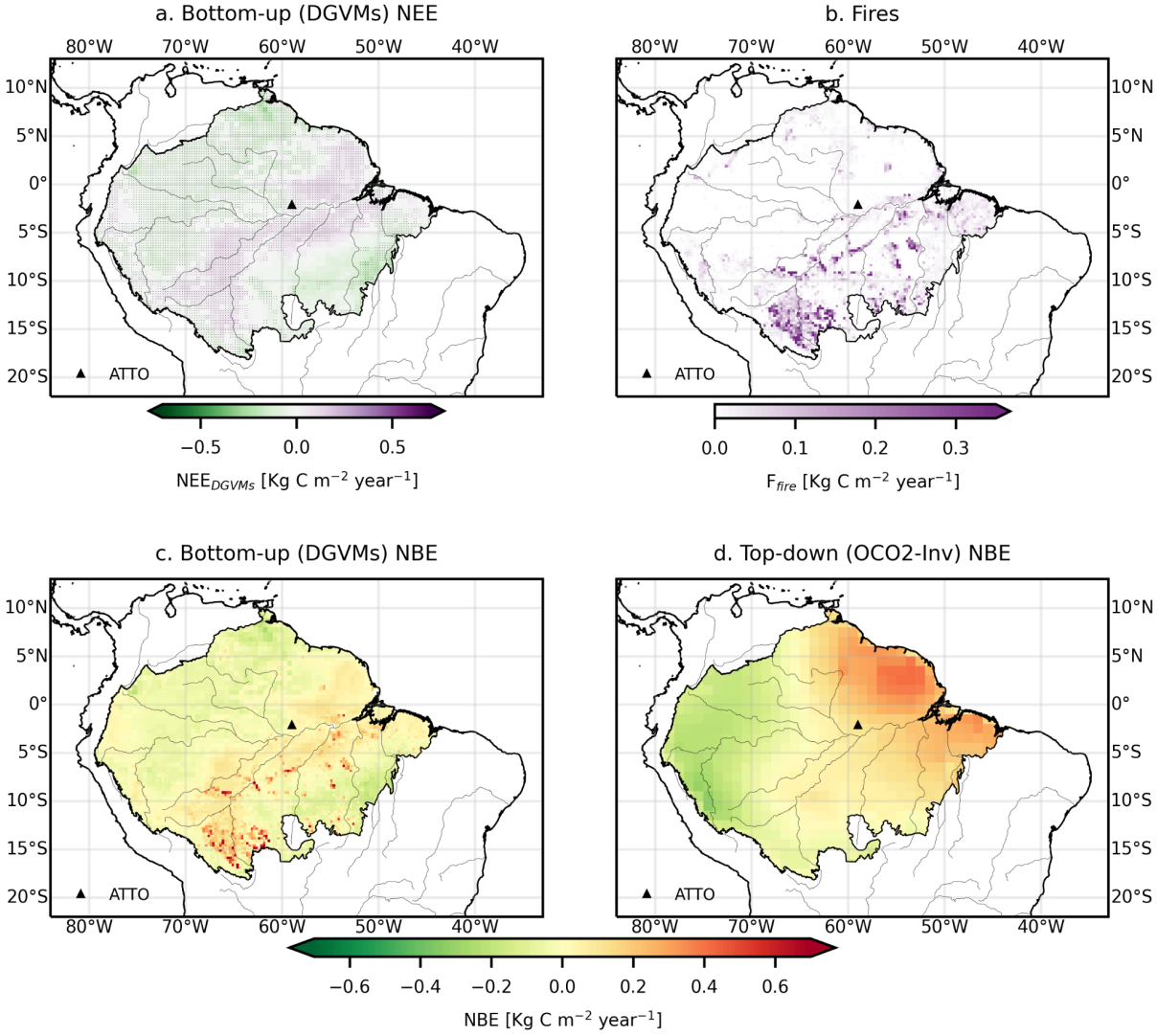

Figure 5. Bottom-up and top-down carbon cycle components for the biogeographic Amazon in 2023. In (a) the mean NEE for the DGVMs, in (b) the mean fire emissions between GFAS and GFED4s, in (c) the NBE calculated as the sum of panels a and b (NBE = NEE_{DGVMs} + F_{fire}) and in (d) the NBE of the OCO2-Inv. In (a) the grid cells in which at least three of the DGVMs coincide in the sign of NEE are highlighted with a marker.

The OCO2-Inv estimates a strong uptake (NBE) in the first months of 2023, but followed by a switch from sink to source in May and a return to a sink in December (Figure 6 e). This is consistent with uptake anomalies (NEE) in DGVMs in the beginning of the year, but the magnitude of uptake in the OCO2-Inv (NBE) relative to the mean of the reference period is larger than in the DGVMs. We find that in the DGVMs and the OCO2-Inv, October is the month in which NEE and NBE reach the seasonal maximum or the largest carbon source in 2023, coinciding with the temperature and VPD anomalies shown in Figure 3 and with the peak in fire activity at the Amazon region scale. Given the seasonal development, we conclude that the NBE maximum in the second semester was driven by a combination of fires and a positive NEE, but the switch from sink to source in May (only in the OCO2-Inv) is only driven by a positive NEE as fire activity with a late onset began only in August (Figure 4). Nevertheless, the enhanced uptake from January to May, evident in both OCO2-Inv and DGVMs, compensated for the relatively large source in the second part of the year.

Over the whole year (2023), the NBE ranges from 0.01 PgC $year^{-1}$ (DGVMs) to 0.17 PgC $year^{-1}$ (OCO2-Inv). In the top-down estimate the NBE implicitly includes fires, and degradation and deforestation emissions that do not occur through burning (although these were not prescribed in the priors) over the Amazon (Figure 6f). Interestingly, the NBE in DGVMs and the OCO2-Inv during 2023 was similar in magnitude to 2015 (DGVMs, -0.06 PgC $year^{-1}$ and OCO2-Inv, 0.16 PgC $year^{-1}$), but contrastingly different than in 2016 (DGVMs, -0.10 PgC $year^{-1}$ and OCO2-Inv, 0.83 PgC $year^{-1}$). Without fires (0.15 [0.13-0.17] PgC $year^{-1}$), the NEE ranges from a sink (DGVMs, -0.13 PgC $year^{-1}$) to a small source (OCO2-Inv, 0.02 PgC $year^{-1}$) in 2023. Note that compared to previous years, the DGVMs show the largest difference in NEE relative to the long-term mean, indicating a carbon sink weakened by more than 30%. It is worth noting that the shape of the seasonal cycle differs between the OCO2-Inv and DGVMs, which might be because DGVMs tend to not capture well the seasonality of GPP in the evergreen tropical forests (Restrepo-Coupe et al., 2017; X. Chen et al., 2020). Therefore, even differing in seasonality and in the absolute magnitude of the fluxes, both DGVMs and the OCO2-Inv estimate a large anomaly in 2023 relative to the reference period.

GPP anomaly and Aboveground biomass change

To confirm the negative anomaly in GPP given by the DGVMs, we further analyzed independent GPP proxies for the same region. First, we compared each GPP proxy (OCO2-SiF, Tropomi-SiF and NIRv) to the local EC-GPP at ATTO (Figure S13), which indicate that the SiF products (OCO2-SiF and Tropomi-SiF) are closer to the local GPP ($r = 0.49$; p-value$<<0.01$, $r = 0.47$; p-value$<<0.01$, $n=72$) than NIRv ($r = 0.32$; p-value$=0.01$, $n=72$). Using the SiF products for the Amazon, we found that the sign of the anomalies in October, November and December is the same as for the DGVMs (Figure 7 a). Earlier in the dry season, in August and September, the SiF products and the DGVMs are not consistent and in September the DGVMs show a rather

large negative anomaly. Therefore, it is likely that the GPP anomaly in DGVMs had an earlier onset compared to the GPP proxies. However, from October to December, a reduced vegetation uptake, as the DGVMs and the GPP proxies suggest, is likely.

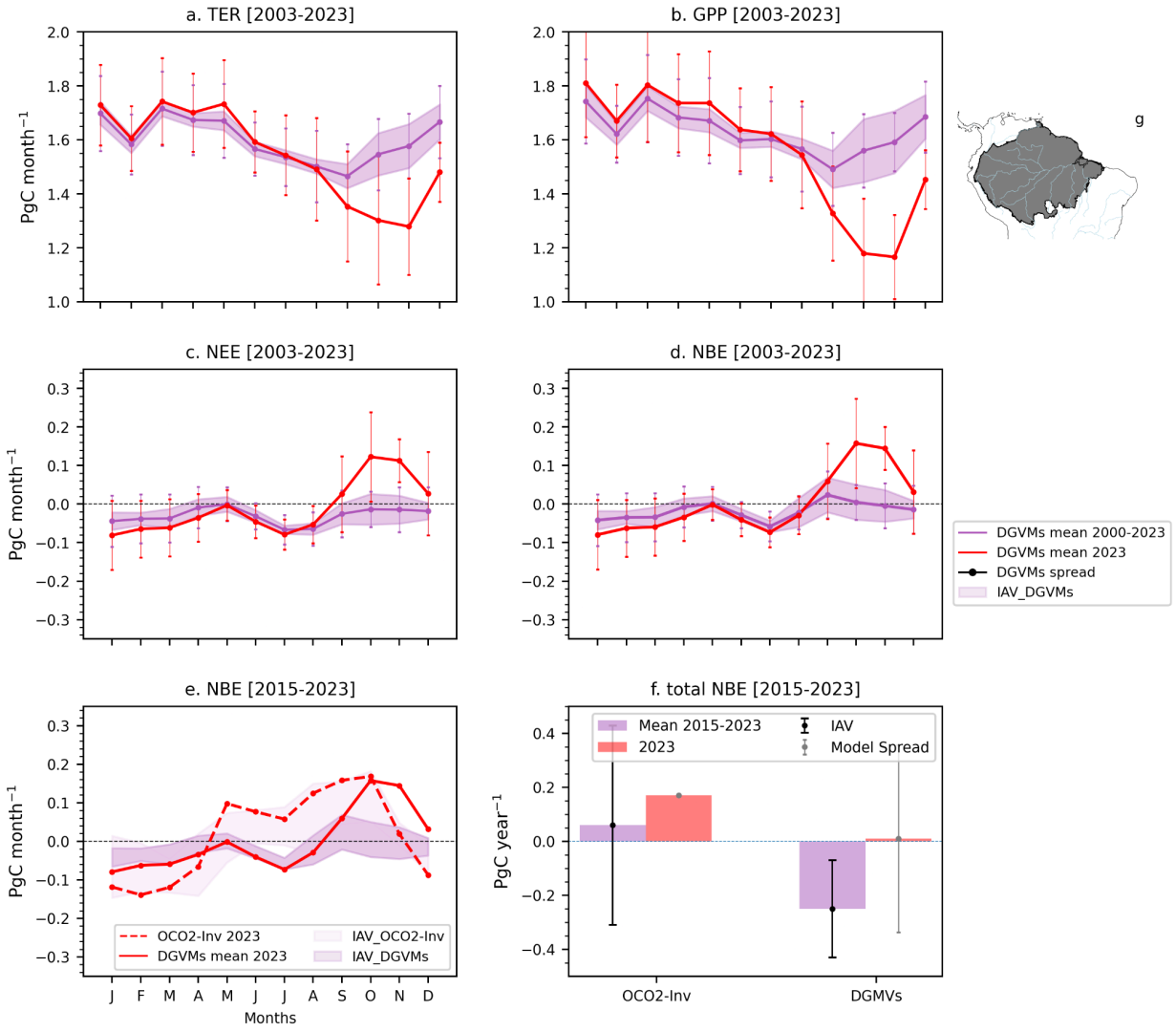

Figure 6. Mean seasonal cycle of gross and net carbon fluxes from DGVMs, having the period from 2003 to 2023 as a reference for the biogeographic Amazon. The climatological mean for the DGVM ensemble is shown for TER (a) and GPP (b) highlighting the standard deviation for each month with a shaded area. Net ecosystem exchange (NEE) based on the DGVM ensemble mean is shown in (c). Net biome exchange (NBE) for the DGVM ensemble mean is shown in (d). In (e) and (f) the seasonal NBE and total NBE for both OCO2-Inv and DGVMs is shown with the reference period corresponding to 2015-2023. Note that NBE for the DGMV ensemble mean was calculated adding the mean fire emission from the GFED4s and the GFAS fire emission products.

We find that the average Aboveground Carbon (AGC) loss in the Amazon from 2011 to 2023 was -0.39 +- 0.15 PgC $year^{-1}$ (average value over all years with losses) while for 2023 it was -0.61 PgC (Figure 7 b). Changes in AGC (ΔAGC) have been associated with tree mortality, deforestation and subsequent degradation at forest edges due to fire and logging, but also to secondary forest growth (Fawcett et al., 2023; Silva Junior et al., 2020), so a ΔAGC represents a net exchange which can have a fraction not emitted directly into the atmosphere. For example, selective logging or tree mortality are processes that can cause a ΔAGC but not an immediate CO_2 source to the atmosphere. The losses in 2023 could have been influenced by the decreasing trend in the L-VOD signal since 2016 (Figure S14). However, the spatial patterns in the AGC anomalies were found to correlate well with Enhanced Vegetation Index (EVI) and SiF (Wigneron et al., 2020), both proxies of GPP. As a comparison, relative to the long-term mean the reduction in DGVMs-GPP was 0.88 PgC $year^{-1}$ in 2023. Thus, while the AGC change in 2023 could in part be associated with a reduction in GPP due to deforestation, the mismatch (GPP_{losses} > AGC_{losses}) suggests that the reduction in GPP in the DGVMs could be slightly overestimated, like in the beginning of the dry season.

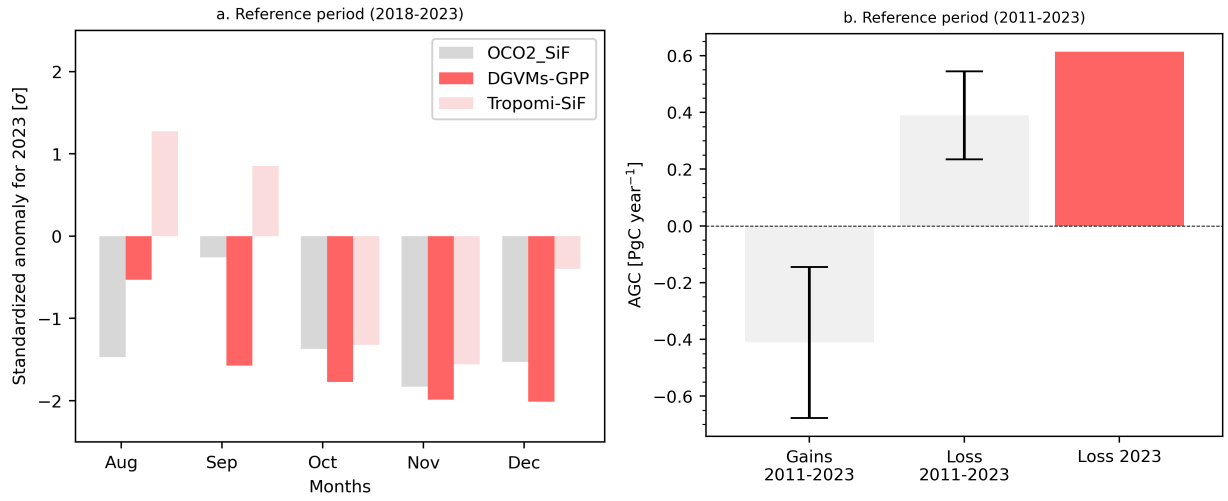

Figure 7. Magnitude of the standardized anomalies in OCO2-SiF, Tropomi-SiF and ensemble mean GPP of the DGVMs for the biogeographic Amazon a) and mean net aboveground carbon loss estimated from L-VOD for the same Amazon region b). Note that the anomalies in a) were calculated with the OCO2-SiF period as a reference (2018-2013), for the OCO2-SiF, Tropomi-SiF and the DGVMs. For b), we calculated the difference in AGC from $year_{t+1}$ to $year_t$ ($year_{t+1}$-$year_t$) from 2011 to 2023 and selected the years with losses (negative numbers) and gains (positive numbers), from that we got the mean for the entire record and the individual loss for 2023. The bars in b) show the interannual variability.

3.3 Local response of the carbon cycle in 2023: ATTO as independent benchmark

CO_2 mole fraction measurements at ATTO (Figure 8 a), representative of a large footprint (Figure 8 b and Figure S1) show a large enhancement over the background (ΔCO_2, Figure 8 a),

peaking in September and consistent with a larger-than-normal fire activity north of 5ºS during this month. Note that the concentration footprint of the 80-m tower covers the area east of the ATTO site, where some of the largest carbon sources were estimated by both the OCO2-Inv and by the DGVMs-ensemble mean (Figure 5), coinciding with the highest VPD and Temperature anomalies (see Figure 3). However, at the same location, the local eddy covariance measurement had a different response.

In the absence of large disturbances, the eddy covariance measurements indicate that the forest close to ATTO was on average a sink of carbon in 2023 (Figure 8c). At ATTO we observe a large (close to but within 1σ) uptake from January to March, interrupted by a positive peak (source) in May and followed by a consistent sink from July to November. The first part of the year is consistent with the seasonal pattern in OCO2-Inv coinciding on a large carbon uptake. The EC-NEE sink is mainly controlled by a large (close to and larger than 1σ) decrease in ecosystem respiration (R_{eco}) in the beginning of the year (February - April), and during the dry season (August - October). Note that GPP also attains the lowest values in June and September, but most of the development in 2023 is within the normal variability of the record. Given these findings, the 2023 drought at ATTO had a stronger effect in R_{eco} than GPP, leading to a net sink at the local ecosystem scale (i.e. ATTO).

The seasonal development of simulated NEE, R_{eco} and GPP in the DGVMs at the grid cell including ATTO (Figure 8 d,f,i) is in contrast to the local EC measurements. The DGVMs show a stronger decline in GPP than in R_{eco} mainly during the dry season, leading to a positive NEE from September to November in 2023. It is worth noting that the seasonality of the DGVMs is very different to the measured one at ATTO, mainly during the wet season, not being able to reproduce the uptake of carbon from January to March. The EC measurements indicate that such uptake was amplified during 2023, reaching values close to 1σ from January to March in EC-NEE. We find that such mismatch could be associated with the forcing data in the DGVMs, as the measured precipitation and shortwave radiation at ATTO were higher than ERA5 in February and March (Figure S15).

The flux response at ATTO deserves more context due to its contrasting development relative to the DGVMs. Local measurements at ATTO show that VPD, air and soil temperature anomalies in 2023 were consistent with the regional pattern shown in Figure 3, reaching values larger than 1σ (Figure S16, S17). Interestingly, soil moisture in the first 50 cm layer did not show anomalous values and precipitation was above the average with 200 mm more than normal years. Therefore, we believe that the normal levels of soil moisture sustained photosynthetic uptake throughout 2023, buffering the effect of air temperature and VPD, which could be a local response associated with the forest close to ATTO and not a general response regionally.

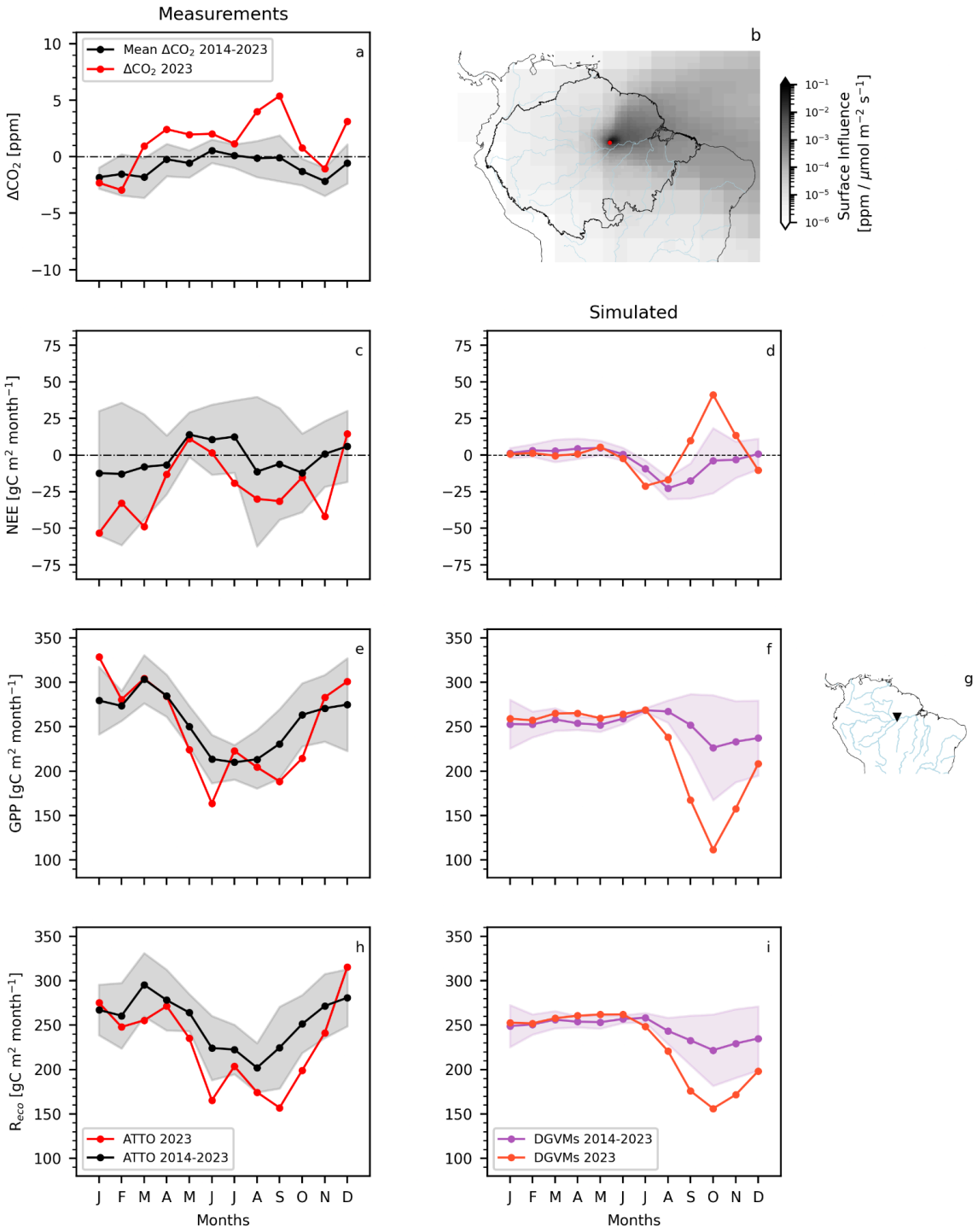

Figure 8. Seasonal evolution of the CO_2 mole fractions and eddy covariance fluxes (NEE, GPP and R_{eco}) at ATTO. On the first column (a, c, e, h) the measurements (ΔCO_2, NEE, GPP and R_{eco}) are shown. In the second column (d, f, i) the simulations (NEE, GPP and R_{eco}) are presented. The surface influence of the ΔCO_2 is shown in b) and in g) a marker is shown indicating the very local influence of the eddy covariance flux data.

4 Discussion

The drivers and consequences of drought

Our results show how elevated SST anomalies in the tropical Atlantic and Pacific oceans and associated changes in atmospheric circulation and surface hydroclimatic conditions, contributed to intensifying widespread soil water deficits across the Amazon during the second half of 2023 (Figure 2), consistent with the extremely low water levels reported by Espinoza et al., (2024) for the Rio Negro in Manaus. An interesting feature of the 2023 drought is that the onset coincided with a transition to an El Niño phase that followed three years of consecutive La Niña conditions (https://psl.noaa.gov/enso/mei/, last accessed August 15, 2024). Compared to the previous El Niño event of 2015/16, 2023 registered higher SST anomalies over the tropical Pacific and especially the tropical Atlantic (Figure S9), which played an important role in the atmospheric circulation anomalies, extremes in air temperature and atmospheric and surface dryness (PCWD). Temperature and precipitation anomalies in the Amazon basin have surpassed the previous record in 2015/16 (Espinoza et al., 2024; Jiménez-Muñoz et al., 2016b) and their extreme magnitude has been attributed to climate change (WWA, 2024). Compared with 2015/16 and previous droughts, the potential cumulative water deficits and extremely high vapor pressure anomalies registered in late 2023 progressed deeper into the humid Amazon forest, extending the dry season by several months and thus contributing to increased vegetation stress.

Here, we calculate PCWD as the balance between potential evapotranspiration and precipitation adapted from Stocker et al., (2023). This estimate is less conservative than other commonly used estimates for the Amazon such as CWD in Aragão et al., (2007), which assume constant evapotranspiration (ET) of 100 mm month^{-1}. Even though there are no reported trends in regional ET, there are spatial gradients (Baker et al., 2021) that could be important for water deficit calculation. For example, at ATTO the mean ET is 120 mm month^{-1}, so a CWD calculated using 100 mm month^{-1} would result in weaker CWD. Furthermore, evaporative demand depends on atmospheric humidity, which, as we have shown, reached extreme values in 2023 (Figure 3). Thus, we consider that estimating PCWD based on potential evapotranspiration, instead of a fixed value, can better represent the spatial patterns of the surface drought, especially under such extreme conditions.

Summary of responses by different data streams

In this paper, we have reported on the response of the Amazon forest to the 2023 event across various spatial scales using multiple data streams (Figure 9). In the absence of anthropogenic disturbances at the ecosystem scale at ATTO (Figure 9c) and with no precipitation deficit, the forest remained a carbon sink due to a large reduction in respiratory carbon loss together with a mild decline in photosynthetic uptake, resulting in a persistent sink

of carbon due to vegetation uptake (EC-NEE). Based on individual measurements of leaf, live wood and soil respiration in the Amazon, Chambers et al., (2004) found that autotrophic respiration contributes a large portion (~70%) of the ecosystem respiration, so a decline in GPP and in autotrophic respiration due to drought (Doughty et al., 2015) could explain the observed decline in R_{eco} in this study. However, an increase in autotrophic respiration and thus an overall increment in ecosystem respiration was found in a rainfall exclusion experiment in the eastern Amazon (Metcalfe et al., 2010), suggesting that there might not be a unidirectional response of R_{eco} to drought in the Amazon given than each drought is unique in its development and preceding conditions (S. Liu et al., 2024). Furthermore, it is worth noting that our estimate of ecosystem respiration (R_{eco}) relies on nighttime NEE that inherently assumes that daytime R_{eco} is equal to nighttime R_{eco} , leading to a source of uncertainty in our total ecosystem respiration estimates.

At a larger scale (Figure 9 b) the positive ΔCO_2 indicates that the ATTO footprint area was likely a source of carbon with a combined effect of reduced vegetation uptake, fires and land use change emissions. There are several implications of these findings. At the ecosystem scale, the forest close to ATTO buffered the effects of the large VPD and temperature anomalies with sufficient soil moisture availability (Figure S17). Such a localized response is not captured by the DGVMs, presenting a challenge for the bottom-up estimates. However, the atmospheric CO_2 signal indicates a larger-than-normal carbon source in the ATTO concentration footprint (which is much larger than the flux footprint). This is consistent with fire activity, the NEE source in the DGVMs, and the NBE source in OCO2-Inv that we report here.

At the biogeographic Amazon scale (Figure 9 a), the source of carbon including fires (NBE) ranges from 0.01 PgC $year^{-1}$ (bottom-up, DGVMs) to 0.17 PgC $year^{-1}$ (top-down, OCO2-Inv), with the main difference being the magnitude of the vegetation uptake (NEE), which, depending on the method used, can represent a small carbon source of 0.02 PgC $year^{-1}$ (OCO2-Inv) or a sink of -0.13 PgC $year^{-1}$ (DGVMs) in 2023. Note that relative to the long-term mean (2003-2023, -0.36 PgC $year^{-1}$), -0.13 PgC $year^{-1}$ represents more than a 30% reduction in NEE. According to the DGVMs the reduction in NEE was driven by a larger decline in GPP than R_{eco}, similar to the findings of Liu et al., (2017) for the 2015/2016 event. Nevertheless, the local response in NEE, GPP and R_{eco} at ATTO, challenges the regional response in the DGVMs, yet we can not rely on the ATTO fluxes to infer a regional-scale response, even more in the absence (at ATTO) of anthropogenic disturbances. Including fires, the NBE source we find here based on the OCO2-Inv represents about half of that reported by Ke et al., (2024) for the Amazon. This difference is mainly because their definition of Amazon is larger than ours, the biogeographic Amazon. Therefore, the definition of the Amazon influences the region-wide fluxes as a large contribution of the fire activity is at the boundary of the Amazon and Cerrado biomes (Botía et al., 2024).

Spatially we attribute the NEE source to the northeast part of the Amazon (Figure 5), consistent with a negative SiF and GPP anomaly during Oct-Dec (Figure 7) and a decline in greenness reported for 2023 by Jiménez et al., (2024). Including fires, based on the OCO2-Inv and the study by Wang et al., (2023), the NBE source was similar to 2015 and lower than 2016. We find that such a response, given the extreme temperature and VPD anomalies, was due to a seasonal compensation, with a large carbon uptake in the beginning of 2023 evident in both OCO2-Inv and DGVMs. This compensation can be associated with more rainfall in the beginning of 2023, driven by La Niña conditions in the Pacific Ocean. It remains to be confirmed whether the findings by Wang et al., (2023) for the 2015/2016 El Niño, in which temperature dominated the total NBE flux, but the spatial patterns were controlled by deficits in soil moisture, still hold true for 2023 and the post-El Niño development in 2024. Therefore, we believe that the use of several large scale data streams and in-situ measurements enhance the comprehensive understanding of drought impacts.

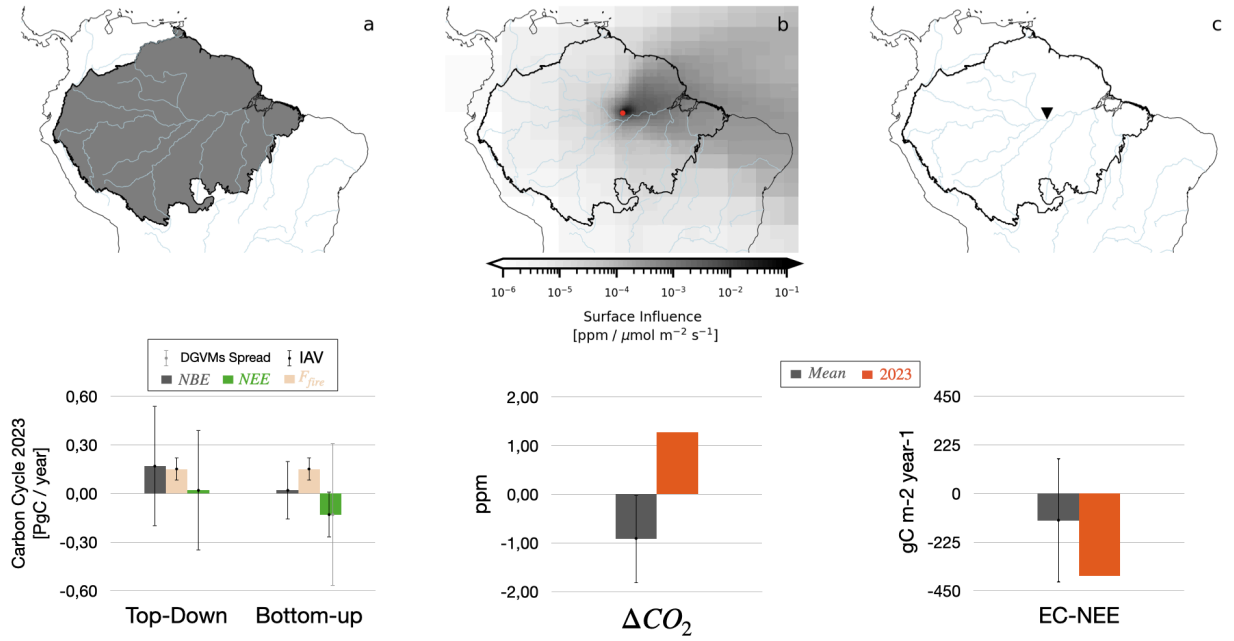

Figure 9. Summary of the drought response across scales and different data streams. In (a) the bottom-up (DGVMs) vs top-down (OCO2-Inv) carbon budget is shown. In panel (b) we present the ΔCO_2 or regional signal at ATTO, which is affected by the areas (i.e. footprint) covered by the gray polygons in the map. The mean response of the ecosystem level EC-NEE is shown in (c). Note that the footprint of the EC-NEE is less than 100 km^2.

Role of fire in NBE

We showed that the fire season was extended until November/December, mainly driven by the progression of surface and atmospheric dryness conditions (Figure 2 and Figure 3). These resulted in an early onset (July to September) with more (less) fire activity in the north (south)

and an offset (November and December) with more (less) fire activity in the south (north), relative to the total fire activity regionally. The north to south dynamic in fire activity reported here, is consistent with the timing of the rainfall anomalies in Espinoza et al., (2024) and in Figures S5 and S6. Furthermore, our results follow the fire anomalies in Jiménez et al., (2024). Even though we find pronounced spatial differences relative to the long-term mean, the total fire counts over the Amazon were similar in magnitude to 2015 and 2016. Fires and deforestation have been linked to drought (Aragão et al., 2007, 2018), with more fires during years of drought (Aragão et al., 2018; Basso et al., 2023; Gatti et al., 2014; Rosan et al., 2024; Silva Junior et al., 2019; van der Laan-Luijkx et al., 2015). Nevertheless, fire emissions in 2023 within the Amazon (0.15 [0.13-0.17] PgC $year^{-1}$, mean between GFAS and GFED4s) were comparable and even lower than non-drought years (e.g. 2022) and similar to the long-term average (see Figure 4 and S7). The individual estimates for GFED4s and GFAS were equal or lower than their long-term averages, respectively. In both products there were less fires compared to the long-term mean in the southeastern border of the Amazon from July to September (Figure 4), when the rainfall anomalies were not as pronounced as in the following months (Oct-Dec). Therefore, our analysis suggests that regardless of an extended fire season, the fire carbon emissions had a smaller contribution to the NBE source in 2023 relative to previous droughts, in which fire changed the sign of NBE from sink to source (Basso et al., 2023; Gatti et al., 2021; van der Laan-Luijkx et al., 2015). We note, though, that the fire inventory products used here (GFAS and GFED4s) tend to underestimate fire emissions, likely due to missing understory fires and small scale fires (Naus et al., 2022; Pessôa et al., 2020). However, the results of Naus et al., (2022) suggest that such underestimation is more pronounced outside of the biogeographic Amazon, in the neighboring Cerrado biome, as also shown by Botía et al., (2024).

Remaining challenges reconciling top-down and bottom-up approaches

The most important differences between top-down and bottom-up NBE are associated with the seasonal timing and the absolute magnitude of NBE. This mismatch is likely due to a misrepresentation of the dry and wet season contrast of NEE, GPP and R_{eco} in DGVMs (Figure 6 and Figure 8), as well as large uncertainty in the bottom-up NBE driven by disturbances and land use change emissions (Rosan et al., 2024). The response of the DGVMs to the development of the drought in 2023 was limited to the dry season when there was a larger spread between models (Figure 6 and Figure 8) and larger inter-annual variability, coinciding with the positive anomalies in VPD and temperature and the negative anomalies in terrestrial water storage and large PCWD (Figure 2 and Figure 3). Conversely, during the wet season, the DGVMs showed a flat and more uniform GPP and TER, suggesting a reduced sensitivity to wet season anomalies, notwithstanding potential biases in the forcing data that would attenuate the severity of the drought (Figure S15). Our study thus adds to the body of literature indicating the limitations

DGVMs have for tropical regions and specifically the Amazon, lacking processes such as (i) leaf phenology and demography, which affect the seasonality in GPP (X. Chen et al., 2020; Kim et al., 2012; Restrepo-Coupe et al., 2017), (ii) low sensitivity of GPP to soil texture (Meunier et al., 2022), (iii) lacking a representation of drought induced tree mortality and therefore biomass reductions (de Almeida Castanho et al., 2016; Powell et al., 2013) and (iv) not simulating secondary forest regrowth leading to difficulties reproducing gains in biomass and thus hindering the simulated changes in AGC (O'Sullivan et al., 2024; Pugh et al., 2019) in DGVMs.

For the top-down approach used here (OCO2-Inv), we acknowledge that cloud cover during the wet season could limit the number of successful XCO_2 retrievals (Frankenberg et al., 2024), inducing a dry-season adjustment bias in the inversion (Crowell et al., 2019; Massie et al., 2017). Furthermore, in-situ data is scarce in the region hindering evaluation of posterior fluxes in satellite-driven inversions and for inversions assimilating flask or in-situ data, leaving no choice but to assimilate most of the available data (Basso et al., 2023; Botía et al., 2024). Additionally, the spatial distribution of the posterior fluxes and their overlap with DGVMs, could be affected by the spatial correlation length scale, which in this study was 500 km. We showed that the strongest carbon sources in the DGVMs overlap to some extent but not entirely, with those in the OCO2-Inv. Therefore, we acknowledge that understanding the causes of the spatial mismatch between top-down and bottom-up approaches should be prioritized in future studies.

The missing disturbance sources in bottom-up NBE assessments that are reported in existing literature include low intensity understory fires (Alencar et al., 2022), missing carbon emissions due to edge effects caused by forest fragmentation (Silva Junior et al., 2020), and an enhanced post-logging respiratory flux which is difficult to quantify as it is a function of recovery time and requires long-term observations (Mills et al., 2023). In addition, a remaining challenge to improve the seasonal development of bottom-up NBE is related with non-fire carbon emissions due to forest degradation (Lapola et al., 2023) and how these vary seasonally and inter-annually. Moreover, the role of CO_2 outgassing from river and aquatic surfaces remains as an ignored flux in recent bottom-up and top-down assessments (Basso et al., 2023; Gatti et al., 2021; Gloor et al., 2012; Rosan et al., 2024), and its role in the Amazon basin seems to result in a weakening of the vegetation (NEE) carbon sink (Hastie et al., 2019). These processes are the remaining challenges in reconciling top-down and bottom-up processes for regional assessments of the carbon cycle response to drought.

5 Conclusions

We studied the Amazon carbon cycle response to the extreme drought in 2023 by using multiple data streams, including land surface models, an atmospheric inversion, remotely-sensed vegetation dynamics and aboveground carbon at the regional scale. In addition we used in-situ measurements from the Amazon Tall Tower Observatory, including eddy covariance fluxes and a decade long CO_2 mole fraction time series to complement the large scale

analysis. At the regional scale, we report that in 2023 the Amazon drought led to a substantial shift in the carbon dynamics of the region, with a net carbon emission (NBE), driven primarily by reduced vegetation uptake. While the fire season extended into November, fire contributions remained near the long-term average, indicating that fires had a smaller influence on the Amazon carbon source compared to vegetation responses. The decline in gross primary productivity (GPP) was particularly strong during October to December coinciding with anomalies in remotely-sensed GPP proxies (i.e. Sun-Induced Fluorescence). During these months anomalously high temperatures, vapor pressure deficits and potential cumulative water deficits were recorded.

Our findings highlight that in early 2023 a relatively large uptake helped to offset the dry-season emissions, possibly driven by a transition from La Niña to El Niño, which was characterized by high precipitation in the beginning of the year in the northern part of the Amazon. Such wet season response was consistent in the atmospheric transport inversion and the local eddy flux measurements, but to a lesser extent in the DGVMs. The low sensitivity of DGVMs to the wet season anomalies in precipitation are partly explained by a bias in the forcing data. However, the observed balance between photosynthesis and respiration in the eddy flux measurements was not reproduced by the DGVMs throughout the year. At ATTO, the seasonal development of NEE was mainly controlled by a large (close to and larger than 1σ) decrease in ecosystem respiration (R_{eco}) in the beginning of the year (January - March), and during the dry season (August - October). Even though we can not attribute the ATTO-eddy-fluxes to all the Amazon region, we believe the comparison points to processes that should be improved in DGVMs to better represent the inter-annual variability of the carbon dynamics in the Amazon.

As Applicable – Inclusion in Global Research Statement

We thank the Instituto Nacional de Pesquisas da Amazonia (Manaus, Brazil) for their technical support managing and running the ATTO research station. Specifically we thank Roberta Pereira de Souza, Bruno Takeshi, Leonardo Ramos de Oliveira, Nagib Alberto de Castro Souza, Amauri Rodriguês Pereira, Hermes Braga Xavier, Jailson da Mata, Valmir Ferreira de Lima, Wallace Rabelo Costa, Antonio Huxley Melo Nascimento, Uwe Schultz, Thomas Seifert, Steffen Schmidt, Thomas Disper, and Sipko Bulthuis.

Acknowledgments

This work and the ATTO project were funded by the German Federal Ministry of Education and Research (BMBF, contracts 01LB1001A and 01LK1602A). The ATTO project is furthermore funded by the Brazilian Ministério da Ciencia, Tecnologia e Inovação (MCTI/FINEP contract

01.11.01248.00) and the Max Planck Society. We acknowledge the Instituto Nacional de Pesquisas da Amazonia as well as the Amazon State University (UEA), FAPEAM, LBA/INPA and SDS/CEUC/RDS-Uatumã for continuous support and logistical management. WP and GK were funded by an ERC-Consolidator grant (649087) as part of the ASICA (Airborne Stable Isotopes of Carbon from the Amazon) project. This study was supported by funding from the European Space Agency Carbon-RO (4000140982/23/I-EF). AB, PC and SS acknowledge support from the CALIPSO project (Carbon Loss in Plant Soils and Oceans) project, funded through the generosity of Eric and Wendy Schmidt by recommendation of the Schmidt Futures program. AB acknowledges funding by the European Union (ERC StG, ForExD, grant agreement No. 101039567). CQD acknowledges support from CNPQ (Processes 440170/2022-2, 406884/2022-6, 307530/2022-1). ITL received funding from the Netherlands Organisation for Scientific Research (grant no. VI.Vidi.213.143). SiB4 simulations were carried out on the Dutch national e-infrastructure with the support of SURF Cooperative (project number NWO-2023.003).

Open Research

The biogeographic Amazon area used for the climate (VPD and 2m temperature) and carbon cycle (DGVMs, OCO2-Inv, and GPP proxies) analysis can be found here: https://edmond.mpg.de/privateurl.xhtml?token=a4af161f-1b77-4611-aa01-7de9203639b8. The ERA5 and ERA5-Land datasets are under public access available here: https://cds.climate.copernicus.eu/datasets/reanalysis-era5-land?tab=overview. For the PCWD calculation we used the following R package: https://zenodo.org/records/5359053. All the processed data integrated for the biogeographic Amazon area can be found here: https://edmond.mpg.de/privateurl.xhtml?token=a062e1cb-9c28-4880-9f99-b9b8a9125dff. This includes the DGVM output and fire emissions (GFED4s and GFAS) from 2003 to 2023, the OCO2-Inv prior and posterior from 2015 to 2023 and the fire counts from MODIS (terra and aqua) from 2003 to 2023. Additionally, on the same repository, the monthly totals of NEE, GPP and Reco at ATTO, together with the monthly mean ΔCO_2 can be also found in tabular form. The GRACE data for the Amazon basin used here can be freely downloaded here: https://grace.jpl.nasa.gov/data-analysis-tool/. The ATTO meteorological data is available at https://www.attodata.org/home/Start. The OCO2-Inv gridded files are available via the atmospheric data store: https://ads.atmosphere.copernicus.eu/datasets. TROPOMI SIF data is available through the S5P-PAL Data Portal (https://data-portal.s5p-pal.com/products/troposif.html). MODIS BRDF-corrected surface reflectance (MCD43C4v061) is available at the Land Processes Distributed Active Archive Center (LP DAAC; https://lpdaac.usgs.gov/products/mcd43c4v061/). The OCO2-SiF data is available from https://oco2.gesdisc.eosdis.nasa.gov/data/OCO2_DATA/OCO2_L2_Lite_SIF.11r/. The L-VOD data can be downloaded here: https://doi.org/10.5281/zenodo.14171387.

References

Alencar, A. A. C., Arruda, V. L. S., Silva, W. V. da, Conciani, D. E., Costa, D. P., Crusco, N., Duverger, S. G., Ferreira, N. C., Franca-Rocha, W., Hasenack, H., Martenexen, L. F. M., Piontekowski, V. J., Ribeiro, N. V., Rosa, E. R., Rosa, M. R., dos Santos, S. M. B., Shimbo, J. Z., & Vélez-Martin, E. (2022). Long-Term Landsat-Based Monthly Burned Area Dataset for the Brazilian Biomes Using Deep Learning. *Remote Sensing*, *14*(11), Article 11. https://doi.org/10.3390/rs14112510

Anderson, L. O., Ribeiro Neto, G., Cunha, A. P., Fonseca, M. G., Mendes de Moura, Y., Dalagnol, R., Wagner, F. H., & de Aragão, L. E. O. e C. (2018). Vulnerability of Amazonian forests to repeated droughts. *Philosophical Transactions of the Royal Society B: Biological Sciences*, *373*(1760), 20170411. https://doi.org/10.1098/rstb.2017.0411

Andreae, M. O., Acevedo, O. C., Araùjo, A., Artaxo, P., Barbosa, C. G. G., Barbosa, H. M. J., Brito, J., Carbone, S., Chi, X., Cintra, B. B. L., da Silva, N. F., Dias, N. L., Dias-Júnior, C. Q., Ditas, F., Ditz, R., Godoi, A. F. L., Godoi, R. H. M., Heimann, M., Hoffmann, T., … Yáñez-Serrano, A. M. (2015). The Amazon Tall Tower Observatory (ATTO): Overview of pilot measurements on ecosystem ecology, meteorology, trace gases, and aerosols. *Atmospheric Chemistry and Physics*, *15*(18), 10723–10776. https://doi.org/10.5194/acp-15-10723-2015

Aragão, L. E. O. C., Anderson, L. O., Fonseca, M. G., Rosan, T. M., Vedovato, L. B., Wagner, F. H., Silva, C. V. J., Junior, C. H. L. S., Arai, E., Aguiar, A. P., Barlow, J., Berenguer, E., Deeter, M. N., Domingues, L. G., Gatti, L., Gloor, M., Malhi, Y., Marengo, J. A., Miller, J. B., … Saatchi, S. (2018). 21st Century drought-related fires counteract the decline of Amazon deforestation carbon emissions. *Nature Communications*, *9*(1), 1–12. https://doi.org/10.1038/s41467-017-02771-y

Aragão, L. E. O. C., Malhi, Y., Roman-Cuesta, R. M., Saatchi, S., Anderson, L. O., & Shimabukuro, Y. E. (2007). Spatial patterns and fire response of recent Amazonian droughts. *Geophysical Research Letters*, *34*(7). https://doi.org/10.1029/2006GL028946

Baker, J. C. A., Garcia-Carreras, L., Gloor, M., Marsham, J. H., Buermann, W., da Rocha, H. R., Nobre, A. D., de Araujo, A. C., & Spracklen, D. V. (2021). Evapotranspiration in the Amazon: Spatial patterns, seasonality, and recent trends in observations, reanalysis, and climate models. *Hydrology and Earth System Sciences*, *25*(4), 2279–2300. https://doi.org/10.5194/hess-25-2279-2021

Basso, L. S., Wilson, C., Chipperfield, M. P., Tejada, G., Cassol, H. L. G., Arai, E., Williams, M., Smallman, T. L., Peters, W., Naus, S., Miller, J. B., & Gloor, M. (2023). Atmospheric CO_2 inversion reveals the Amazon as a minor carbon source caused by fire emissions, with forest uptake offsetting about half of these emissions. *Atmospheric Chemistry and Physics*, *23*(17), 9685–9723. https://doi.org/10.5194/acp-23-9685-2023

Bastos, A., Friedlingstein, P., Sitch, S., Chen, C., Mialon, A., Wigneron, J.-P., Arora, V. K., Briggs, P. R., Canadell, J. G., & Ciais, P. (2018). Impact of the 2015/2016 El Niño on the terrestrial carbon cycle constrained by bottom-up and top-down approaches. *Philosophical Transactions of the Royal Society B: Biological Sciences*, *373*(1760), 20170304.

Berenguer, E., Lennox, G. D., Ferreira, J., Malhi, Y., Aragão, L. E. O. C., Barreto, J. R., Del Bon Espírito-Santo, F., Figueiredo, A. E. S., França, F., Gardner, T. A., Joly, C. A., Palmeira, A. F., Quesada, C. A., Rossi, L. C., de Seixas, M. M. M., Smith, C. C., Withey, K., & Barlow, J. (2021). Tracking the impacts of El Niño drought and fire in human-modified Amazonian forests. *Proceedings of the National Academy of Sciences*, *118*(30), e2019377118. https://doi.org/10.1073/pnas.2019377118

Berenguer, E., Malhi, Y., Brando, P., Cardoso Nunes Cordeiro, A., Ferreira, J., França, F., Chesini Rossi, L., Maria Moraes de Seixas, M., & Barlow, J. (2018). Tree growth and stem carbon accumulation in human-modified Amazonian forests following drought and fire. *Philosophical Transactions of the Royal Society B: Biological Sciences*, *373*(1760), 20170308. https://doi.org/10.1098/rstb.2017.0308

Botía, S., Komiya, S., Marshall, J., Koch, T., Gałkowski, M., Lavric, J., Gomes-Alves, E., Walter, D., Fisch, G., Pinho, D. M., Nelson, B. W., Martins, G., Luijkx, I. T., Koren, G., Florentie, L., Carioca de Araújo, A., Sá, M., Andreae, M. O., Heimann, M., … Gerbig, C. (2022). The CO2 record at the Amazon Tall Tower Observatory: A new opportunity to study processes on seasonal and inter-annual scales. *Global Change Biology*, *28*(2), 588–611. https://doi.org/10.1111/gcb.15905

Botía, S., Munassar, S., Koch, T., Custodio, D., Basso, L. S., Komiya, S., Lavric, J. V., Walter, D., Gloor, M., Martins, G., Naus, S., Koren, G., Luijkx, I., Hantson, S., Miller, J. B., Peters, W., Rödenbeck, C., & Gerbig, C. (2024). Combined CO_2 measurement record indicates decreased Amazon forest carbon uptake, offset by Savannah carbon release. *EGUsphere*, 1–55. https://doi.org/10.5194/egusphere-2024-1735

Brando, P. M., Balch, J. K., Nepstad, D. C., Morton, D. C., Putz, F. E., Coe, M. T., Silvério, D., Macedo, M. N., Davidson, E. A., Nóbrega, C. C., Alencar, A., & Soares-Filho, B. S. (2014). Abrupt increases in Amazonian

tree mortality due to drought–fire interactions. *Proceedings of the National Academy of Sciences*, *111*(17), 6347–6352. https://doi.org/10.1073/pnas.1305499111

Byrne, B., Liu, J., Bowman, K. W., Pascolini-Campbell, M., Chatterjee, A., Pandey, S., Miyazaki, K., van der Werf, G. R., Wunch, D., Wennberg, P. O., Roehl, C. M., & Sinha, S. (2024). Carbon emissions from the 2023 Canadian wildfires. *Nature*, *633*(8031), 835–839. https://doi.org/10.1038/s41586-024-07878-z

Chambers, J. Q., Tribuzy, E. S., Toledo, L. C., Crispim, B. F., Higuchi, N., Santos, J. dos, Araújo, A. C., Kruijt, B., Nobre, A. D., & Trumbore, S. E. (2004). Respiration from a Tropical Forest Ecosystem: Partitioning of Sources and Low Carbon Use Efficiency. *Ecological Applications*, *14*(sp4), 72–88. https://doi.org/10.1890/01-6012

Chen, S., Stark, S. C., Nobre, A. D., Cuartas, L. A., de Jesus Amore, D., Restrepo-Coupe, N., Smith, M. N., Chitra-Tarak, R., Ko, H., Nelson, B. W., & Saleska, S. R. (2024). Amazon forest biogeography predicts resilience and vulnerability to drought. *Nature*, *631*(8019), 111–117. https://doi.org/10.1038/s41586-024-07568-w

Chen, X., Maignan, F., Viovy, N., Bastos, A., Goll, D., Wu, J., Liu, L., Yue, C., Peng, S., Yuan, W., Conceição, A. C. da, O'Sullivan, M., & Ciais, P. (2020). Novel Representation of Leaf Phenology Improves Simulation of Amazonian Evergreen Forest Photosynthesis in a Land Surface Model. *Journal of Advances in Modeling Earth Systems*, *12*(1). https://doi.org/10.1029/2018MS001565

Copernicus. (2024). *Copernicus: 2023 is the hottest year on record, with global temperatures close to the 1.5°C limit | Copernicus*. https://climate.copernicus.eu/copernicus-2023-hottest-year-record

Crowell, S., Baker, D., Schuh, A., Basu, S., Jacobson, A. R., Chevallier, F., Liu, J., Deng, F., Feng, L., McKain, K., Chatterjee, A., Miller, J. B., Stephens, B. B., Eldering, A., Crisp, D., Schimel, D., Nassar, R., O'Dell, C. W., Oda, T., … Jones, D. B. A. (2019). The 2015–2016 carbon cycle as seen from OCO-2 and the global in situ network. *Atmospheric Chemistry and Physics*, *19*(15), 9797–9831. https://doi.org/10.5194/acp-19-9797-2019

de Almeida Castanho, A. D., Galbraith, D., Zhang, K., Coe, M. T., Costa, M. H., & Moorcroft, P. (2016). Changing Amazon biomass and the role of atmospheric CO2 concentration, climate, and land use. *Global Biogeochemical Cycles*, *30*(1), 18–39. https://doi.org/10.1002/2015GB005135

Doughty, C. E., Metcalfe, D. B., Girardin, C. A. J., Amézquita, F. F., Cabrera, D. G., Huasco, W. H., Silva-Espejo, J.

E., Araujo-Murakami, A., da Costa, M. C., Rocha, W., Feldpausch, T. R., Mendoza, A. L. M., da Costa, A. C. L., Meir, P., Phillips, O. L., & Malhi, Y. (2015). Drought impact on forest carbon dynamics and fluxes in Amazonia. *Nature*, *519*(7541), 78–82. https://doi.org/10.1038/nature14213

Erik, van S., Lars, K., Smith Naomi, E., Gerbrand, K., H, van B. L. P., Wouter, P., & T, van der L.-L. I. (2018). Changes in surface hydrology, soil moisture and gross primary production in the Amazon during the 2015/2016 El Niño. *Philosophical Transactions of the Royal Society B: Biological Sciences*, *373*(1760), 20180084. https://doi.org/10.1098/rstb.2018.0084

Espinoza, J.-C., Jimenez, J. C., Marengo, J. A., Schongart, J., Ronchail, J., Lavado-Casimiro, W., & Ribeiro, J. V. M. (2024). The new record of drought and warmth in the Amazon in 2023 related to regional and global climatic features. *Scientific Reports*, *14*(1), 8107. https://doi.org/10.1038/s41598-024-58782-5

Esquivel-Muelbert, A., Phillips, O. L., Brienen, R. J. W., Fauset, S., Sullivan, M. J. P., Baker, T. R., Chao, K.-J., Feldpausch, T. R., Gloor, E., Higuchi, N., Houwing-Duistermaat, J., Lloyd, J., Liu, H., Malhi, Y., Marimon, B., Marimon Junior, B. H., Monteagudo-Mendoza, A., Poorter, L., Silveira, M., … Galbraith, D. (2020). Tree mode of death and mortality risk factors across Amazon forests. *Nature Communications*, *11*(1), 5515. https://doi.org/10.1038/s41467-020-18996-3

Fawcett, D., Sitch, S., Ciais, P., Wigneron, J. P., Silva-Junior, C. H. L., Heinrich, V., Vancutsem, C., Achard, F., Bastos, A., Yang, H., Li, X., Albergel, C., Friedlingstein, P., & Aragão, L. E. O. C. (2023). Declining Amazon biomass due to deforestation and subsequent degradation losses exceeding gains. *Global Change Biology*, *29*(4), 1106–1118. https://doi.org/10.1111/gcb.16513

Feldpausch, T. R., Phillips, O. L., Brienen, R. J. W., Gloor, E., Lloyd, J., Lopez-Gonzalez, G., Monteagudo-Mendoza, A., Malhi, Y., Alarcón, A., Álvarez Dávila, E., Alvarez-Loayza, P., Andrade, A., Aragao, L. E. O. C., Arroyo, L., Aymard C., G. A., Baker, T. R., Baraloto, C., Barroso, J., Bonal, D., … Vos, V. A. (2016). Amazon forest response to repeated droughts. *Global Biogeochemical Cycles*, *30*(7), 964–982. https://doi.org/10.1002/2015GB005133

Foken, T., Göockede, M., Mauder, M., Mahrt, L., Amiro, B., & Munger, W. (2005). Post-Field Data Quality Control. In X. Lee, W. Massman, & B. Law (Eds.), *Handbook of Micrometeorology: A Guide for Surface Flux Measurement and Analysis* (pp. 181–208). Springer Netherlands. https://doi.org/10.1007/1-4020-2265-4_9

Frankenberg, C., Bar-On, Y. M., Yin, Y., Wennberg, P. O., Jacob, D. J., & Michalak, A. M. (2024). Data Drought in

the Humid Tropics: How to Overcome the Cloud Barrier in Greenhouse Gas Remote Sensing. *Geophysical Research Letters*, *51*(8), e2024GL108791. https://doi.org/10.1029/2024GL108791

Friedlingstein, P., O'Sullivan, M., Jones, M. W., Andrew, R. M., Hauck, J., Landschützer, P., Le Quéré, C., Li, H., Luijkx, I. T., Olsen, A., Peters, G. P., Peters, W., Pongratz, J., Schwingshackl, C., Sitch, S., Canadell, J. G., Ciais, P., Jackson, R. B., Alin, S. R., … Zeng, J. (2024). Global Carbon Budget 2024. *Earth System Science Data Discussions*, 1–133. https://doi.org/10.5194/essd-2024-519

Gatti, L. V., Basso, L. S., Miller, J. B., Gloor, M., Gatti Domingues, L., Cassol, H. L. G., Tejada, G., Aragão, L. E. O. C., Nobre, C., Peters, W., Marani, L., Arai, E., Sanches, A. H., Corrêa, S. M., Anderson, L., Von Randow, C., Correia, C. S. C., Crispim, S. P., & Neves, R. A. L. (2021). Amazonia as a carbon source linked to deforestation and climate change. *Nature*, *595*(7867), 388–393. https://doi.org/10.1038/s41586-021-03629-6

Gatti, L. V., Gloor, M., Miller, J. B., Doughty, C. E., Malhi, Y., Domingues, L. G., Basso, L. S., Martinewski, A., Correia, C. S. C., Borges, V. F., Freitas, S., Braz, R., Anderson, L. O., Rocha, H., Grace, J., Phillips, O. L., & Lloyd, J. (2014). Drought sensitivity of Amazonian carbon balance revealed by atmospheric measurements. *Nature*, *506*(7486), 76–80. https://doi.org/10.1038/nature12957

Gloor, M., Gatti, L., Brienen, R., Feldpausch, T. R., Phillips, O. L., Miller, J., Ometto, J. P., Rocha, H., Baker, T., de Jong, B., Houghton, R. A., Malhi, Y., Aragão, L. E. O. C., Guyot, J.-L., Zhao, K., Jackson, R., Peylin, P., Sitch, S., Poulter, B., … Lloyd, J. (2012). The carbon balance of South America: A review of the status, decadal trends and main determinants. *Biogeosciences*, *9*(12), 5407–5430. https://doi.org/10.5194/bg-9-5407-2012

Gloor, M., Wilson, C., Chipperfield, M. P., Chevallier, F., Buermann, W., Boesch, H., Parker, R., Somkuti, P., Gatti, L. V., Correia, C., Domingues, L. G., Peters, W., Miller, J., Deeter, M. N., & Sullivan, M. J. P. (2018). Tropical land carbon cycle responses to 2015/16 El Niño as recorded by atmospheric greenhouse gas and remote sensing data. *Philosophical Transactions of the Royal Society B: Biological Sciences*, *373*(1760), 20170302. https://doi.org/10.1098/rstb.2017.0302

Hartmann, H., Bastos, A., Das, A. J., Esquivel-Muelbert, A., Hammond, W. M., Martínez-Vilalta, J., McDowell, N. G., Powers, J. S., Pugh, T. A., & Ruthrof, K. X. (2022). Climate change risks to global forest health: Emergence of unexpected events of elevated tree mortality worldwide. *Annual Review of Plant Biology*, *73*,

673–702.

Hastie, A., Lauerwald, R., Ciais, P., & Regnier, P. (2019). Aquatic carbon fluxes dampen the overall variation of net ecosystem productivity in the Amazon basin: An analysis of the interannual variability in the boundless carbon cycle. *Global Change Biology*, *25*(6), 2094–2111. https://doi.org/10.1111/gcb.14620

Hersbach, H., Bell, B., Berrisford, P., Hirahara, S., Horányi, A., Muñoz-Sabater, J., Nicolas, J., Peubey, C., Radu, R., Schepers, D., Simmons, A., Soci, C., Abdalla, S., Abellan, X., Balsamo, G., Bechtold, P., Biavati, G., Bidlot, J., Bonavita, M., … Thépaut, J.-N. (2020). The ERA5 global reanalysis. *Quarterly Journal of the Royal Meteorological Society*, *146*(730), 1999–2049. https://doi.org/10.1002/qj.3803

Jimenez, J. C., Barichivich, J., Mattar, C., Takahashi, K., Santamaría-Artigas, A., Sobrino, J. A., & Malhi, Y. (2018). Spatio-temporal patterns of thermal anomalies and drought over tropical forests driven by recent extreme climatic anomalies. *Philosophical Transactions of the Royal Society B: Biological Sciences*, *373*(1760), 20170300. https://doi.org/10.1098/rstb.2017.0300

Jiménez, J. C., Miranda, V., Trigo, I., Libonati, R., Albuquerque, R., Peres, L. F., Espinoza, J.-C., & Marengo, J. A. (2024). Vegetation Warming and Greenness Decline across Amazonia during the Extreme Drought of 2023. *Remote Sensing*, *16*(14), Article 14. https://doi.org/10.3390/rs16142519

Jiménez-Muñoz, J. C., Mattar, C., Barichivich, J., Santamaría-Artigas, A., Takahashi, K., Malhi, Y., Sobrino, J. A., & Schrier, G. van der. (2016a). Record-breaking warming and extreme drought in the Amazon rainforest during the course of El Niño 2015–2016. *Scientific Reports*, *6*(1), 33130. https://doi.org/10.1038/srep33130

Jiménez-Muñoz, J. C., Mattar, C., Barichivich, J., Santamaría-Artigas, A., Takahashi, K., Malhi, Y., Sobrino, J. A., & Schrier, G. van der. (2016b). Record-breaking warming and extreme drought in the Amazon rainforest during the course of El Niño 2015–2016. *Scientific Reports*, *6*(1). https://doi.org/10.1038/srep33130

Kaiser, J. W., Heil, A., Andreae, M. O., Benedetti, A., Chubarova, N., Jones, L., Morcrette, J.-J., Razinger, M., Schultz, M. G., Suttie, M., & van der Werf, G. R. (2012). Biomass burning emissions estimated with a global fire assimilation system based on observed fire radiative power. *Biogeosciences*, *9*(1), 527–554. https://doi.org/10.5194/bg-9-527-2012

Ke, P., Ciais, P., Sitch, S., Li, W., Bastos, A., Liu, Z., Xu, Y., Gui, X., Bian, J., Goll, D. S., Xi, Y., Li, W., O'Sullivan, M., de Souza, J. G., Friedlingstein, P., & Chevallier, F. (2024). Low latency carbon budget analysis reveals a large decline of the land carbon sink in 2023. *National Science Review*, nwae367.

https://doi.org/10.1093/nsr/nwae367

Kim, Y., Knox, R. G., Longo, M., Medvigy, D., Hutyra, L. R., Pyle, E. H., Wofsy, S. C., Bras, R. L., & Moorcroft, P. R. (2012). Seasonal carbon dynamics and water fluxes in an Amazon rainforest. *Global Change Biology*, *18*(4), 1322–1334. https://doi.org/10.1111/j.1365-2486.2011.02629.x

Lan, X., Mund, J. W., Crotwell, A. M., Thoning, K. W., Moglia, E., Madronich, M., Baugh, K., Petron, G., Crotwell, M. J., Neff, D., Wolter, S., Mefford, T., & DeVogel, S. (2024). *Atmospheric Carbon Dioxide Dry Air Mole Fractions from the NOAA GML Carbon Cycle Cooperative Global Air Sampling Network, 1968-2023* (Version 2024-07-30) [Dataset]. https://doi.org/10.15138/wkgj-f215

Lan, X., Tans, P., & Thoning, K. W. (2024). *Trends in globally-averaged CO2 determined from NOAA Global Monitoring Laboratory measurements* (Version Tuesday, 05-Nov-2024 13:17:54 MST) [Dataset]. https://doi.org/10.15138/9N0H-ZH07

Lapola, D. M., Pinho, P., Barlow, J., Aragão, L. E. O. C., Berenguer, E., Carmenta, R., Liddy, H. M., Seixas, H., Silva, C. V. J., Silva-Junior, C. H. L., Alencar, A. A. C., Anderson, L. O., Armenteras, D., Brovkin, V., Calders, K., Chambers, J., Chini, L., Costa, M. H., Faria, B. L., … Walker, W. S. (2023). The drivers and impacts of Amazon forest degradation. *Science*, *379*(6630), eabp8622. https://doi.org/10.1126/science.abp8622

Liu, J., Bowman, K. W., Schimel, D. S., Parazoo, N. C., Jiang, Z., Lee, M., Bloom, A. A., Wunch, D., Frankenberg, C., Sun, Y., & others. (2017). Contrasting carbon cycle responses of the tropical continents to the 2015–2016 El Niño. *Science*, *358*(6360), eaam5690.

Liu, S., McVicar, T. R., Wu, X., Cao, X., & Liu, Y. (2024). Assessing the relative importance of dry-season incoming solar radiation and water storage dynamics during the 2005, 2010 and 2015 southern Amazon droughts: Not all droughts are created equal. *Environmental Research Letters*, *19*(3), 034027. https://doi.org/10.1088/1748-9326/ad281e

MacCarthy, J., Tyukavina, A., Weisse, M. J., Harris, N., & Glen, E. (2024). Extreme wildfires in Canada and their contribution to global loss in tree cover and carbon emissions in 2023. *Global Change Biology*, *30*(6), e17392. https://doi.org/10.1111/gcb.17392

Marengo, J. A., Tomasella, J., Alves, L. M., Soares, W. R., & Rodriguez, D. A. (2011). The drought of 2010 in the context of historical droughts in the Amazon region. *Geophysical Research Letters*, *38*(12).

https://doi.org/10.1029/2011GL047436

Massie, S. T., Sebastian Schmidt, K., Eldering, A., & Crisp, D. (2017). Observational evidence of 3-D cloud effects in OCO-2 CO2 retrievals. *Journal of Geophysical Research: Atmospheres*, *122*(13), 7064–7085. https://doi.org/10.1002/2016JD026111

Mauder, M., & Foken, T. (2004). *Documentation and Instruction Manual of the Eddy Covariance Software Package TK2*.

Metcalfe, D. B., Meir, P., Aragão, L. E. O. C., Lobo-do-Vale, R., Galbraith, D., Fisher, R. A., Chaves, M. M., Maroco, J. P., da Costa, A. C. L., de Almeida, S. S., Braga, A. P., Gonçalves, P. H. L., de Athaydes, J., da Costa, M., Portela, T. T. B., de Oliveira, A. a. R., Malhi, Y., & Williams, M. (2010). Shifts in plant respiration and carbon use efficiency at a large-scale drought experiment in the eastern Amazon. *New Phytologist*, *187*(3), 608–621. https://doi.org/10.1111/j.1469-8137.2010.03319.x

Meunier, F., Verbruggen, W., Verbeeck, H., & Peaucelle, M. (2022). Low sensitivity of three terrestrial biosphere models to soil texture over the South American tropics. *Geoscientific Model Development*, *15*(20), 7573–7591. https://doi.org/10.5194/gmd-15-7573-2022

Mills, M. B., Malhi, Y., Ewers, R. M., Kho, L. K., Teh, Y. A., Both, S., Burslem, D. F. R. P., Majalap, N., Nilus, R., Huaraca Huasco, W., Cruz, R., Pillco, M. M., Turner, E. C., Reynolds, G., & Riutta, T. (2023). Tropical forests post-logging are a persistent net carbon source to the atmosphere. *Proceedings of the National Academy of Sciences*, *120*(3), e2214462120. https://doi.org/10.1073/pnas.2214462120

Muñoz-Sabater, J., Dutra, E., Agustí-Panareda, A., Albergel, C., Arduini, G., Balsamo, G., Boussetta, S., Choulga, M., Harrigan, S., Hersbach, H., Martens, B., Miralles, D. G., Piles, M., Rodríguez-Fernández, N. J., Zsoter, E., Buontempo, C., & Thépaut, J.-N. (2021). ERA5-Land: A state-of-the-art global reanalysis dataset for land applications. *Earth System Science Data*, *13*(9), 4349–4383. https://doi.org/10.5194/essd-13-4349-2021

Naus, S., Domingues, L. G., Krol, M., Luijkx, I. T., Gatti, L. V., Miller, J. B., Gloor, E., Basu, S., Correia, C., Koren, G., Worden, H. M., Flemming, J., Pétron, G., & Peters, W. (2022). Sixteen years of MOPITT satellite data strongly constrain Amazon CO fire emissions. *Atmospheric Chemistry and Physics*, *22*(22), 14735–14750. https://doi.org/10.5194/acp-22-14735-2022

O'Sullivan, M., Sitch, S., Friedlingstein, P., Luijkx, I. T., Peters, W., Rosan, T. M., Arneth, A., Arora, V. K.,

Chandra, N., Chevallier, F., Ciais, P., Falk, S., Feng, L., Gasser, T., Houghton, R. A., Jain, A. K., Kato, E., Kennedy, D., Knauer, J., … Zaehle, S. (2024). The key role of forest disturbance in reconciling estimates of the northern carbon sink. *Communications Earth & Environment*, *5*(1), 1–10. https://doi.org/10.1038/s43247-024-01827-4

Palmer, P. I., Feng, L., Baker, D., Chevallier, F., Bösch, H., & Somkuti, P. (2019). Net carbon emissions from African biosphere dominate pan-tropical atmospheric CO2 signal. *Nature Communications*, *10*(1), 3344. https://doi.org/10.1038/s41467-019-11097-w

Pessôa, A. C. M., Anderson, L. O., Carvalho, N. S., Campanharo, W. A., Junior, C. H. L. S., Rosan, T. M., Reis, J. B. C., Pereira, F. R. S., Assis, M., Jacon, A. D., Ometto, J. P., Shimabukuro, Y. E., Silva, C. V. J., Pontes-Lopes, A., Morello, T. F., & Aragão, L. E. O. C. (2020). Intercomparison of Burned Area Products and Its Implication for Carbon Emission Estimations in the Amazon. *Remote Sensing*, *12*(23), Article 23. https://doi.org/10.3390/rs12233864

Phillips, O. L., Aragao, L. E. O. C., Lewis, S. L., Fisher, J. B., Lloyd, J., Lopez-Gonzalez, G., Malhi, Y., Monteagudo, A., Peacock, J., Quesada, C. A., van der Heijden, G., Almeida, S., Amaral, I., Arroyo, L., Aymard, G., Baker, T. R., Banki, O., Blanc, L., Bonal, D., … Torres-Lezama, A. (2009). Drought Sensitivity of the Amazon Rainforest. *Science*, *323*(5919), 1344–1347. https://doi.org/10.1126/science.1164033

Powell, T. L., Galbraith, D. R., Christoffersen, B. O., Harper, A., Imbuzeiro, H. M. A., Rowland, L., Almeida, S., Brando, P. M., da Costa, A. C. L., Costa, M. H., Levine, N. M., Malhi, Y., Saleska, S. R., Sotta, E., Williams, M., Meir, P., & Moorcroft, P. R. (2013). Confronting model predictions of carbon fluxes with measurements of Amazon forests subjected to experimental drought. *New Phytologist*, *200*(2), 350–365. https://doi.org/10.1111/nph.12390

Powers, J. S., Vargas G., G., Brodribb, T. J., Schwartz, N. B., Pérez-Aviles, D., Smith-Martin, C. M., Becknell, J. M., Aureli, F., Blanco, R., Calderón-Morales, E., Calvo-Alvarado, J. C., Calvo-Obando, A. J., Chavarría, M. M., Carvajal-Vanegas, D., Jiménez-Rodríguez, C. D., Murillo Chacon, E., Schaffner, C. M., Werden, L. K., Xu, X., & Medvigy, D. (2020). A catastrophic tropical drought kills hydraulically vulnerable tree species. *Global Change Biology*, *26*(5), 3122–3133. https://doi.org/10.1111/gcb.15037

Pugh, T. A. M., Lindeskog, M., Smith, B., Poulter, B., Arneth, A., Haverd, V., & Calle, L. (2019). Role of forest

regrowth in global carbon sink dynamics. *Proceedings of the National Academy of Sciences*, *116*(10), 4382–4387. https://doi.org/10.1073/pnas.1810512116

Restrepo‐Coupe, N., Levine, N. M., Christoffersen, B. O., Albert, L. P., Wu, J., Costa, M. H., Galbraith, D., Imbuzeiro, H., Martins, G., Araujo, A. C. da, Malhi, Y. S., Zeng, X., Moorcroft, P., & Saleska, S. R. (2017). Do dynamic global vegetation models capture the seasonality of carbon fluxes in the Amazon basin? A data-model intercomparison. *Global Change Biology*, *23*(1), 191–208. https://doi.org/10.1111/gcb.13442

Rödenbeck, C., Zaehle, S., Keeling, R., & Heimann, M. (2018). History of El Niño impacts on the global carbon cycle 1957–2017: A quantification from atmospheric CO_2 data. *Philosophical Transactions of the Royal Society B: Biological Sciences*, *373*(1760), 20170303. https://doi.org/10.1098/rstb.2017.0303

Rosan, T. M., Sitch, S., O'Sullivan, M., Basso, L. S., Wilson, C., Silva, C., Gloor, E., Fawcett, D., Heinrich, V., Souza, J. G., Bezerra, F. G. S., von Randow, C., Mercado, L. M., Gatti, L., Wiltshire, A., Friedlingstein, P., Pongratz, J., Schwingshackl, C., Williams, M., … Aragão, L. E. O. C. (2024). Synthesis of the land carbon fluxes of the Amazon region between 2010 and 2020. *Communications Earth & Environment*, *5*(1), 1–15. https://doi.org/10.1038/s43247-024-01205-0

Schimel, D., Stephens, B. B., & Fisher, J. B. (2015). Effect of increasing CO_2 on the terrestrial carbon cycle. *Proceedings of the National Academy of Sciences*, *112*(2), 436–441. https://doi.org/10.1073/pnas.1407302112

Silva Junior, C. H. L., Anderson, L. O., Silva, A. L., Almeida, C. T., Dalagnol, R., Pletsch, M. A. J. S., Penha, T. V., Paloschi, R. A., & Aragão, L. E. O. C. (2019). Fire Responses to the 2010 and 2015/2016 Amazonian Droughts. *Frontiers in Earth Science*, *7*. https://doi.org/10.3389/feart.2019.00097

Silva Junior, C. H. L., Aragão, L. E. O. C., Anderson, L. O., Fonseca, M. G., Shimabukuro, Y. E., Vancutsem, C., Achard, F., Beuchle, R., Numata, I., Silva, C. A., Maeda, E. E., Longo, M., & Saatchi, S. S. (2020). Persistent collapse of biomass in Amazonian forest edges following deforestation leads to unaccounted carbon losses. *Science Advances*, *6*(40), eaaz8360. https://doi.org/10.1126/sciadv.aaz8360

Stocker, B. D., Tumber-Dávila, S. J., Konings, A. G., Anderson, M. C., Hain, C., & Jackson, R. B. (2023). Global patterns of water storage in the rooting zones of vegetation. *Nature Geoscience*, *16*(3), 250–256. https://doi.org/10.1038/s41561-023-01125-2

Trenberth, K. E., Caron, J. M., Stepaniak, D. P., & Worley, S. (2002). Evolution of El Niño–Southern Oscillation and

global atmospheric surface temperatures. *Journal of Geophysical Research: Atmospheres*, *107*(D8), AAC 5-1-AAC 5-17. https://doi.org/10.1029/2000JD000298

van Asperen, H., Jones, S., Lavric, J., Walter, D., Sierra, C., Horna, V., Komiya, S., Botía, S., Warneke, T., Griffith, D., Heimann, M., Andreae, M., & Trumbore, S. (2024). *Long term continuous high-precision greenhouse gas observation at the ATTO fieldsite: An overview*. https://proceedings.science/icdc-2024/papers/long-term-continuous-high-precision-greenhouse-gas-observation-at-the-atto-field?lang=en

van der Laan-Luijkx, I. T., van der Velde, I. R., Krol, M. C., Gatti, L. V., Domingues, L. G., Correia, C. S. C., Miller, J. B., Gloor, M., van Leeuwen, T. T., Kaiser, J. W., Wiedinmyer, C., Basu, S., Clerbaux, C., & Peters, W. (2015). Response of the Amazon carbon balance to the 2010 drought derived with CarbonTracker South America. *Global Biogeochemical Cycles*, *29*(7), 1092–1108. https://doi.org/10.1002/2014GB005082

van der Werf, G. R., Randerson, J. T., Giglio, L., Leeuwen, T. T. van, Chen, Y., Rogers, B. M., Mu, M., Marle, M. J. E. van, Morton, D. C., Collatz, G. J., Yokelson, R. J., & Kasibhatla, P. S. (2017). Global fire emissions estimates during 1997–2016. *Earth System Science Data*, *9*(2), 697–720. https://doi.org/10.5194/essd-9-697-2017

Vickers, D., & Mahrt, L. (1997). Quality Control and Flux Sampling Problems for Tower and Aircraft Data. *Journal of Atmospheric and Oceanic Technology*, *14*(3), 512–526. https://doi.org/10.1175/1520-0426(1997)014<0512:QCAFSP>2.0.CO;2

Wang, J., Zeng, N., Wang, M., Jiang, F., Chevallier, F., Crowell, S., He, W., Johnson, M. S., Liu, J., Liu, Z., Miller, S. M., Philip, S., Wang, H., Wu, M., Ju, W., Feng, S., & Jia, M. (2023). Anomalous Net Biome Exchange Over Amazonian Rainforests Induced by the 2015/16 El Niño: Soil Dryness-Shaped Spatial Pattern but Temperature-dominated Total Flux. *Geophysical Research Letters*, *50*(11), e2023GL103379. https://doi.org/10.1029/2023GL103379

Wigneron, J.-P., Fan, L., Ciais, P., Bastos, A., Brandt, M., Chave, J., Saatchi, S., Baccini, A., & Fensholt, R. (2020). Tropical forests did not recover from the strong 2015–2016 El Niño event. *Science Advances*, *6*(6). https://doi.org/10.1126/sciadv.aay4603

Winderlich, J., Gerbig, C., Kolle, O., & Heimann, M. (2014). Inferences from CO_2 and CH_4 concentration profiles at the Zotino Tall Tower Observatory (ZOTTO) on regional summertime ecosystem fluxes. *Biogeosciences*,

11(7), 2055–2068. https://doi.org/10.5194/bg-11-2055-2014

WWA. (2024). *Climate change, not El Niño, main driver of exceptional drought in highly vulnerable Amazon River Basin – World Weather Attribution*. https://www.worldweatherattribution.org/climate-change-not-el-nino-main-driver-of-exceptional-drought-in-highly-vulnerable-amazon-river-basin/

Yang, H., Ciais, P., Wigneron, J.-P., Chave, J., Cartus, O., Chen, X., Fan, L., Green, J. K., Huang, Y., Joetzjer, E., Kay, H., Makowski, D., Maignan, F., Santoro, M., Tao, S., Liu, L., & Yao, Y. (2022). Climatic and biotic factors influencing regional declines and recovery of tropical forest biomass from the 2015/16 El Niño. *Proceedings of the National Academy of Sciences*, *119*(26), e2101388119. https://doi.org/10.1073/pnas.2101388119

Yang, J., Tian, H., Pan, S., Chen, G., Zhang, B., & Dangal, S. (2018). Amazon drought and forest response: Largely reduced forest photosynthesis but slightly increased canopy greenness during the extreme drought of 2015/2016. *Global Change Biology*, *24*(5), 1919–1934. https://doi.org/10.1111/gcb.14056

Reduced vegetation uptake during the extreme 2023 drought turns the Amazon into a weak carbon source

S. Botía[1], C. Q. Dias-Junior[2], S. Komiya[3], A. M. van der Woude[4], M. Terristi[5,9], R.J. de Kok[4,8], G. Koren[7], H. van Asperen[3], S. P. Jones[3], F.A.F. D'Oliveira[2], U. Weber[9], E. P. Marques-Filho[10], I.M. Cely[11], A. Araujo[12], J. V. Lavric[13], D. Walter[14], X. Li[15], J.P. Wigneron[15], B. D. Stocker[6,21], J. Gonçalves de Souza[16], M. O'Sullivan[16], S. Sitch[16], P. Ciais[17], F. Chevallier[17], W. Li[18], I. Luijkx[4], W. Peters[4,19], C. A. Quesada[20], S. Zaehle[1], S. Trumbore[3], and A. Bastos[5,9]

[1]Biogeochemical Signals Department, Max Planck Institute for Biogeochemistry, Jena, Germany

[2]Departamento de Física, Instituto Federal de Educação, Ciência e Tecnologia do Pará, Belém, Brazil

[3]Biogeochemical Processes Department, Max Planck Institute for Biogeochemistry, Jena, Germany

[4]Wageningen University, Meteorology & Air Quality Dept, Wageningen, The Netherlands

[5]Institute for Earth System Science and Remote Sensing, Leipzig University

[6]Institute of Geography, University of Bern, Hallerstrasse 12, 3012 Bern, Switzerland

[7]Copernicus Institute of Sustainable Development, Utrecht University, Utrecht, The Netherlands

[8]ICOS ERIC, Carbon Portal, Geocentrum II, Sölvegatan 12, SE-22362, Lund, Sweden

[9]Biogeochemical Integration Department, Max Planck Institute for Biogeochemistry, Jena, Germany

[10]Departamento de Física, Universidade Federal da Bahia, Salvador, Brazil

[11]Atmospheric Physics Laboratory, University of São Paulo, São Paulo, Brazil

[12]Embrapa Amazônia Oriental, Belém, Pará, Brazil

[13]Acoem GmbH, Hallbergmoos, Germany

[14]Multiphase Chemistry Department, Max Planck Institute for Chemistry, Mainz, Germany

[15]INRAE, UMR1391 ISPA, 33140 Villenave d'Ornon, France

[16]Faculty of Environment, Science and Economy, University of Exeter, Exeter, UK.

[17]LSCE/IPSL, CEA-CNRS-UVSQ, Université Paris-Saclay, 91191 Gif-sur-Yvette, France

[18]Department of Earth System Science, Ministry of Education Key Laboratory for Earth System Modeling, Institute for Global Change Studies, Tsinghua University, Beijing, China

[19]University of Groningen, Centre for Isotope Research, Nijenborgh 6, Groningen, The Netherlands

[20]Instituto Nacional de Pesquisas da Amazônia (INPA), Manaus, Brazil

[21]Oeschger Centre for Climate Change Research, University of Bern, Bern, Switzerland

Corresponding author: Santiago Botía (sbotia@bgc-jena.mpg.de)

Key Points:

- Drought turned the biogeographic Amazon in 2023 to a weak carbon source, with magnitude similar to the drought of 2015 but less than 2016.
- Seasonal development of net carbon exchange in 2023 was marked by early uptake that partly compensated the carbon source of the dry season.
- The 2023 fire season in the Amazon was extended until November, though annual fire emissions were close to the long-term average.

Abstract

In 2023, the biogeographic Amazon experienced temperature anomalies of 1.5°C above the 1991-2020 average from September to November. These conditions were driven by high sea surface temperature in the Atlantic and Pacific oceans, together with reduced moisture advection from the Atlantic, causing large vapor pressure and water deficits in the second semester of 2023. Here, we evaluate the response of the Amazon carbon cycle to this extreme event across different spatial scales. We combined atmospheric CO_2 mole fractions and eddy covariance flux data from the Amazon Tall Tower Observatory (ATTO), near-real-time simulations by Dynamic Global Vegetation Models (DGVMs), an atmospheric inversion, and remote sensing data. We find that in 2023 the Amazon region was, including fires, a net carbon source of 0.01 to 0.17 PgC. Fire emissions (0.15 [0.13-0.17] PgC) were within typical variability of the 2003-2023 period, thus we attribute the weak carbon source to reduced vegetation uptake during the dry season. A stronger-than-normal vegetation uptake early in the year (January to April), consistent across data streams and spatial scales, mitigated the total carbon losses by the end of the year. We find a shift from carbon sink to source in May and a peak source in October. Our findings show a reduced vegetation carbon uptake over the Amazon region, leading to a weak carbon source that contributed 30% of the net carbon loss in the tropical land in 2023.

Plain Language Summary

The Amazon rainforest is a fundamental component in the Earth system as it stores large amounts of carbon in standing biomass. In 2023, unusually high temperatures (1.5°C above typical levels from 1991-2020) and dryness were recorded in the region from September to November. These conditions were caused by less moisture from the Atlantic ocean and warmer water temperatures in the Atlantic and Pacific oceans, which led to low humidity and drought across the Amazon region in the second half of 2023. We studied how these extreme conditions affected the Amazon's ability to absorb and store carbon. Using CO_2 measurements from the Amazon Tall Tower Observatory (ATTO), along with computer simulations and satellite data, we observed that the Amazon became a source of carbon emissions in 2023, releasing between 0.01 and 0.17 billion tons of carbon, rather than absorbing it. Carbon emissions from fires were 0.15 billion tons, which was within normal levels for the last two decades (2003-2023). We therefore attribute the anomalous carbon release in 2023 mostly to weakened vegetation uptake, rather than increased losses from fires. The seasonal development diagnosed by computer models suggest that vegetation absorbed more carbon than usual from January to April, helping offset emissions, but this shifted in May when the Amazon began releasing more carbon, with the highest emissions in October. Our results suggest that the Amazon's reduced carbon absorption accounted for 30% of the net carbon source across the tropical land in 2023.

1 Introduction

The global atmospheric CO_2 growth rate in 2023 was 2.79 +- 0.08 ppm (Ke et al., 2024; Lan, Tans, et al., 2024), the third largest since 2000 and fourth since 1959. The average growth rate for the 2010-2020 decade was close to 2.5 ppm (https://gml.noaa.gov/ccgg/trends/gl_gr.html, last accessed Dec 12, 2024), so this large anomaly, can not be solely explained by an increase of 1.3% in anthropogenic emissions from 2022 to 2023 (Friedlingstein et al., 2024), suggesting a reduction in the global carbon sinks (Ke et al., 2024). Tropical land plays an important role in determining the mean magnitude of the land carbon sink (Schimel et al., 2015), which is controlled by a balance between net carbon sources resulting from deforestation and carbon sinks where uptake surpasses carbon losses in less disturbed forest vegetation. Net release of carbon in the tropical land has been associated with positive phases of El Niño Southern Oscillation events (Gloor et al., 2018; J. Liu et al., 2017; Palmer et al., 2019; Rödenbeck et al., 2018), which in turn is linked to positive surface temperature anomalies globally (Trenberth et al., 2002) and in tropical forests (Jimenez et al., 2018).

Globally, the year 2023 was the first one in which daily global mean temperatures were continuously 1^{o}C above the 1850-1900 reference period, marking an unprecedented record. In about 50% of the days, most of them in the second half of the year, daily global mean temperatures reached values 1.5^{o}C above the 1850-1900 reference period, and from April to December global surface ocean temperatures registered record values (Copernicus, 2024). Associated with these record warming conditions, extreme events were observed both over land and ocean, including major heatwaves and droughts across many regions. For example, in Canada, extreme temperatures combined with low humidity led to unprecedented wildfires which contributed to ca. 25% of total tree cover loss that year (MacCarthy et al., 2024) and released over 0.6 PgC, more than the national fossil fuel emissions (Byrne et al., 2024). In the Amazon basin, historical drought and heat conditions were registered in 2023, with temperatures in October greater than 3^{o}C above the 1981-2020 average, and the Port of Manaus reaching the lowest water levels since records began in 1902 (Espinoza et al., 2024).

These extreme conditions have been linked to a transition from La-Niña conditions in 2022-23 to El-Niño from mid 2023, combined with widespread anomalous warming over the oceans worldwide (Espinoza et al., 2024). Previous droughts in the Amazon region, such as the ones in 2005 and 2010, and those associated with El-Niño conditions like in 2015-16, have resulted in reduced net carbon uptake by the Amazon forest, due to decreased productivity despite a slight increase in greenness (Bastos et al., 2018; Erik et al., 2018; J. Liu et al., 2017; J. Yang et al., 2018), reduced tree growth (Phillips et al., 2009; Feldpausch et al., 2016; H. Yang et al., 2022) and increased mortality (Hartmann et al., 2022; Powers et al., 2020). Hot and dry conditions tend to be associated with high fire activity and increased tree mortality (Brando et

al., 2014) resulting in persistent impacts that compound with human-driven disturbances, and can accelerate forest degradation (Berenguer et al., 2021; Fawcett et al., 2023; Lapola et al., 2023). Furthermore, in previous droughts in 2010 and 2015/2016, intensified fire emissions in the south and east of the Amazon have shifted the region from a carbon sink to a source (Basso et al., 2023; Gatti et al., 2014; Rosan et al., 2024; van der Laan-Luijkx et al., 2015; Alden et al., 2016; Gloor et al, 2018). However, regional differences in drought severity (Aragão et al., 2018; Lapola et al., 2023; Phillips et al., 2009) and thus resistance and resilience to drought (S. Chen et al., 2024) and fires (Berenguer et al., 2018; Esquivel-Muelbert et al., 2020), together with long-term rainfall trends, make impacts of each drought unique (Anderson et al., 2018).

Here, we examine the impacts of the 2023 extreme heat and drought conditions on the Amazon carbon cycle by combining multiple sources of information on ecosystem productivity, changes in biomass growth, fire activity and resulting net carbon fluxes. The combination of different types of surface and atmospheric measurements together with satellite observations of vegetation condition, aboveground biomass and fire activity, as well as atmospheric inversions and dynamical global model simulations, enables a distillation of robust patterns and the linking of atmospheric drivers with continental-to-regional-scale impacts on the land carbon balance. We first study the development of the 2023 drought by analyzing the seasonal evolution of the large-scale atmospheric circulation anomalies over tropical South America, and compare these with previous events such as the El-Niño in 2015/16. Then we analyze the spatiotemporal patterns of the most relevant climatic drivers of vegetation dynamics over the Amazon basin and the evolution of fire activity, contrasting when possible with previous events. We compare net land-atmosphere carbon exchanges, gross primary productivity, and ecosystem respiration from global vegetation models and an atmospheric inversion, analyzing their agreement and differences in magnitude and seasonality during the 2023 extreme event. As a benchmark, we compare the large-scale patterns with in-situ measurements of carbon fluxes and atmospheric CO_2 at the Amazon Tall Tower Observatory (ATTO), which is located in the central Brazilian Amazon in a well preserved location and is one of the few sites in the region providing carbon cycle in-situ data. By combining these multiple lines of evidence, our study aims to provide a robust assessment of the carbon cycle impacts of the 2023 extreme drought in the Amazon, and their relevance in the context of the global carbon cycle anomalies in 2023 (Friedlingstein et al., 2024; Ke et al., 2024).

2 Materials and Methods

2.1 Data sources and carbon cycle flux terms at regional scale

We used ERA5 reanalysis data (Hersbach et al., 2020) and ERA5-Land (Muñoz-Sabater et al., 2021) to analyze climatic drivers and anomalies over the Amazon. Monthly anomalies for sea surface temperature (SST), winds, geopotential height, and water vapor flux were computed

relative to 2000–2023 (Figure 1, Text S1). Potential cumulative water deficit (PCWD) was derived from precipitation and potential evapotranspiration (PET) following Stocker et al., (2023) and vapor pressure deficit (VPD) was calculated using 2m air temperature and relative humidity from ERA5-Land, with anomalies also referenced to 2000–2023. We refer the reader to Text S1 for more details on the reanalysis data.

To calculate the carbon cycle components (see Figure 1 and Text S2 and S3 for more details) we use four land surface models (bottom-up approach): Simple Biosphere model Version 4 (SiB4, Haynes et al., 2019), ORCHIDEE-MICT (Guimberteau et al., 2018; Krinner et al., 2005) , O-CN (hereafter referred to as OCN, Zaehle et al., 2010) and JULES (Clark et al., 2011). Three of the land surface models are Dynamic Global Vegetation Models (DGVMs) and one is a process-based model (SiB4), but for practical reasons we will refer to DGVMs throughout the text. As the top-down approach we use one satellite-driven atmospheric inversion (OCO2-Inv) that has a high resolution globally (1 x 1 degree) and is driven by the OCO-2 satellite atmospheric CO_2 concentration data. The remote sensing data (Figure 1, Text S4), like fire counts and emissions, GPP proxies (Sun Induced Fluorescence - SIF and Near Infrared of Vegetation - NIRv) and the Aboveground Carbon (AGC) based on L-band derived Vegetation Optical Depth (L-VOD) are all described in Text S4.

We define the carbon cycle components as the net flux over land (F_{land}) which results from the Net Biome Exchange (NBE) and the anthropogenic emissions (F_{ff}) from fossil fuels.

$$F_{land} = NBE + F_{ff}$$

NBE is composed by the Net Ecosystem Exchange (NEE) and fire emissions, including deforestation and degradation (F_{fire}) .

$$NBE = NEE + F_{fire}$$

And finally, NEE is given by the difference between terrestrial ecosystem respiration (TER) and photosynthesis (GPP). A negative sign (-) in F_{land}, NBE and NEE indicates a net uptake of carbon over land, whereas a positive (+) sign denotes a net source of carbon over land.

$$NEE = TER - GPP$$

To obtain the bottom-up NBE, we use the ensemble mean of the DGVMs and the mean F_{fire} between GFAS (Kaiser et al., 2012) and GFED4s (van der Werf et al., 2017). The top-down approach NBE is obtained using the OCO2-Inv and by subtracting F_{fire} from NBE, we obtain NEE. In Figure 1, we provide a summary of the data streams used to calculate the bottom-up and top-down NBE and NEE, together with the data used as proxies in this study.

The uncertainty of the F_{fire} is reported in terms of the min-max range [min-max], between GFAS and GFED4s. For the flux components (GPP, TER, NEE and NBE) calculated with the DGVMs we use the standard deviation of the model ensemble mean. For the OCO2-Inv we do not report uncertainty for 2023, but we note that as the global uncertainty (1-σ) for a single year is 3 PgC year^{-1}, the posterior uncertainty for the biogeographic Amazon will be less given the smaller domain and the data constraint, likely within 0.3-0.5 PgC year^{-1}. The inter-annual variability (IAV) is also reported explicitly and is calculated as the standard deviation of the multi-year mean for a given data source (e.g. $\overline{NEE}$ +- IAV). For the DGVMs, the multiyear mean is calculated from the ensemble mean of each individual year.

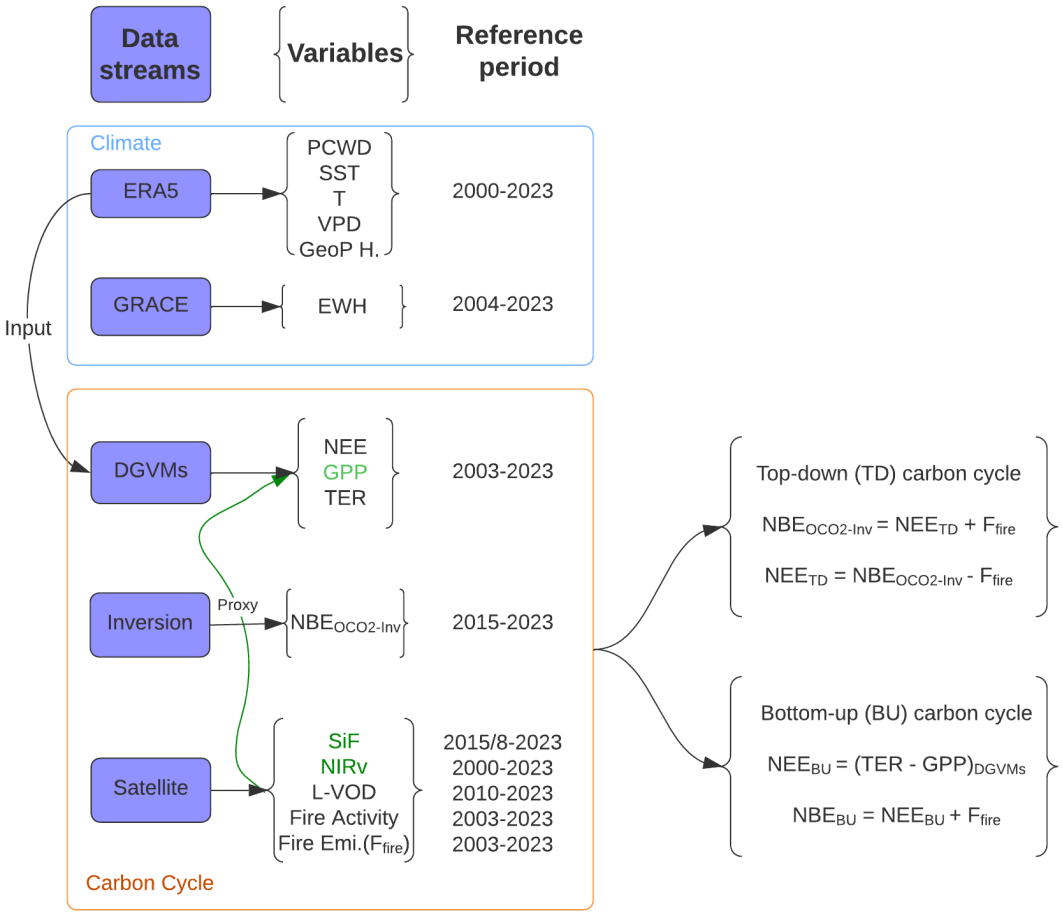

Figure 1. Data streams for climate and carbon cycle cycle components used to obtain the carbon budget for the biogeographic Amazon based on top-down and bottom-up approaches. Note that for SIF, as we describe in Text S4 we are using two products with different reference periods. The green highlight shows that SiF and NIRv are used as GPP proxies.

2.2 Local Measurements of carbon and climate variables

We use several data streams measured at the ATTO site (-2.1441, -58.999, https://www.attoproject.org/). In-situ continuous CO_2 mole fractions covering the period from

2014 to 2023 were used. The ATTO site and most of the measurement systems have been described by Andreae et al., (2015) and the footprint of the CO_2 mole fractions were characterized by Botía et al., (2022) and added in Figure S1. The half-hourly eddy covariance (EC) data was measured with a 3D sonic anemometer (CSAT3, Campbell Scientific Inc., Logan, UT, USA) and an open-path infrared gas analyzer (LI-7500A, Li-COR Inc., Lincoln, NE, USA), both mounted at 81 m above ground level on the ATTO 80 m Instant tower. The filtered high-quality and half-hourly turbulent EC-CO_2 fluxes were used for further data analysis: net ecosystem exchange (EC-NEE) calculation, gap-filling and EC-NEE partitioning to Gross Primary Productivity (GPP) and Ecosystem Respiration (R_{eco}). The complete details on the processing, partitioning, data quality assessment and calibration of the eddy covariance data and the CO_2 mole fraction datasets can be found in Text S5.

3 Results

3.1 Regional climate anomalies

In 2023, large PCWD (Figure 2) were found in the beginning of the year for the areas surrounding the Amazon, but remained low through the first semester within the biogeographic Amazon (hereafter Amazon). PCWD remained particularly low in the southern and eastern sectors of the Amazon forest, while other parts experienced relatively higher water deficits. By July, an increasing PCWD started to develop primarily in the southern sector of the Amazon, intensifying and expanding into central Amazonia. The progressive increase of PCWD is associated with high pressure anomalies between 5-20^{o}S (Figures S2-S3) and a weakening of the trade winds that persisted from June until October 2023 (Figures S7-S8). The persistence of high-pressure anomalies south of the equator in the second half of 2023 further induced a northward shift of the ITCZ (Figure S4) that suppressed regional convection and rainfall (Figure S4, S5) over the Amazon.

The weakened winds coming from the east and northeast flow contributed to reduced moisture transport from the Atlantic Ocean into the Amazon region; such wind anomalies were more pronounced from March to August (Figures S10). This led to the intensification of PCWD, potentially reinforcing anomalous anticyclonic circulation, especially in the eastern and central Amazon. The anomalous circulation patterns from May to December 2023 were likely induced by the above-average sea surface temperatures (SSTs) registered in both the Pacific and Atlantic Oceans (Figure 2). In the eastern Pacific, strong positive SST anomalies developed from April to November, consistent with the predominance of El Niño conditions (Espinoza et al., 2024), as in 2010 and 2015/16 (Marengo et al., 2011; Jiménez-Muñoz et al., 2016). The coincidence of warming in both ocean basins is particularly noteworthy, as it likely amplified the drought effects beyond what would be expected from a typical El Niño event alone.

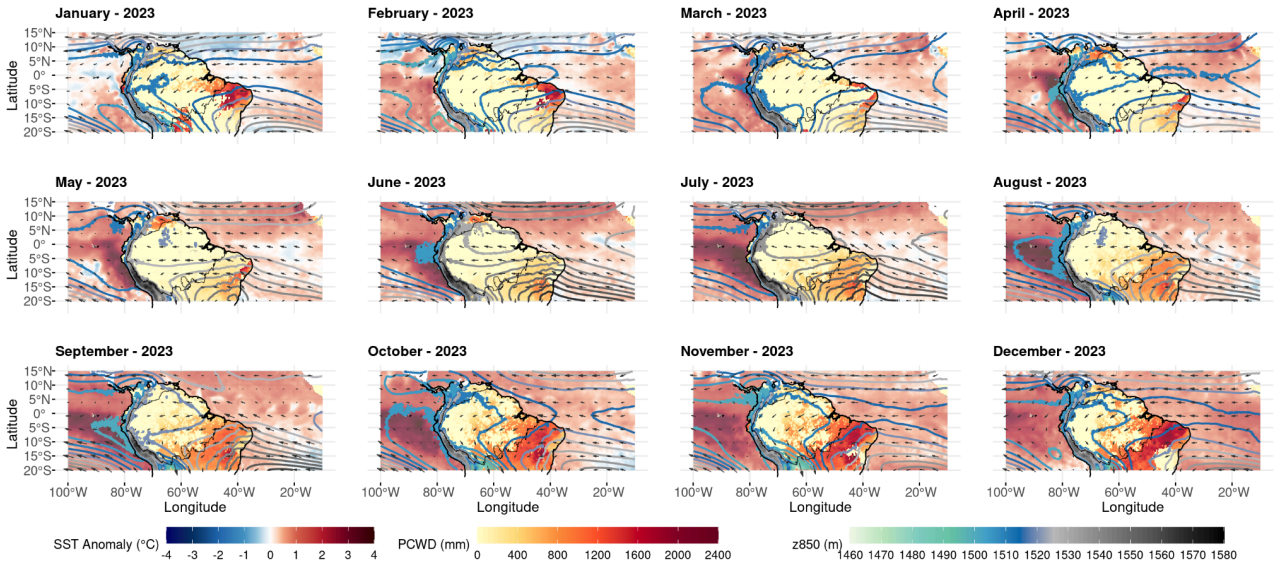

Figure 2. Regional climate analysis for 2023. Sea Surface Temperature (SST, plotted over sea surface), Cumulative water deficit (PCWD, plotted over continental surface), geopotential height contours at 850hPa (plotted as colored contour lines) and wind fields at 850hPa (black arrows). All variables were calculated using ERA5 reanalysis data, and the monthly anomalies were calculated relative to 2000-2023 baseline.

To better understand the 2023 event we compare the large-scale anomalies in climatic drivers in 2023 with those in 2015, the previous El Niño event in the origin year. Compared to 2015, the 2023 drought extended deeper into the Amazon, as shown by positive differences in PCWD emerging from September to December (Figure S9) and by the precipitation anomalies (Figures S5-S6). The exacerbated warming in 2023 is also evident in SST anomalies in 2023 compared to 2015 (Figure S9), which were consistently higher in 2023 than 2015 for most of the year in both the Atlantic and the Pacific oceans. Over the eastern Pacific, 2023 was colder than 2015 from September until December, consistent with it being a weaker El-Niño.

PCWD differences between 2023 and 2015 are partly driven by differences in VPD between those years and linked to 2023 having recorded record air temperatures and VPD over the last 24 years (Figure 3). Moreover, the seasonal evolution of temperature and VPD anomalies were concentrated in the second half of 2023 (Figure 3a,b,c,d), presenting a peak in October (Figure 3f,g). In addition, the equivalent water height from GRACE, was the lowest in this century in the Amazon basin (Figure 3e). Therefore, our results show that other mechanisms additional to El Niño in 2023, like the anomalous sea surface temperature in the Atlantic ocean, contributed to stronger drought conditions over most of the Amazon than in 2015, and are consistent with the attribution of the extreme drought conditions in 2023 to climate change by the World Weather Attribution project (WWA, 2024).

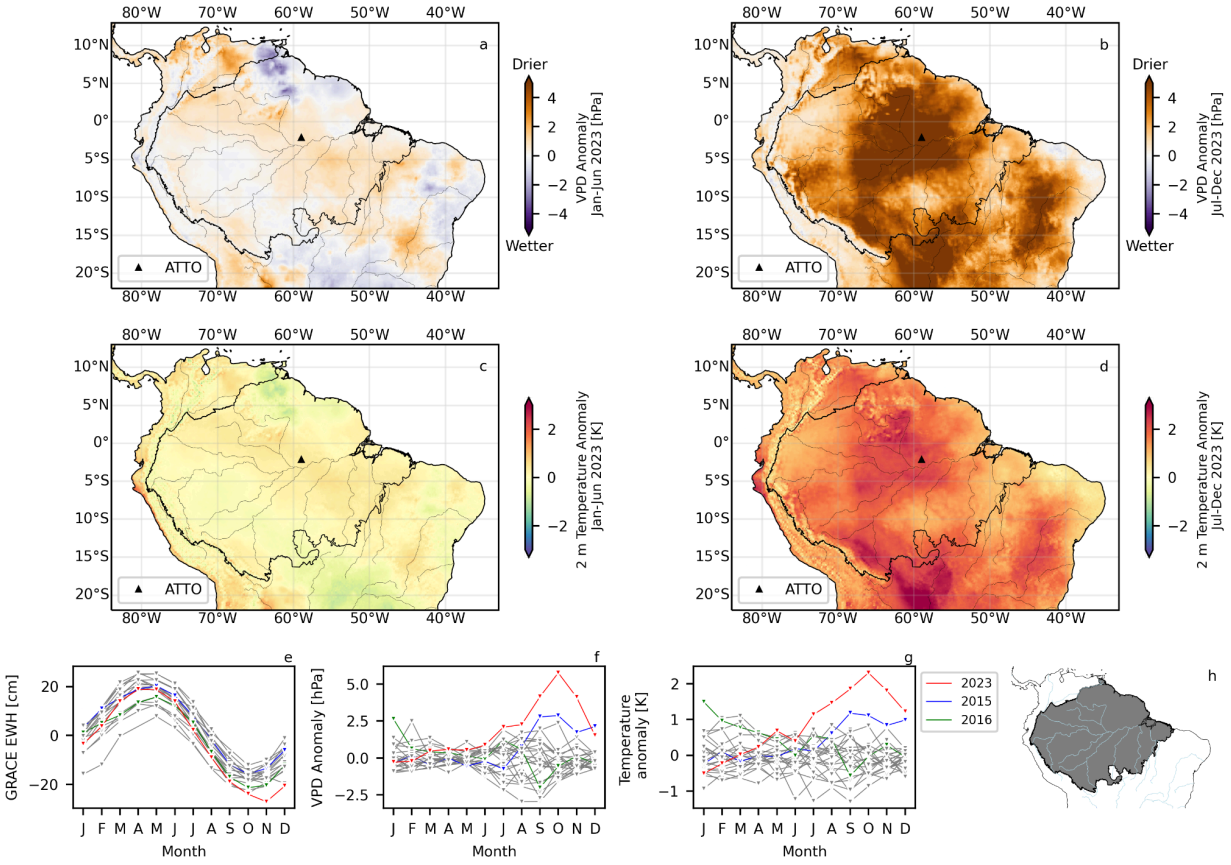

Figure 3. Regional scale climate anomalies for tropical South America. The spatial anomalies of VPD for both semesters in 2023 (a,b) and the same for the 2m temperature (c,d) were calculated using ERA5 land data (Hersbach et al., 2020). The seasonal evolution of the Equivalent Water Height (EWH) anomalies for the Amazon basin (e) were taken from the Gravity Recovery and Climate Experiment (GRACE) (available at: https://grace.jpl.nasa.gov/data-analysis-tool/. Last access: July 17, 2024). The seasonal evolution of VPD (f) and 2m temperature (g) anomalies are shown for the shaded area in (h) that corresponds to the biogeographic Amazon. The anomalies are based on a reference time period from 2000 to 2023.

3.2 Seasonal evolution and spatial distribution of carbon cycle components

Seasonal F_{fire} anomalies

The fire season in 2023 was extended well into November, different from normal years when the fire season offset is in October (Figure 4b,d). This extended fire season was driven by a north-to-south shift, but not necessarily leading to anomalous fire activity and carbon emissions (Figure 4b,c,d,e). Fires were largely concentrated in the Arc of Deforestation, along the southern border of the Amazon (between 70-60ºW and 15ºS), but also further north in the state of Pará and along the main branch of the Amazon river (Figure 4a). The highest fire counts and emissions were in October and November (Figure 4b,d). On average, the fire activity is dominated by fires occurring south of 5ºS, with an increasing contribution in October and November (Figure 4f,g). In 2023, from July to September the relative contribution of fires north of 5ºS was 10% larger than the long-term mean (2003-2023), consistent with the study of Jiménez et al., (2024). Later (November and December), the fire counts in the south (below 5ºS) were doubled relative to the 2003-2023 mean. Note that these spatial patterns are consistent with the development of the PCWD in the second half of 2023 (Figure 2). Furthermore, ATTO carbon monoxide data shows larger than average enhancements of CO, especially in September and October, confirming the larger than average contribution of fires north of 5ºS (Figure S11).

Even though there was an extended fire season, total fire emissions in 2023 (0.15 [0.13-0.17] PgC $year^{-1}$, see Figure 4c) were the same as the long-term (2003-2023) average between the two fire products (0.15 [0.13-0.16] PgC $year^{-1}$) with an interannual variability of +- 0.07 PgC $year^{-1}$. Individually, over the entire record (2003-2023, Figure S12), GFED4s emissions and its inter-annual variability (0.16 +- 0.08 PgC $year^{-1}$) are on average larger than GFAS (0.13 +- 0.07 PgC $year^{-1}$). Our estimate for the biogeographic Amazon in 2023 is similar to 2015 and 2016 (0.13 and 0.14 PgC $year^{-1}$), consistent with the total fire counts in 2023 (~180,000), which were marginally higher than 2015 (~163,000) and 2016 (~145,000). Given these findings, we conclude that fires were within the long-term variability and had a close-to-normal contribution to the NBE in 2023.

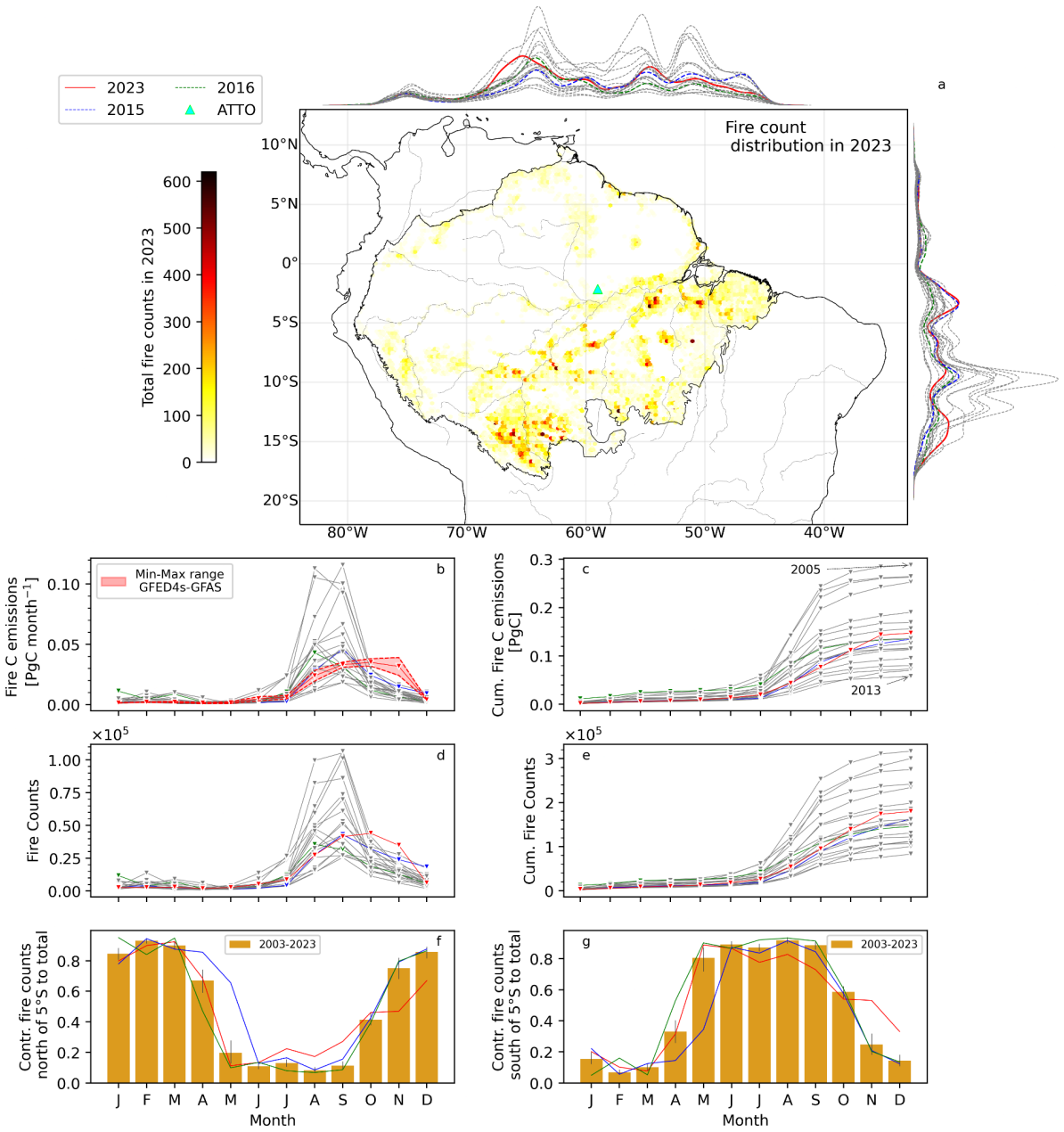

Figure 4. Fire counts and carbon emissions from fire in the biogeographic Amazon. Spatial distribution of total Fire counts in 2023 (a) with the latitudinal and longitudinal marginal distributions on y and x. We calculated the mean fire carbon emissions based on the GFED4s (van der Werf et al., 2017) and GFAS (Kaiser et al., 2012) products for each month from 2003 to 2023 (b). The red shading in (b) indicates the maximum and minimum fire emission between GFED4s and GFAS for the months in 2023. The cumulative fire carbon emissions are shown in (c). The seasonal evolution of fire counts (d) and cumulative fire counts from 2003 to 2023 (e). The relative contribution (%) of fire counts north (f) and south (g) of the latitude 5ºS to the total fire counts per month for 2023 and the mean for 2003 to 2023.

Spatial distribution of NEE, NBE and Fires

In 2023, the spatial patterns of vegetation carbon sources and sinks (NEE), as simulated by DGVMs, show high consistency, with at least three out of four models agreeing on the sign of NEE (Figure 5a). According to these models, vegetation acted as a carbon source south of the main branch of the Amazon River and northeast of ATTO. The source regions south of the Amazon River (e.g., between 70°W–60°W) overlap with fire emissions (Figure 5b), whereas this overlap is not observed in the northeast near ATTO. Spatial patterns of NEE partially align with the temperature and VPD anomalies shown in Figure 3 and with PCWD in Figure 2, particularly in the central, southern, and eastern Amazon. Conversely, regions in the north and northwest, where DGVMs simulate vegetation uptake, do not show significant VPD or temperature anomalies, nor large PCWD throughout the year. Therefore, DGVMs and fire data suggest that vegetation carbon sources were enhanced by fire activity in the south of the Amazon but not in the northeast.

The spatial distribution of NBE in the DGVMs and the OCO2-Inv is broadly consistent in an east-west sink-to-source gradient in the Amazon (Figure 5c,d). The OCO2-Inv indicates a net uptake of carbon concentrated over the west (west of 70°W), but the DGVMs simulate the uptake in the northwest. While DGVMs simulate larger carbon sources than the OCO2-Inv in the south of the Amazon where most of the fires are located, the OCO2-Inv shows a large source northeast of ATTO. Note that northeast of ATTO, fire emissions were low suggesting that the positive NBE (carbon sources) is mainly driven by vegetation. The differences between NEE and NBE in Figure 5a versus 4c,d are indicative of fire emissions in the regions where NBE > NEE, but only where fire emissions overlap. On the other hand, in the grid cells in which NEE (Figure 5 a) is close to NBE (Figure 5 d), the role of the vegetation in the sink or source of carbon is more relevant than fires. Based on this, we found a carbon source (+NEE) due to reduced vegetation uptake in the north of the main branch of the Amazon river and northeast of ATTO.

Seasonal evolution of NEE, NBE and GPP, TER

We compared the calculated seasonal evolution of the gross and net carbon fluxes over the whole basin in 2023 with the long-term mean, both for DGVMs (2003-2023) and the OCO2-Inv (2015-2023) (Figure 6). We use different reference periods as the OCO2-Inv is limited to the OCO2 data coverage. DGVMs simulate positive (slightly above 1σ) TER and GPP anomalies in the beginning of 2023, which result in equally strong negative NEE (increased uptake) until May (Figure 6 a,b,c). Starting in August, DGVMs indicate a steep decline in GPP, shifting from moderately positive values in August to extremely low (<-2σ) levels from September to December. This decline is accompanied by a consistent but less pronounced decrease in TER, with the most significant negative anomalies (also below -2σ) in November. As a result, the NEE over the Amazon shifts from negative (carbon uptake) to positive (carbon source) in September, remaining positive through the end of the year (Figure 6c). Adding fire,

the NBE from DGVMs shows a similar trajectory, with more evident contributions from fire since July onwards (Figure 6d). Note that the anomalies given by the DGVMs are based on a reference period between 2003 and 2023 and represent the largest simulated decline in gross fluxes and net sources (NEE and NBE) during the dry season in the current century.

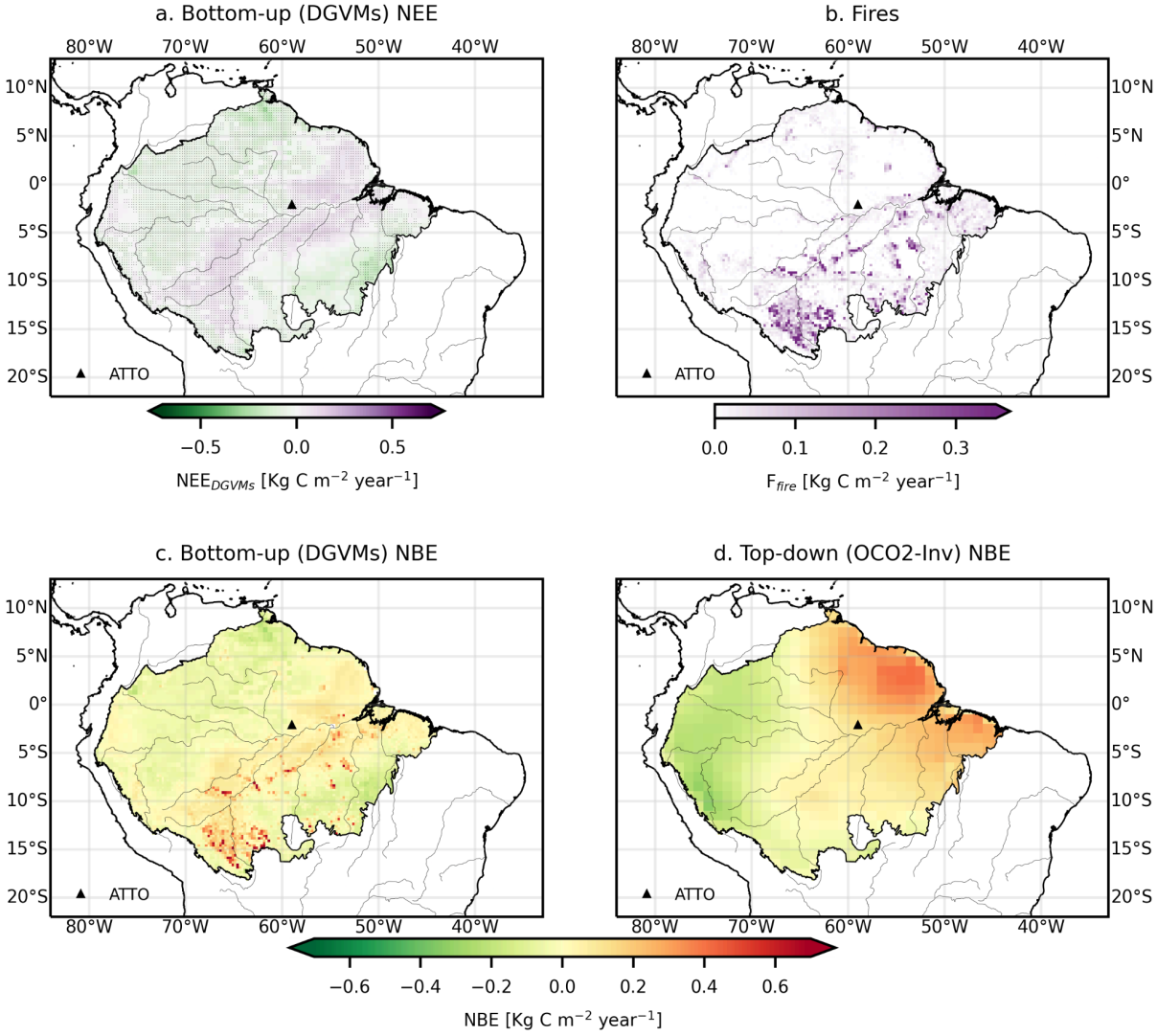

Figure 5. Bottom-up and top-down carbon cycle components for the biogeographic Amazon in 2023. In (a) the mean NEE for the DGVMs, in (b) the mean fire emissions between GFAS and GFED4s, in (c) the NBE calculated as the sum of panels a and b (NBE = NEE_{DGVMs} + F_{fire}) and in (d) the NBE of the OCO2-Inv. In (a) the grid cells in which at least three of the DGVMs coincide in the sign of NEE are highlighted with a marker.

The OCO2-Inv estimates a strong uptake (NBE) in the first months of 2023, but followed by a switch from sink to source in May and a return to a sink in December (Figure 6 e). This is consistent with uptake anomalies (NEE) in DGVMs in the beginning of the year, but the magnitude of uptake in the OCO2-Inv (NBE) relative to the mean of the reference period is larger than in the DGVMs. We find that in the DGVMs and the OCO2-Inv, October is the month in which NEE and NBE reach the seasonal maximum or the largest carbon source in 2023, coinciding with the temperature and VPD anomalies shown in Figure 3 and with the peak in fire activity at the Amazon region scale. Given the seasonal development, we conclude that the NBE maximum in the second semester was driven by a combination of fires and a positive NEE, but the switch from sink to source in May (only in the OCO2-Inv) is only driven by a positive NEE as fire activity with a late onset began only in August (Figure 4). Nevertheless, the enhanced uptake from January to May, evident in both OCO2-Inv and DGVMs, compensated for the relatively large source in the second part of the year.

Over the whole year (2023), the NBE ranges from 0.01 PgC $year^{-1}$ (DGVMs) to 0.17 PgC $year^{-1}$ (OCO2-Inv). In the top-down estimate the NBE implicitly includes fires, and degradation and deforestation emissions that do not occur through burning (although these were not prescribed in the priors) over the Amazon (Figure 6f). Interestingly, the NBE in DGVMs and the OCO2-Inv during 2023 was similar in magnitude to 2015 (DGVMs, -0.06 PgC $year^{-1}$ and OCO2-Inv, 0.16 PgC $year^{-1}$), but contrastingly different than in 2016 (DGVMs, -0.10 PgC $year^{-1}$ and OCO2-Inv, 0.83 PgC $year^{-1}$). Without fires (0.15 [0.13-0.17] PgC $year^{-1}$), the NEE ranges from a sink (DGVMs, -0.13 PgC $year^{-1}$) to a small source (OCO2-Inv, 0.02 PgC $year^{-1}$) in 2023. Note that compared to previous years, the DGVMs show the largest difference in NEE relative to the long-term mean, indicating a carbon sink weakened by more than 30%. It is worth noting that the shape of the seasonal cycle differs between the OCO2-Inv and DGVMs, which might be because DGVMs tend to not capture well the seasonality of GPP in the evergreen tropical forests (Restrepo-Coupe et al., 2017; X. Chen et al., 2020). Therefore, even differing in seasonality and in the absolute magnitude of the fluxes, both DGVMs and the OCO2-Inv estimate a large anomaly in 2023 relative to the reference period.

GPP anomaly and Aboveground biomass change

To confirm the negative anomaly in GPP given by the DGVMs, we further analyzed independent GPP proxies for the same region. First, we compared each GPP proxy (OCO2-SiF, Tropomi-SiF and NIRv) to the local EC-GPP at ATTO (Figure S13), which indicate that the SiF products (OCO2-SiF and Tropomi-SiF) are closer to the local GPP ($r = 0.49$; p-value$<<0.01$, $r = 0.47$; p-value$<<0.01$, $n=72$) than NIRv ($r = 0.32$; p-value$=0.01$, $n=72$). Using the SiF products for the Amazon, we found that the sign of the anomalies in October, November and December is the same as for the DGVMs (Figure 7 a). Earlier in the dry season, in August and September, the SiF products and the DGVMs are not consistent and in September the DGVMs show a rather

large negative anomaly. Therefore, it is likely that the GPP anomaly in DGVMs had an earlier onset compared to the GPP proxies. However, from October to December, a reduced vegetation uptake, as the DGVMs and the GPP proxies suggest, is likely.

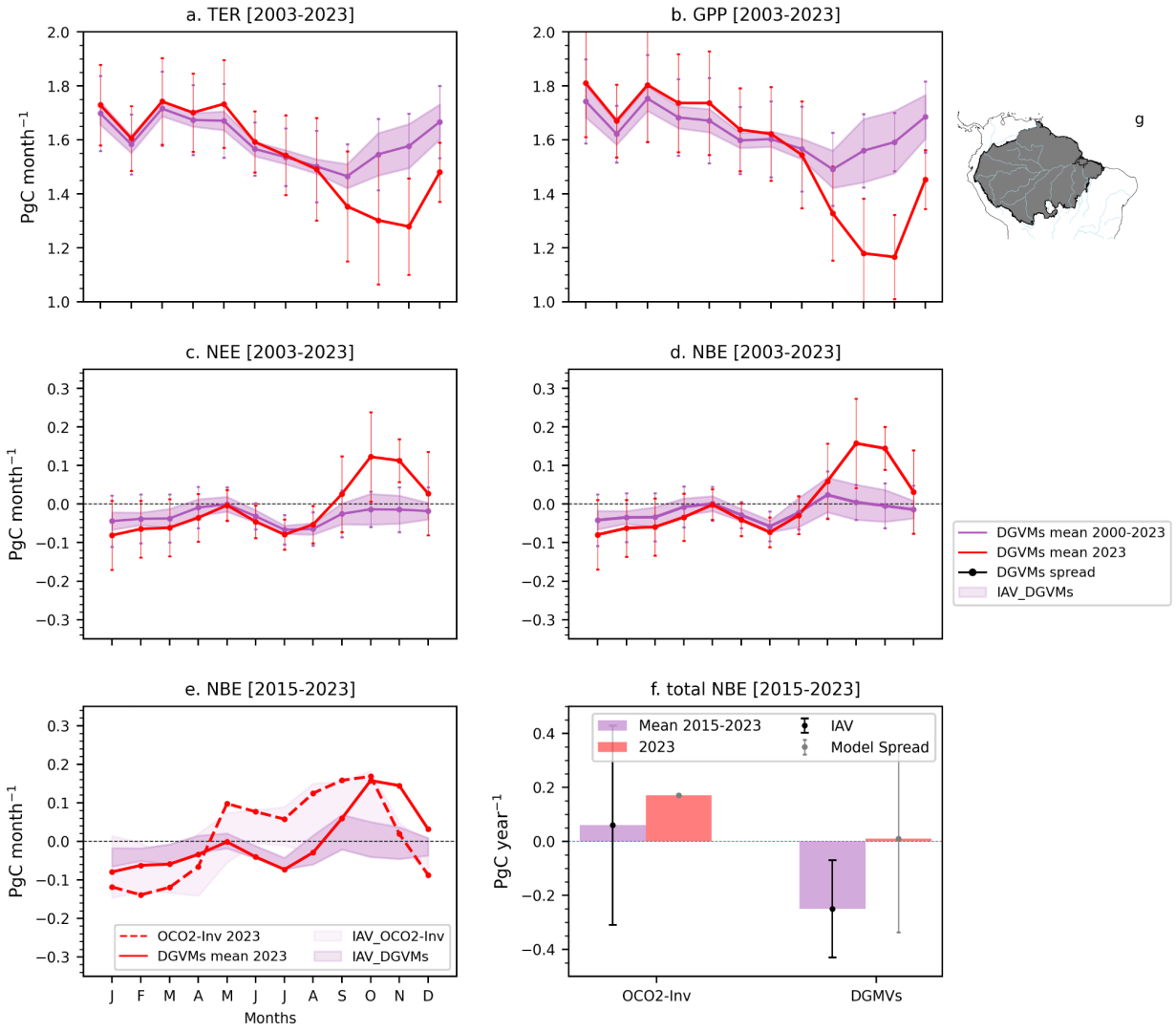

Figure 6. Mean seasonal cycle of gross and net carbon fluxes from DGVMs, having the period from 2003 to 2023 as a reference for the biogeographic Amazon. The climatological mean for the DGVM ensemble is shown for TER (a) and GPP (b) highlighting the standard deviation for each month with a shaded area. Net ecosystem exchange (NEE) based on the DGVM ensemble mean is shown in (c). Net biome exchange (NBE) for the DGVM ensemble mean is shown in (d). In (e) and (f) the seasonal NBE and total NBE for both OCO2-Inv and DGVMs is shown with the reference period corresponding to 2015-2023. Note that NBE for the DGMV ensemble mean was calculated adding the mean fire emission from the GFED4s and the GFAS fire emission products.

We find that the average Aboveground Carbon (AGC) loss in the Amazon from 2011 to 2023 was -0.39 +- 0.15 PgC $year^{-1}$ (average value over all years with losses) while for 2023 it was -0.61 PgC (Figure 7 b). Changes in AGC (ΔAGC) have been associated with tree mortality, deforestation and subsequent degradation at forest edges due to fire and logging, but also to secondary forest growth (Fawcett et al., 2023; Silva Junior et al., 2020), so a ΔAGC represents a net exchange which can have a fraction not emitted directly into the atmosphere. For example, selective logging or tree mortality are processes that can cause a ΔAGC but not an immediate CO_2 source to the atmosphere. The losses in 2023 could have been influenced by the decreasing trend in the L-VOD signal since 2016 (Figure S14). However, the spatial patterns in the AGC anomalies were found to correlate well with Enhanced Vegetation Index (EVI) and SiF (Wigneron et al., 2020), both proxies of GPP. As a comparison, relative to the long-term mean the reduction in DGVMs-GPP was 0.88 PgC $year^{-1}$ in 2023. Thus, while the AGC change in 2023 could in part be associated with a reduction in GPP due to deforestation, the mismatch (GPP_{losses} > AGC_{losses}) suggests that the reduction in GPP in the DGVMs could be slightly overestimated, like in the beginning of the dry season.

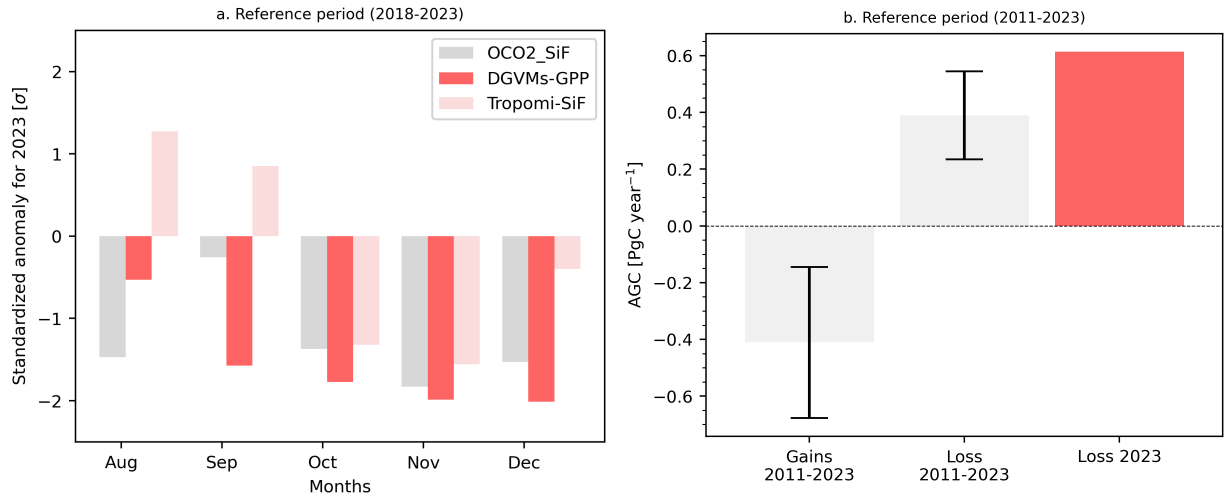

Figure 7. Magnitude of the standardized anomalies in OCO2-SiF, Tropomi-SiF and ensemble mean GPP of the DGVMs for the biogeographic Amazon a) and mean net aboveground carbon loss estimated from L-VOD for the same Amazon region b). Note that the anomalies in a) were calculated with the OCO2-SiF period as a reference (2018-2013), for the OCO2-SiF, Tropomi-SiF and the DGVMs. For b), we calculated the difference in AGC from $year_{t+1}$ to $year_t$ ($year_{t+1}$-$year_t$) from 2011 to 2023 and selected the years with losses (negative numbers) and gains (positive numbers), from that we got the mean for the entire record and the individual loss for 2023. The bars in b) show the interannual variability.

3.3 Local response of the carbon cycle in 2023: ATTO as independent benchmark

CO_2 mole fraction measurements at ATTO (Figure 8 a), representative of a large footprint (Figure 8 b and Figure S1) show a large enhancement over the background (ΔCO_2, Figure 8 a),

peaking in September and consistent with a larger-than-normal fire activity north of 5ºS during this month. Note that the concentration footprint of the 80-m tower covers the area east of the ATTO site, where some of the largest carbon sources were estimated by both the OCO2-Inv and by the DGVMs-ensemble mean (Figure 5), coinciding with the highest VPD and Temperature anomalies (see Figure 3). However, at the same location, the local eddy covariance measurement had a different response.

In the absence of large disturbances, the eddy covariance measurements indicate that the forest close to ATTO was on average a sink of carbon in 2023 (Figure 8c). At ATTO we observe a large (close to but within 1σ) uptake from January to March, interrupted by a positive peak (source) in May and followed by a consistent sink from July to November. The first part of the year is consistent with the seasonal pattern in OCO2-Inv coinciding on a large carbon uptake. The EC-NEE sink is mainly controlled by a large (close to and larger than 1σ) decrease in ecosystem respiration (R_{eco}) in the beginning of the year (February - April), and during the dry season (August - October). Note that GPP also attains the lowest values in June and September, but most of the development in 2023 is within the normal variability of the record. Given these findings, the 2023 drought at ATTO had a stronger effect in R_{eco} than GPP, leading to a net sink at the local ecosystem scale (i.e. ATTO).

The seasonal development of simulated NEE, R_{eco} and GPP in the DGVMs at the grid cell including ATTO (Figure 8 d,f,i) is in contrast to the local EC measurements. The DGVMs show a stronger decline in GPP than in R_{eco} mainly during the dry season, leading to a positive NEE from September to November in 2023. It is worth noting that the seasonality of the DGVMs is very different to the measured one at ATTO, mainly during the wet season, not being able to reproduce the uptake of carbon from January to March. The EC measurements indicate that such uptake was amplified during 2023, reaching values close to 1σ from January to March in EC-NEE. We find that such mismatch could be associated with the forcing data in the DGVMs, as the measured precipitation and shortwave radiation at ATTO were higher than ERA5 in February and March (Figure S15).

The flux response at ATTO deserves more context due to its contrasting development relative to the DGVMs. Local measurements at ATTO show that VPD, air and soil temperature anomalies in 2023 were consistent with the regional pattern shown in Figure 3, reaching values larger than 1σ (Figure S16, S17). Interestingly, soil moisture in the first 50 cm layer did not show anomalous values and precipitation was above the average with 200 mm more than normal years. Therefore, we believe that the normal levels of soil moisture sustained photosynthetic uptake throughout 2023, buffering the effect of air temperature and VPD, which could be a local response associated with the forest close to ATTO and not a general response regionally.

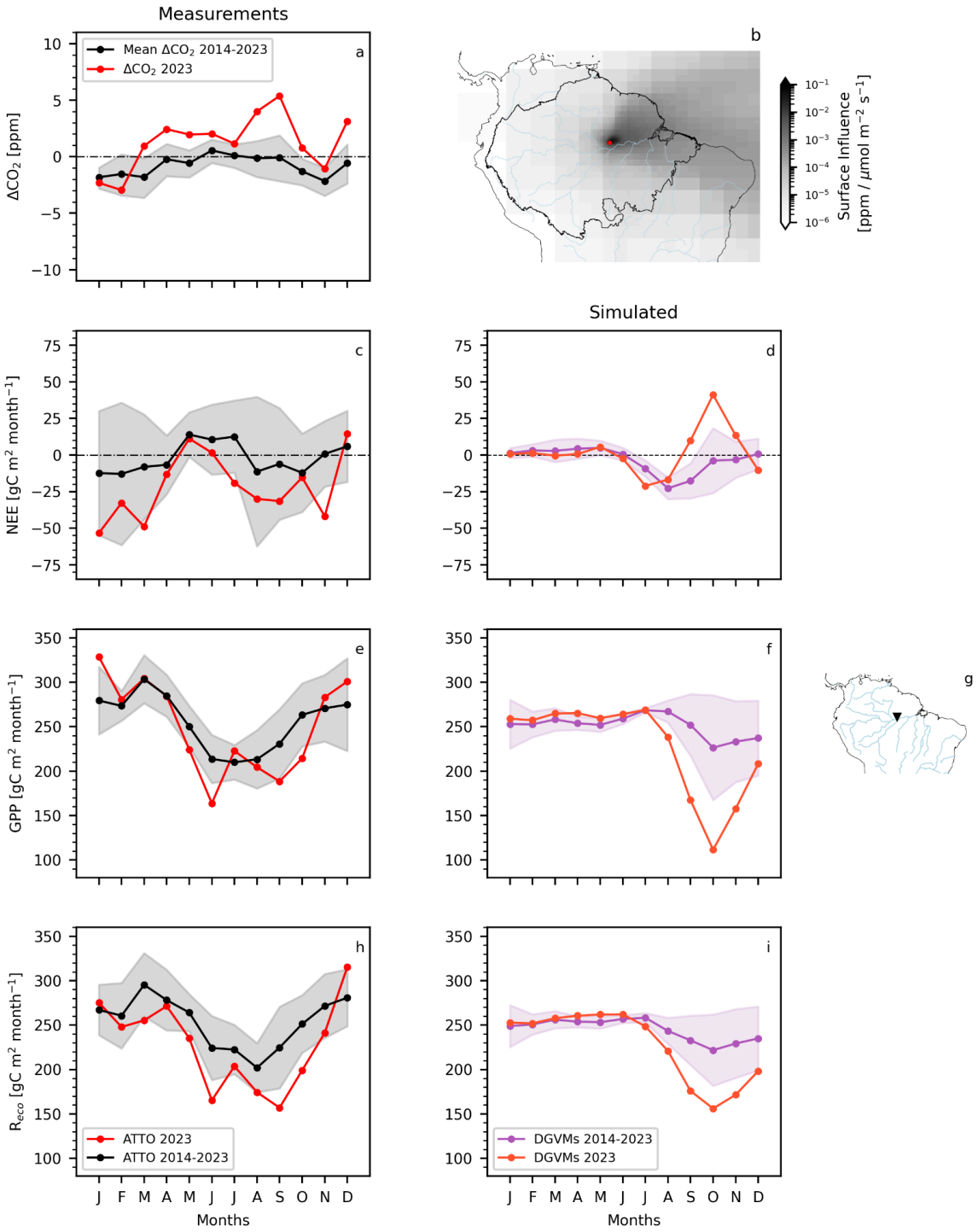

Figure 8. Seasonal evolution of the CO_2 mole fractions and eddy covariance fluxes (NEE, GPP and R_{eco}) at ATTO. On the first column (a, c, e, h) the measurements (ΔCO_2, NEE, GPP and R_{eco}) are shown. In the second column (d, f, i) the simulations (NEE, GPP and R_{eco}) are presented. The surface influence of the ΔCO_2 is shown in b) and in g) a marker is shown indicating the very local influence of the eddy covariance flux data.

4 Discussion

The drivers and consequences of drought

Our results show how elevated SST anomalies in the tropical Atlantic and Pacific oceans and associated changes in atmospheric circulation and surface hydroclimatic conditions, contributed to intensifying widespread soil water deficits across the Amazon during the second half of 2023 (Figure 2), consistent with the extremely low water levels reported by Espinoza et al., (2024) for the Rio Negro in Manaus. An interesting feature of the 2023 drought is that the onset coincided with a transition to an El Niño phase that followed three years of consecutive La Niña conditions (https://psl.noaa.gov/enso/mei/, last accessed August 15, 2024). Compared to the previous El Niño event of 2015/16, 2023 registered higher SST anomalies over the tropical Pacific and especially the tropical Atlantic (Figure S9), which played an important role in the atmospheric circulation anomalies, extremes in air temperature and atmospheric and surface dryness (PCWD). Temperature and precipitation anomalies in the Amazon basin have surpassed the previous record in 2015/16 (Espinoza et al., 2024; Jiménez-Muñoz et al., 2016b) and their extreme magnitude has been attributed to climate change (WWA, 2024). Compared with 2015/16 and previous droughts, the potential cumulative water deficits and extremely high vapor pressure anomalies registered in late 2023 progressed deeper into the humid Amazon forest, extending the dry season by several months and thus contributing to increased vegetation stress.

Here, we calculate PCWD as the balance between potential evapotranspiration and precipitation adapted from Stocker et al., (2023). This estimate is less conservative than other commonly used estimates for the Amazon such as CWD in Aragão et al., (2007), which assume constant evapotranspiration (ET) of 100 mm month^{-1}. Even though there are no reported trends in regional ET, there are spatial gradients (Baker et al., 2021) that could be important for water deficit calculation. For example, at ATTO the mean ET is 120 mm month^{-1}, so a CWD calculated using 100 mm month^{-1} would result in weaker CWD. Furthermore, evaporative demand depends on atmospheric humidity, which, as we have shown, reached extreme values in 2023 (Figure 3). Thus, we consider that estimating PCWD based on potential evapotranspiration, instead of a fixed value, can better represent the spatial patterns of the surface drought, especially under such extreme conditions.

Summary of responses by different data streams

In this paper, we have reported on the response of the Amazon forest to the 2023 event across various spatial scales using multiple data streams (Figure 9). In the absence of anthropogenic disturbances at the ecosystem scale at ATTO (Figure 9c) and with no precipitation deficit, the forest remained a carbon sink due to a large reduction in respiratory carbon loss together with a mild decline in photosynthetic uptake, resulting in a persistent sink

of carbon due to vegetation uptake (EC-NEE). Based on individual measurements of leaf, live wood and soil respiration in the Amazon, Chambers et al., (2004) found that autotrophic respiration contributes a large portion (~70%) of the ecosystem respiration, so a decline in GPP and in autotrophic respiration due to drought (Doughty et al., 2015) could explain the observed decline in R_{eco} in this study. However, an increase in autotrophic respiration and thus an overall increment in ecosystem respiration was found in a rainfall exclusion experiment in the eastern Amazon (Metcalfe et al., 2010), suggesting that there might not be a unidirectional response of R_{eco} to drought in the Amazon given than each drought is unique in its development and preceding conditions (S. Liu et al., 2024). Furthermore, it is worth noting that our estimate of ecosystem respiration (R_{eco}) relies on nighttime NEE that inherently assumes that daytime R_{eco} is equal to nighttime R_{eco} , leading to a source of uncertainty in our total ecosystem respiration estimates.

At a larger scale (Figure 9 b) the positive ΔCO_2 indicates that the ATTO footprint area was likely a source of carbon with a combined effect of reduced vegetation uptake, fires and land use change emissions. There are several implications of these findings. At the ecosystem scale, the forest close to ATTO buffered the effects of the large VPD and temperature anomalies with sufficient soil moisture availability (Figure S17). Such a localized response is not captured by the DGVMs, presenting a challenge for the bottom-up estimates. However, the atmospheric CO_2 signal indicates a larger-than-normal carbon source in the ATTO concentration footprint (which is much larger than the flux footprint). This is consistent with fire activity, the NEE source in the DGVMs, and the NBE source in OCO2-Inv that we report here.

At the biogeographic Amazon scale (Figure 9 a), the source of carbon including fires (NBE) ranges from 0.01 PgC $year^{-1}$ (bottom-up, DGVMs) to 0.17 PgC $year^{-1}$ (top-down, OCO2-Inv), with the main difference being the magnitude of the vegetation uptake (NEE), which, depending on the method used, can represent a small carbon source of 0.02 PgC $year^{-1}$ (OCO2-Inv) or a sink of -0.13 PgC $year^{-1}$ (DGVMs) in 2023. Note that relative to the long-term mean (2003-2023, -0.36 PgC $year^{-1}$), -0.13 PgC $year^{-1}$ represents more than a 30% reduction in NEE. According to the DGVMs the reduction in NEE was driven by a larger decline in GPP than R_{eco}, similar to the findings of Liu et al., (2017) for the 2015/2016 event. Nevertheless, the local response in NEE, GPP and R_{eco} at ATTO, challenges the regional response in the DGVMs, yet we can not rely on the ATTO fluxes to infer a regional-scale response, even more in the absence (at ATTO) of anthropogenic disturbances. Including fires, the NBE source we find here based on the OCO2-Inv represents about half of that reported by Ke et al., (2024) for the Amazon. This difference is mainly because their definition of Amazon is larger than ours, the biogeographic Amazon. Therefore, the definition of the Amazon influences the region-wide fluxes as a large contribution of the fire activity is at the boundary of the Amazon and Cerrado biomes (Botía et al., 2024).

Spatially we attribute the NEE source to the northeast part of the Amazon (Figure 5), consistent with a negative SiF and GPP anomaly during Oct-Dec (Figure 7) and a decline in greenness reported for 2023 by Jiménez et al., (2024). Including fires, based on the OCO2-Inv and the study by Wang et al., (2023), the NBE source was similar to 2015 and lower than 2016. We find that such a response, given the extreme temperature and VPD anomalies, was due to a seasonal compensation, with a large carbon uptake in the beginning of 2023 evident in both OCO2-Inv and DGVMs. This compensation can be associated with more rainfall in the beginning of 2023, driven by La Niña conditions in the Pacific Ocean. It remains to be confirmed whether the findings by Wang et al., (2023) for the 2015/2016 El Niño, in which temperature dominated the total NBE flux, but the spatial patterns were controlled by deficits in soil moisture, still hold true for 2023 and the post-El Niño development in 2024. Therefore, we believe that the use of several large scale data streams and in-situ measurements enhance the comprehensive understanding of drought impacts.

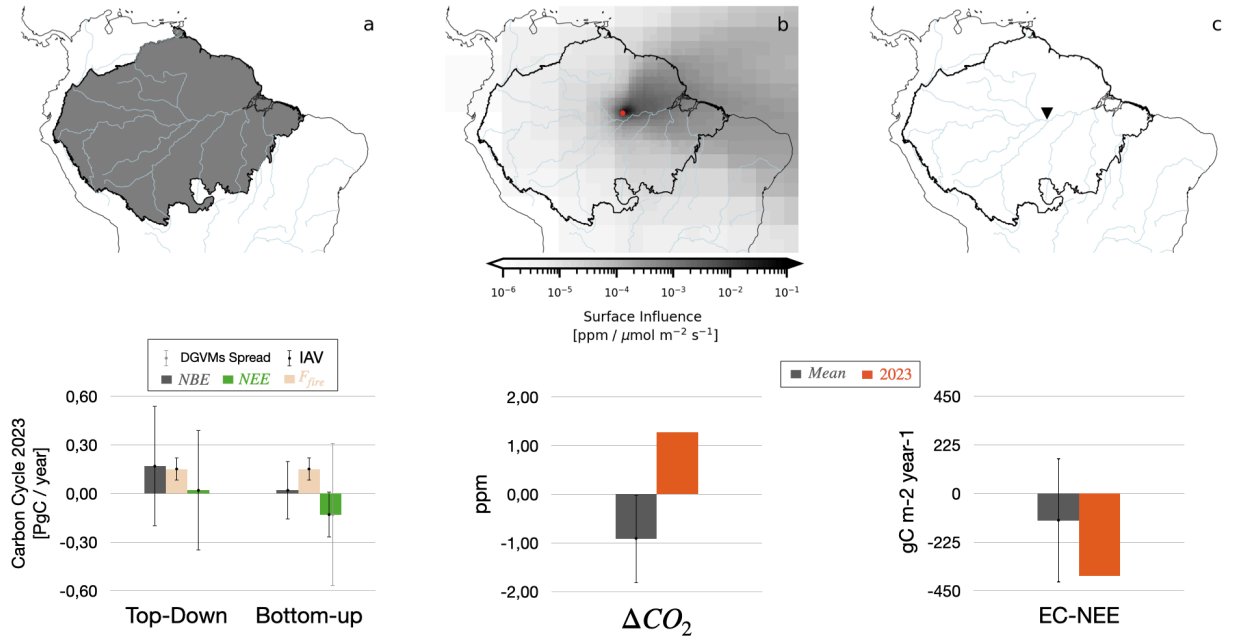

Figure 9. Summary of the drought response across scales and different data streams. In (a) the bottom-up (DGVMs) vs top-down (OCO2-Inv) carbon budget is shown. In panel (b) we present the ΔCO_2 or regional signal at ATTO, which is affected by the areas (i.e. footprint) covered by the gray polygons in the map. The mean response of the ecosystem level EC-NEE is shown in (c). Note that the footprint of the EC-NEE is less than 100 km^2.

Role of fire in NBE

We showed that the fire season was extended until November/December, mainly driven by the progression of surface and atmospheric dryness conditions (Figure 2 and Figure 3). These resulted in an early onset (July to September) with more (less) fire activity in the north (south)

and an offset (November and December) with more (less) fire activity in the south (north), relative to the total fire activity regionally. The north to south dynamic in fire activity reported here, is consistent with the timing of the rainfall anomalies in Espinoza et al., (2024) and in Figures S5 and S6. Furthermore, our results follow the fire anomalies in Jiménez et al., (2024). Even though we find pronounced spatial differences relative to the long-term mean, the total fire counts over the Amazon were similar in magnitude to 2015 and 2016. Fires and deforestation have been linked to drought (Aragão et al., 2007, 2018), with more fires during years of drought (Aragão et al., 2018; Basso et al., 2023; Gatti et al., 2014; Rosan et al., 2024; Silva Junior et al., 2019; van der Laan-Luijkx et al., 2015). Nevertheless, fire emissions in 2023 within the Amazon (0.15 [0.13-0.17] PgC $year^{-1}$, mean between GFAS and GFED4s) were comparable and even lower than non-drought years (e.g. 2022) and similar to the long-term average (see Figure 4 and S7). The individual estimates for GFED4s and GFAS were equal or lower than their long-term averages, respectively. In both products there were less fires compared to the long-term mean in the southeastern border of the Amazon from July to September (Figure 4), when the rainfall anomalies were not as pronounced as in the following months (Oct-Dec). Therefore, our analysis suggests that regardless of an extended fire season, the fire carbon emissions had a smaller contribution to the NBE source in 2023 relative to previous droughts, in which fire changed the sign of NBE from sink to source (Basso et al., 2023; Gatti et al., 2021; van der Laan-Luijkx et al., 2015). We note, though, that the fire inventory products used here (GFAS and GFED4s) tend to underestimate fire emissions, likely due to missing understory fires and small scale fires (Naus et al., 2022; Pessôa et al., 2020). However, the results of Naus et al., (2022) suggest that such underestimation is more pronounced outside of the biogeographic Amazon, in the neighboring Cerrado biome, as also shown by Botía et al., (2024).

Remaining challenges reconciling top-down and bottom-up approaches

The most important differences between top-down and bottom-up NBE are associated with the seasonal timing and the absolute magnitude of NBE. This mismatch is likely due to a misrepresentation of the dry and wet season contrast of NEE, GPP and R_{eco} in DGVMs (Figure 6 and Figure 8), as well as large uncertainty in the bottom-up NBE driven by disturbances and land use change emissions (Rosan et al., 2024). The response of the DGVMs to the development of the drought in 2023 was limited to the dry season when there was a larger spread between models (Figure 6 and Figure 8) and larger inter-annual variability, coinciding with the positive anomalies in VPD and temperature and the negative anomalies in terrestrial water storage and large PCWD (Figure 2 and Figure 3). Conversely, during the wet season, the DGVMs showed a flat and more uniform GPP and TER, suggesting a reduced sensitivity to wet season anomalies, notwithstanding potential biases in the forcing data that would attenuate the severity of the drought (Figure S15). Our study thus adds to the body of literature indicating the limitations

DGVMs have for tropical regions and specifically the Amazon, lacking processes such as (i) leaf phenology and demography, which affect the seasonality in GPP (X. Chen et al., 2020; Kim et al., 2012; Restrepo-Coupe et al., 2017), (ii) low sensitivity of GPP to soil texture (Meunier et al., 2022), (iii) lacking a representation of drought induced tree mortality and therefore biomass reductions (de Almeida Castanho et al., 2016; Powell et al., 2013) and (iv) not simulating secondary forest regrowth leading to difficulties reproducing gains in biomass and thus hindering the simulated changes in AGC (O'Sullivan et al., 2024; Pugh et al., 2019) in DGVMs.

For the top-down approach used here (OCO2-Inv), we acknowledge that cloud cover during the wet season could limit the number of successful XCO_2 retrievals (Frankenberg et al., 2024), inducing a dry-season adjustment bias in the inversion (Crowell et al., 2019; Massie et al., 2017). Furthermore, in-situ data is scarce in the region hindering evaluation of posterior fluxes in satellite-driven inversions and for inversions assimilating flask or in-situ data, leaving no choice but to assimilate most of the available data (Basso et al., 2023; Botía et al., 2024). Additionally, the spatial distribution of the posterior fluxes and their overlap with DGVMs, could be affected by the spatial correlation length scale, which in this study was 500 km. We showed that the strongest carbon sources in the DGVMs overlap to some extent but not entirely, with those in the OCO2-Inv. Therefore, we acknowledge that understanding the causes of the spatial mismatch between top-down and bottom-up approaches should be prioritized in future studies.

The missing disturbance sources in bottom-up NBE assessments that are reported in existing literature include low intensity understory fires (Alencar et al., 2022), missing carbon emissions due to edge effects caused by forest fragmentation (Silva Junior et al., 2020), and an enhanced post-logging respiratory flux which is difficult to quantify as it is a function of recovery time and requires long-term observations (Mills et al., 2023). In addition, a remaining challenge to improve the seasonal development of bottom-up NBE is related with non-fire carbon emissions due to forest degradation (Lapola et al., 2023) and how these vary seasonally and inter-annually. Moreover, the role of CO_2 outgassing from river and aquatic surfaces remains as an ignored flux in recent bottom-up and top-down assessments (Basso et al., 2023; Gatti et al., 2021; Gloor et al., 2012; Rosan et al., 2024), and its role in the Amazon basin seems to result in a weakening of the vegetation (NEE) carbon sink (Hastie et al., 2019). These processes are the remaining challenges in reconciling top-down and bottom-up processes for regional assessments of the carbon cycle response to drought.

5 Conclusions

We studied the Amazon carbon cycle response to the extreme drought in 2023 by using multiple data streams, including land surface models, an atmospheric inversion, remotely-sensed vegetation dynamics and aboveground carbon at the regional scale. In addition we used in-situ measurements from the Amazon Tall Tower Observatory, including eddy covariance fluxes and a decade long CO_2 mole fraction time series to complement the large scale

analysis. At the regional scale, we report that in 2023 the Amazon drought led to a substantial shift in the carbon dynamics of the region, with a net carbon emission (NBE), driven primarily by reduced vegetation uptake. While the fire season extended into November, fire contributions remained near the long-term average, indicating that fires had a smaller influence on the Amazon carbon source compared to vegetation responses. The decline in gross primary productivity (GPP) was particularly strong during October to December coinciding with anomalies in remotely-sensed GPP proxies (i.e. Sun-Induced Fluorescence). During these months anomalously high temperatures, vapor pressure deficits and potential cumulative water deficits were recorded.

Our findings highlight that in early 2023 a relatively large uptake helped to offset the dry-season emissions, possibly driven by a transition from La Niña to El Niño, which was characterized by high precipitation in the beginning of the year in the northern part of the Amazon. Such wet season response was consistent in the atmospheric transport inversion and the local eddy flux measurements, but to a lesser extent in the DGVMs. The low sensitivity of DGVMs to the wet season anomalies in precipitation are partly explained by a bias in the forcing data. However, the observed balance between photosynthesis and respiration in the eddy flux measurements was not reproduced by the DGVMs throughout the year. At ATTO, the seasonal development of NEE was mainly controlled by a large (close to and larger than 1σ) decrease in ecosystem respiration (R_{eco}) in the beginning of the year (January - March), and during the dry season (August - October). Even though we can not attribute the ATTO-eddy-fluxes to all the Amazon region, we believe the comparison points to processes that should be improved in DGVMs to better represent the inter-annual variability of the carbon dynamics in the Amazon.

As Applicable – Inclusion in Global Research Statement

We thank the Instituto Nacional de Pesquisas da Amazonia (Manaus, Brazil) for their technical support managing and running the ATTO research station. Specifically we thank Roberta Pereira de Souza, Bruno Takeshi, Leonardo Ramos de Oliveira, Nagib Alberto de Castro Souza, Amauri Rodriguês Pereira, Hermes Braga Xavier, Jailson da Mata, Valmir Ferreira de Lima, Wallace Rabelo Costa, Antonio Huxley Melo Nascimento, Uwe Schultz, Thomas Seifert, Steffen Schmidt, Thomas Disper, and Sipko Bulthuis.

Acknowledgments

This work and the ATTO project were funded by the German Federal Ministry of Education and Research (BMBF, contracts 01LB1001A and 01LK1602A). The ATTO project is furthermore funded by the Brazilian Ministério da Ciencia, Tecnologia e Inovação (MCTI/FINEP contract

01.11.01248.00) and the Max Planck Society. We acknowledge the Instituto Nacional de Pesquisas da Amazonia as well as the Amazon State University (UEA), FAPEAM, LBA/INPA and SDS/CEUC/RDS-Uatumã for continuous support and logistical management. WP and GK were funded by an ERC-Consolidator grant (649087) as part of the ASICA (Airborne Stable Isotopes of Carbon from the Amazon) project. This study was supported by funding from the European Space Agency Carbon-RO (4000140982/23/I-EF). AB, PC and SS acknowledge support from the CALIPSO project (Carbon Loss in Plant Soils and Oceans) project, funded through the generosity of Eric and Wendy Schmidt by recommendation of the Schmidt Futures program. AB acknowledges funding by the European Union (ERC StG, ForExD, grant agreement No. 101039567). CQD acknowledges support from CNPQ (Processes 440170/2022-2, 406884/2022-6, 307530/2022-1). ITL received funding from the Netherlands Organisation for Scientific Research (grant no. VI.Vidi.213.143). SiB4 simulations were carried out on the Dutch national e-infrastructure with the support of SURF Cooperative (project number NWO-2023.003).

Open Research

The biogeographic Amazon area used for the climate (VPD and 2m temperature) and carbon cycle (DGVMs, OCO2-Inv, and GPP proxies) analysis can be found here: https://edmond.mpg.de/privateurl.xhtml?token=a4af161f-1b77-4611-aa01-7de9203639b8. The ERA5 and ERA5-Land datasets are under public access available here: https://cds.climate.copernicus.eu/datasets/reanalysis-era5-land?tab=overview. For the PCWD calculation we used the following R package: https://zenodo.org/records/5359053. All the processed data integrated for the biogeographic Amazon area can be found here: https://edmond.mpg.de/privateurl.xhtml?token=a062e1cb-9c28-4880-9f99-b9b8a9125dff. This includes the DGVM output and fire emissions (GFED4s and GFAS) from 2003 to 2023, the OCO2-Inv prior and posterior from 2015 to 2023 and the fire counts from MODIS (terra and aqua) from 2003 to 2023. Additionally, on the same repository, the monthly totals of NEE, GPP and Reco at ATTO, together with the monthly mean ΔCO_2 can be also found in tabular form. The GRACE data for the Amazon basin used here can be freely downloaded here: https://grace.jpl.nasa.gov/data-analysis-tool/. The ATTO meteorological data is available at https://www.attodata.org/home/Start. The OCO2-Inv gridded files are available via the atmospheric data store: https://ads.atmosphere.copernicus.eu/datasets. TROPOMI SIF data is available through the S5P-PAL Data Portal (https://data-portal.s5p-pal.com/products/troposif.html). MODIS BRDF-corrected surface reflectance (MCD43C4v061) is available at the Land Processes Distributed Active Archive Center (LP DAAC; https://lpdaac.usgs.gov/products/mcd43c4v061/). The OCO2-SiF data is available from https://oco2.gesdisc.eosdis.nasa.gov/data/OCO2_DATA/OCO2_L2_Lite_SIF.11r/. The L-VOD data can be downloaded here: https://doi.org/10.5281/zenodo.14171387.

References

Alencar, A. A. C., Arruda, V. L. S., Silva, W. V. da, Conciani, D. E., Costa, D. P., Crusco, N., Duverger, S. G., Ferreira, N. C., Franca-Rocha, W., Hasenack, H., Martenexen, L. F. M., Piontekowski, V. J., Ribeiro, N. V., Rosa, E. R., Rosa, M. R., dos Santos, S. M. B., Shimbo, J. Z., & Vélez-Martin, E. (2022). Long-Term Landsat-Based Monthly Burned Area Dataset for the Brazilian Biomes Using Deep Learning. *Remote Sensing*, *14*(11), Article 11. https://doi.org/10.3390/rs14112510

Anderson, L. O., Ribeiro Neto, G., Cunha, A. P., Fonseca, M. G., Mendes de Moura, Y., Dalagnol, R., Wagner, F. H., & de Aragão, L. E. O. e C. (2018). Vulnerability of Amazonian forests to repeated droughts. *Philosophical Transactions of the Royal Society B: Biological Sciences*, *373*(1760), 20170411. https://doi.org/10.1098/rstb.2017.0411

Andreae, M. O., Acevedo, O. C., Araùjo, A., Artaxo, P., Barbosa, C. G. G., Barbosa, H. M. J., Brito, J., Carbone, S., Chi, X., Cintra, B. B. L., da Silva, N. F., Dias, N. L., Dias-Júnior, C. Q., Ditas, F., Ditz, R., Godoi, A. F. L., Godoi, R. H. M., Heimann, M., Hoffmann, T., … Yáñez-Serrano, A. M. (2015). The Amazon Tall Tower Observatory (ATTO): Overview of pilot measurements on ecosystem ecology, meteorology, trace gases, and aerosols. *Atmospheric Chemistry and Physics*, *15*(18), 10723–10776. https://doi.org/10.5194/acp-15-10723-2015

Aragão, L. E. O. C., Anderson, L. O., Fonseca, M. G., Rosan, T. M., Vedovato, L. B., Wagner, F. H., Silva, C. V. J., Junior, C. H. L. S., Arai, E., Aguiar, A. P., Barlow, J., Berenguer, E., Deeter, M. N., Domingues, L. G., Gatti, L., Gloor, M., Malhi, Y., Marengo, J. A., Miller, J. B., … Saatchi, S. (2018). 21st Century drought-related fires counteract the decline of Amazon deforestation carbon emissions. *Nature Communications*, *9*(1), 1–12. https://doi.org/10.1038/s41467-017-02771-y

Aragão, L. E. O. C., Malhi, Y., Roman-Cuesta, R. M., Saatchi, S., Anderson, L. O., & Shimabukuro, Y. E. (2007). Spatial patterns and fire response of recent Amazonian droughts. *Geophysical Research Letters*, *34*(7). https://doi.org/10.1029/2006GL028946

Baker, J. C. A., Garcia-Carreras, L., Gloor, M., Marsham, J. H., Buermann, W., da Rocha, H. R., Nobre, A. D., de Araujo, A. C., & Spracklen, D. V. (2021). Evapotranspiration in the Amazon: Spatial patterns, seasonality, and recent trends in observations, reanalysis, and climate models. *Hydrology and Earth System Sciences*, *25*(4), 2279–2300. https://doi.org/10.5194/hess-25-2279-2021

Basso, L. S., Wilson, C., Chipperfield, M. P., Tejada, G., Cassol, H. L. G., Arai, E., Williams, M., Smallman, T. L., Peters, W., Naus, S., Miller, J. B., & Gloor, M. (2023). Atmospheric CO_2 inversion reveals the Amazon as a minor carbon source caused by fire emissions, with forest uptake offsetting about half of these emissions. *Atmospheric Chemistry and Physics*, *23*(17), 9685–9723. https://doi.org/10.5194/acp-23-9685-2023

Bastos, A., Friedlingstein, P., Sitch, S., Chen, C., Mialon, A., Wigneron, J.-P., Arora, V. K., Briggs, P. R., Canadell, J. G., & Ciais, P. (2018). Impact of the 2015/2016 El Niño on the terrestrial carbon cycle constrained by bottom-up and top-down approaches. *Philosophical Transactions of the Royal Society B: Biological Sciences*, *373*(1760), 20170304.

Berenguer, E., Lennox, G. D., Ferreira, J., Malhi, Y., Aragão, L. E. O. C., Barreto, J. R., Del Bon Espírito-Santo, F., Figueiredo, A. E. S., França, F., Gardner, T. A., Joly, C. A., Palmeira, A. F., Quesada, C. A., Rossi, L. C., de Seixas, M. M. M., Smith, C. C., Withey, K., & Barlow, J. (2021). Tracking the impacts of El Niño drought and fire in human-modified Amazonian forests. *Proceedings of the National Academy of Sciences*, *118*(30), e2019377118. https://doi.org/10.1073/pnas.2019377118

Berenguer, E., Malhi, Y., Brando, P., Cardoso Nunes Cordeiro, A., Ferreira, J., França, F., Chesini Rossi, L., Maria Moraes de Seixas, M., & Barlow, J. (2018). Tree growth and stem carbon accumulation in human-modified Amazonian forests following drought and fire. *Philosophical Transactions of the Royal Society B: Biological Sciences*, *373*(1760), 20170308. https://doi.org/10.1098/rstb.2017.0308

Botía, S., Komiya, S., Marshall, J., Koch, T., Gałkowski, M., Lavric, J., Gomes-Alves, E., Walter, D., Fisch, G., Pinho, D. M., Nelson, B. W., Martins, G., Luijkx, I. T., Koren, G., Florentie, L., Carioca de Araújo, A., Sá, M., Andreae, M. O., Heimann, M., … Gerbig, C. (2022). The CO2 record at the Amazon Tall Tower Observatory: A new opportunity to study processes on seasonal and inter-annual scales. *Global Change Biology*, *28*(2), 588–611. https://doi.org/10.1111/gcb.15905

Botía, S., Munassar, S., Koch, T., Custodio, D., Basso, L. S., Komiya, S., Lavric, J. V., Walter, D., Gloor, M., Martins, G., Naus, S., Koren, G., Luijkx, I., Hantson, S., Miller, J. B., Peters, W., Rödenbeck, C., & Gerbig, C. (2024). Combined CO_2 measurement record indicates decreased Amazon forest carbon uptake, offset by Savannah carbon release. *EGUsphere*, 1–55. https://doi.org/10.5194/egusphere-2024-1735

Brando, P. M., Balch, J. K., Nepstad, D. C., Morton, D. C., Putz, F. E., Coe, M. T., Silvério, D., Macedo, M. N., Davidson, E. A., Nóbrega, C. C., Alencar, A., & Soares-Filho, B. S. (2014). Abrupt increases in Amazonian

tree mortality due to drought–fire interactions. *Proceedings of the National Academy of Sciences*, *111*(17), 6347–6352. https://doi.org/10.1073/pnas.1305499111

Byrne, B., Liu, J., Bowman, K. W., Pascolini-Campbell, M., Chatterjee, A., Pandey, S., Miyazaki, K., van der Werf, G. R., Wunch, D., Wennberg, P. O., Roehl, C. M., & Sinha, S. (2024). Carbon emissions from the 2023 Canadian wildfires. *Nature*, *633*(8031), 835–839. https://doi.org/10.1038/s41586-024-07878-z

Chambers, J. Q., Tribuzy, E. S., Toledo, L. C., Crispim, B. F., Higuchi, N., Santos, J. dos, Araújo, A. C., Kruijt, B., Nobre, A. D., & Trumbore, S. E. (2004). Respiration from a Tropical Forest Ecosystem: Partitioning of Sources and Low Carbon Use Efficiency. *Ecological Applications*, *14*(sp4), 72–88. https://doi.org/10.1890/01-6012

Chen, S., Stark, S. C., Nobre, A. D., Cuartas, L. A., de Jesus Amore, D., Restrepo-Coupe, N., Smith, M. N., Chitra-Tarak, R., Ko, H., Nelson, B. W., & Saleska, S. R. (2024). Amazon forest biogeography predicts resilience and vulnerability to drought. *Nature*, *631*(8019), 111–117. https://doi.org/10.1038/s41586-024-07568-w

Chen, X., Maignan, F., Viovy, N., Bastos, A., Goll, D., Wu, J., Liu, L., Yue, C., Peng, S., Yuan, W., Conceição, A. C. da, O'Sullivan, M., & Ciais, P. (2020). Novel Representation of Leaf Phenology Improves Simulation of Amazonian Evergreen Forest Photosynthesis in a Land Surface Model. *Journal of Advances in Modeling Earth Systems*, *12*(1). https://doi.org/10.1029/2018MS001565

Copernicus. (2024). *Copernicus: 2023 is the hottest year on record, with global temperatures close to the 1.5°C limit | Copernicus*. https://climate.copernicus.eu/copernicus-2023-hottest-year-record

Crowell, S., Baker, D., Schuh, A., Basu, S., Jacobson, A. R., Chevallier, F., Liu, J., Deng, F., Feng, L., McKain, K., Chatterjee, A., Miller, J. B., Stephens, B. B., Eldering, A., Crisp, D., Schimel, D., Nassar, R., O'Dell, C. W., Oda, T., … Jones, D. B. A. (2019). The 2015–2016 carbon cycle as seen from OCO-2 and the global in situ network. *Atmospheric Chemistry and Physics*, *19*(15), 9797–9831. https://doi.org/10.5194/acp-19-9797-2019

de Almeida Castanho, A. D., Galbraith, D., Zhang, K., Coe, M. T., Costa, M. H., & Moorcroft, P. (2016). Changing Amazon biomass and the role of atmospheric CO2 concentration, climate, and land use. *Global Biogeochemical Cycles*, *30*(1), 18–39. https://doi.org/10.1002/2015GB005135

Doughty, C. E., Metcalfe, D. B., Girardin, C. A. J., Amézquita, F. F., Cabrera, D. G., Huasco, W. H., Silva-Espejo, J.

E., Araujo-Murakami, A., da Costa, M. C., Rocha, W., Feldpausch, T. R., Mendoza, A. L. M., da Costa, A. C. L., Meir, P., Phillips, O. L., & Malhi, Y. (2015). Drought impact on forest carbon dynamics and fluxes in Amazonia. *Nature*, *519*(7541), 78–82. https://doi.org/10.1038/nature14213

Erik, van S., Lars, K., Smith Naomi, E., Gerbrand, K., H, van B. L. P., Wouter, P., & T, van der L.-L. I. (2018). Changes in surface hydrology, soil moisture and gross primary production in the Amazon during the 2015/2016 El Niño. *Philosophical Transactions of the Royal Society B: Biological Sciences*, *373*(1760), 20180084. https://doi.org/10.1098/rstb.2018.0084

Espinoza, J.-C., Jimenez, J. C., Marengo, J. A., Schongart, J., Ronchail, J., Lavado-Casimiro, W., & Ribeiro, J. V. M. (2024). The new record of drought and warmth in the Amazon in 2023 related to regional and global climatic features. *Scientific Reports*, *14*(1), 8107. https://doi.org/10.1038/s41598-024-58782-5

Esquivel-Muelbert, A., Phillips, O. L., Brienen, R. J. W., Fauset, S., Sullivan, M. J. P., Baker, T. R., Chao, K.-J., Feldpausch, T. R., Gloor, E., Higuchi, N., Houwing-Duistermaat, J., Lloyd, J., Liu, H., Malhi, Y., Marimon, B., Marimon Junior, B. H., Monteagudo-Mendoza, A., Poorter, L., Silveira, M., … Galbraith, D. (2020). Tree mode of death and mortality risk factors across Amazon forests. *Nature Communications*, *11*(1), 5515. https://doi.org/10.1038/s41467-020-18996-3

Fawcett, D., Sitch, S., Ciais, P., Wigneron, J. P., Silva-Junior, C. H. L., Heinrich, V., Vancutsem, C., Achard, F., Bastos, A., Yang, H., Li, X., Albergel, C., Friedlingstein, P., & Aragão, L. E. O. C. (2023). Declining Amazon biomass due to deforestation and subsequent degradation losses exceeding gains. *Global Change Biology*, *29*(4), 1106–1118. https://doi.org/10.1111/gcb.16513

Feldpausch, T. R., Phillips, O. L., Brienen, R. J. W., Gloor, E., Lloyd, J., Lopez-Gonzalez, G., Monteagudo-Mendoza, A., Malhi, Y., Alarcón, A., Álvarez Dávila, E., Alvarez-Loayza, P., Andrade, A., Aragao, L. E. O. C., Arroyo, L., Aymard C., G. A., Baker, T. R., Baraloto, C., Barroso, J., Bonal, D., … Vos, V. A. (2016). Amazon forest response to repeated droughts. *Global Biogeochemical Cycles*, *30*(7), 964–982. https://doi.org/10.1002/2015GB005133

Foken, T., Göockede, M., Mauder, M., Mahrt, L., Amiro, B., & Munger, W. (2005). Post-Field Data Quality Control. In X. Lee, W. Massman, & B. Law (Eds.), *Handbook of Micrometeorology: A Guide for Surface Flux Measurement and Analysis* (pp. 181–208). Springer Netherlands. https://doi.org/10.1007/1-4020-2265-4_9

Frankenberg, C., Bar-On, Y. M., Yin, Y., Wennberg, P. O., Jacob, D. J., & Michalak, A. M. (2024). Data Drought in

the Humid Tropics: How to Overcome the Cloud Barrier in Greenhouse Gas Remote Sensing. *Geophysical Research Letters*, *51*(8), e2024GL108791. https://doi.org/10.1029/2024GL108791

Friedlingstein, P., O'Sullivan, M., Jones, M. W., Andrew, R. M., Hauck, J., Landschützer, P., Le Quéré, C., Li, H., Luijkx, I. T., Olsen, A., Peters, G. P., Peters, W., Pongratz, J., Schwingshackl, C., Sitch, S., Canadell, J. G., Ciais, P., Jackson, R. B., Alin, S. R., … Zeng, J. (2024). Global Carbon Budget 2024. *Earth System Science Data Discussions*, 1–133. https://doi.org/10.5194/essd-2024-519

Gatti, L. V., Basso, L. S., Miller, J. B., Gloor, M., Gatti Domingues, L., Cassol, H. L. G., Tejada, G., Aragão, L. E. O. C., Nobre, C., Peters, W., Marani, L., Arai, E., Sanches, A. H., Corrêa, S. M., Anderson, L., Von Randow, C., Correia, C. S. C., Crispim, S. P., & Neves, R. A. L. (2021). Amazonia as a carbon source linked to deforestation and climate change. *Nature*, *595*(7867), 388–393. https://doi.org/10.1038/s41586-021-03629-6

Gatti, L. V., Gloor, M., Miller, J. B., Doughty, C. E., Malhi, Y., Domingues, L. G., Basso, L. S., Martinewski, A., Correia, C. S. C., Borges, V. F., Freitas, S., Braz, R., Anderson, L. O., Rocha, H., Grace, J., Phillips, O. L., & Lloyd, J. (2014). Drought sensitivity of Amazonian carbon balance revealed by atmospheric measurements. *Nature*, *506*(7486), 76–80. https://doi.org/10.1038/nature12957

Gloor, M., Gatti, L., Brienen, R., Feldpausch, T. R., Phillips, O. L., Miller, J., Ometto, J. P., Rocha, H., Baker, T., de Jong, B., Houghton, R. A., Malhi, Y., Aragão, L. E. O. C., Guyot, J.-L., Zhao, K., Jackson, R., Peylin, P., Sitch, S., Poulter, B., … Lloyd, J. (2012). The carbon balance of South America: A review of the status, decadal trends and main determinants. *Biogeosciences*, *9*(12), 5407–5430. https://doi.org/10.5194/bg-9-5407-2012

Gloor, M., Wilson, C., Chipperfield, M. P., Chevallier, F., Buermann, W., Boesch, H., Parker, R., Somkuti, P., Gatti, L. V., Correia, C., Domingues, L. G., Peters, W., Miller, J., Deeter, M. N., & Sullivan, M. J. P. (2018). Tropical land carbon cycle responses to 2015/16 El Niño as recorded by atmospheric greenhouse gas and remote sensing data. *Philosophical Transactions of the Royal Society B: Biological Sciences*, *373*(1760), 20170302. https://doi.org/10.1098/rstb.2017.0302

Hartmann, H., Bastos, A., Das, A. J., Esquivel-Muelbert, A., Hammond, W. M., Martínez-Vilalta, J., McDowell, N. G., Powers, J. S., Pugh, T. A., & Ruthrof, K. X. (2022). Climate change risks to global forest health: Emergence of unexpected events of elevated tree mortality worldwide. *Annual Review of Plant Biology*, *73*,

673–702.

Hastie, A., Lauerwald, R., Ciais, P., & Regnier, P. (2019). Aquatic carbon fluxes dampen the overall variation of net ecosystem productivity in the Amazon basin: An analysis of the interannual variability in the boundless carbon cycle. *Global Change Biology*, *25*(6), 2094–2111. https://doi.org/10.1111/gcb.14620

Hersbach, H., Bell, B., Berrisford, P., Hirahara, S., Horányi, A., Muñoz-Sabater, J., Nicolas, J., Peubey, C., Radu, R., Schepers, D., Simmons, A., Soci, C., Abdalla, S., Abellan, X., Balsamo, G., Bechtold, P., Biavati, G., Bidlot, J., Bonavita, M., … Thépaut, J.-N. (2020). The ERA5 global reanalysis. *Quarterly Journal of the Royal Meteorological Society*, *146*(730), 1999–2049. https://doi.org/10.1002/qj.3803

Jimenez, J. C., Barichivich, J., Mattar, C., Takahashi, K., Santamaría-Artigas, A., Sobrino, J. A., & Malhi, Y. (2018). Spatio-temporal patterns of thermal anomalies and drought over tropical forests driven by recent extreme climatic anomalies. *Philosophical Transactions of the Royal Society B: Biological Sciences*, *373*(1760), 20170300. https://doi.org/10.1098/rstb.2017.0300

Jiménez, J. C., Miranda, V., Trigo, I., Libonati, R., Albuquerque, R., Peres, L. F., Espinoza, J.-C., & Marengo, J. A. (2024). Vegetation Warming and Greenness Decline across Amazonia during the Extreme Drought of 2023. *Remote Sensing*, *16*(14), Article 14. https://doi.org/10.3390/rs16142519

Jiménez-Muñoz, J. C., Mattar, C., Barichivich, J., Santamaría-Artigas, A., Takahashi, K., Malhi, Y., Sobrino, J. A., & Schrier, G. van der. (2016a). Record-breaking warming and extreme drought in the Amazon rainforest during the course of El Niño 2015–2016. *Scientific Reports*, *6*(1), 33130. https://doi.org/10.1038/srep33130

Jiménez-Muñoz, J. C., Mattar, C., Barichivich, J., Santamaría-Artigas, A., Takahashi, K., Malhi, Y., Sobrino, J. A., & Schrier, G. van der. (2016b). Record-breaking warming and extreme drought in the Amazon rainforest during the course of El Niño 2015–2016. *Scientific Reports*, *6*(1). https://doi.org/10.1038/srep33130

Kaiser, J. W., Heil, A., Andreae, M. O., Benedetti, A., Chubarova, N., Jones, L., Morcrette, J.-J., Razinger, M., Schultz, M. G., Suttie, M., & van der Werf, G. R. (2012). Biomass burning emissions estimated with a global fire assimilation system based on observed fire radiative power. *Biogeosciences*, *9*(1), 527–554. https://doi.org/10.5194/bg-9-527-2012

Ke, P., Ciais, P., Sitch, S., Li, W., Bastos, A., Liu, Z., Xu, Y., Gui, X., Bian, J., Goll, D. S., Xi, Y., Li, W., O'Sullivan, M., de Souza, J. G., Friedlingstein, P., & Chevallier, F. (2024). Low latency carbon budget analysis reveals a large decline of the land carbon sink in 2023. *National Science Review*, nwae367.

https://doi.org/10.1093/nsr/nwae367

Kim, Y., Knox, R. G., Longo, M., Medvigy, D., Hutyra, L. R., Pyle, E. H., Wofsy, S. C., Bras, R. L., & Moorcroft, P. R. (2012). Seasonal carbon dynamics and water fluxes in an Amazon rainforest. *Global Change Biology*, *18*(4), 1322–1334. https://doi.org/10.1111/j.1365-2486.2011.02629.x

Lan, X., Mund, J. W., Crotwell, A. M., Thoning, K. W., Moglia, E., Madronich, M., Baugh, K., Petron, G., Crotwell, M. J., Neff, D., Wolter, S., Mefford, T., & DeVogel, S. (2024). *Atmospheric Carbon Dioxide Dry Air Mole Fractions from the NOAA GML Carbon Cycle Cooperative Global Air Sampling Network, 1968-2023* (Version 2024-07-30) [Dataset]. https://doi.org/10.15138/wkgj-f215

Lan, X., Tans, P., & Thoning, K. W. (2024). *Trends in globally-averaged CO2 determined from NOAA Global Monitoring Laboratory measurements* (Version Tuesday, 05-Nov-2024 13:17:54 MST) [Dataset]. https://doi.org/10.15138/9N0H-ZH07

Lapola, D. M., Pinho, P., Barlow, J., Aragão, L. E. O. C., Berenguer, E., Carmenta, R., Liddy, H. M., Seixas, H., Silva, C. V. J., Silva-Junior, C. H. L., Alencar, A. A. C., Anderson, L. O., Armenteras, D., Brovkin, V., Calders, K., Chambers, J., Chini, L., Costa, M. H., Faria, B. L., … Walker, W. S. (2023). The drivers and impacts of Amazon forest degradation. *Science*, *379*(6630), eabp8622. https://doi.org/10.1126/science.abp8622

Liu, J., Bowman, K. W., Schimel, D. S., Parazoo, N. C., Jiang, Z., Lee, M., Bloom, A. A., Wunch, D., Frankenberg, C., Sun, Y., & others. (2017). Contrasting carbon cycle responses of the tropical continents to the 2015–2016 El Niño. *Science*, *358*(6360), eaam5690.

Liu, S., McVicar, T. R., Wu, X., Cao, X., & Liu, Y. (2024). Assessing the relative importance of dry-season incoming solar radiation and water storage dynamics during the 2005, 2010 and 2015 southern Amazon droughts: Not all droughts are created equal. *Environmental Research Letters*, *19*(3), 034027. https://doi.org/10.1088/1748-9326/ad281e

MacCarthy, J., Tyukavina, A., Weisse, M. J., Harris, N., & Glen, E. (2024). Extreme wildfires in Canada and their contribution to global loss in tree cover and carbon emissions in 2023. *Global Change Biology*, *30*(6), e17392. https://doi.org/10.1111/gcb.17392

Marengo, J. A., Tomasella, J., Alves, L. M., Soares, W. R., & Rodriguez, D. A. (2011). The drought of 2010 in the context of historical droughts in the Amazon region. *Geophysical Research Letters*, *38*(12).

https://doi.org/10.1029/2011GL047436

Massie, S. T., Sebastian Schmidt, K., Eldering, A., & Crisp, D. (2017). Observational evidence of 3-D cloud effects in OCO-2 CO2 retrievals. *Journal of Geophysical Research: Atmospheres*, *122*(13), 7064–7085. https://doi.org/10.1002/2016JD026111

Mauder, M., & Foken, T. (2004). *Documentation and Instruction Manual of the Eddy Covariance Software Package TK2*.

Metcalfe, D. B., Meir, P., Aragão, L. E. O. C., Lobo-do-Vale, R., Galbraith, D., Fisher, R. A., Chaves, M. M., Maroco, J. P., da Costa, A. C. L., de Almeida, S. S., Braga, A. P., Gonçalves, P. H. L., de Athaydes, J., da Costa, M., Portela, T. T. B., de Oliveira, A. a. R., Malhi, Y., & Williams, M. (2010). Shifts in plant respiration and carbon use efficiency at a large-scale drought experiment in the eastern Amazon. *New Phytologist*, *187*(3), 608–621. https://doi.org/10.1111/j.1469-8137.2010.03319.x

Meunier, F., Verbruggen, W., Verbeeck, H., & Peaucelle, M. (2022). Low sensitivity of three terrestrial biosphere models to soil texture over the South American tropics. *Geoscientific Model Development*, *15*(20), 7573–7591. https://doi.org/10.5194/gmd-15-7573-2022

Mills, M. B., Malhi, Y., Ewers, R. M., Kho, L. K., Teh, Y. A., Both, S., Burslem, D. F. R. P., Majalap, N., Nilus, R., Huaraca Huasco, W., Cruz, R., Pillco, M. M., Turner, E. C., Reynolds, G., & Riutta, T. (2023). Tropical forests post-logging are a persistent net carbon source to the atmosphere. *Proceedings of the National Academy of Sciences*, *120*(3), e2214462120. https://doi.org/10.1073/pnas.2214462120

Muñoz-Sabater, J., Dutra, E., Agustí-Panareda, A., Albergel, C., Arduini, G., Balsamo, G., Boussetta, S., Choulga, M., Harrigan, S., Hersbach, H., Martens, B., Miralles, D. G., Piles, M., Rodríguez-Fernández, N. J., Zsoter, E., Buontempo, C., & Thépaut, J.-N. (2021). ERA5-Land: A state-of-the-art global reanalysis dataset for land applications. *Earth System Science Data*, *13*(9), 4349–4383. https://doi.org/10.5194/essd-13-4349-2021

Naus, S., Domingues, L. G., Krol, M., Luijkx, I. T., Gatti, L. V., Miller, J. B., Gloor, E., Basu, S., Correia, C., Koren, G., Worden, H. M., Flemming, J., Pétron, G., & Peters, W. (2022). Sixteen years of MOPITT satellite data strongly constrain Amazon CO fire emissions. *Atmospheric Chemistry and Physics*, *22*(22), 14735–14750. https://doi.org/10.5194/acp-22-14735-2022

O'Sullivan, M., Sitch, S., Friedlingstein, P., Luijkx, I. T., Peters, W., Rosan, T. M., Arneth, A., Arora, V. K.,

Chandra, N., Chevallier, F., Ciais, P., Falk, S., Feng, L., Gasser, T., Houghton, R. A., Jain, A. K., Kato, E., Kennedy, D., Knauer, J., … Zaehle, S. (2024). The key role of forest disturbance in reconciling estimates of the northern carbon sink. *Communications Earth & Environment*, *5*(1), 1–10. https://doi.org/10.1038/s43247-024-01827-4

Palmer, P. I., Feng, L., Baker, D., Chevallier, F., Bösch, H., & Somkuti, P. (2019). Net carbon emissions from African biosphere dominate pan-tropical atmospheric CO2 signal. *Nature Communications*, *10*(1), 3344. https://doi.org/10.1038/s41467-019-11097-w

Pessôa, A. C. M., Anderson, L. O., Carvalho, N. S., Campanharo, W. A., Junior, C. H. L. S., Rosan, T. M., Reis, J. B. C., Pereira, F. R. S., Assis, M., Jacon, A. D., Ometto, J. P., Shimabukuro, Y. E., Silva, C. V. J., Pontes-Lopes, A., Morello, T. F., & Aragão, L. E. O. C. (2020). Intercomparison of Burned Area Products and Its Implication for Carbon Emission Estimations in the Amazon. *Remote Sensing*, *12*(23), Article 23. https://doi.org/10.3390/rs12233864

Phillips, O. L., Aragao, L. E. O. C., Lewis, S. L., Fisher, J. B., Lloyd, J., Lopez-Gonzalez, G., Malhi, Y., Monteagudo, A., Peacock, J., Quesada, C. A., van der Heijden, G., Almeida, S., Amaral, I., Arroyo, L., Aymard, G., Baker, T. R., Banki, O., Blanc, L., Bonal, D., … Torres-Lezama, A. (2009). Drought Sensitivity of the Amazon Rainforest. *Science*, *323*(5919), 1344–1347. https://doi.org/10.1126/science.1164033

Powell, T. L., Galbraith, D. R., Christoffersen, B. O., Harper, A., Imbuzeiro, H. M. A., Rowland, L., Almeida, S., Brando, P. M., da Costa, A. C. L., Costa, M. H., Levine, N. M., Malhi, Y., Saleska, S. R., Sotta, E., Williams, M., Meir, P., & Moorcroft, P. R. (2013). Confronting model predictions of carbon fluxes with measurements of Amazon forests subjected to experimental drought. *New Phytologist*, *200*(2), 350–365. https://doi.org/10.1111/nph.12390

Powers, J. S., Vargas G., G., Brodribb, T. J., Schwartz, N. B., Pérez-Aviles, D., Smith-Martin, C. M., Becknell, J. M., Aureli, F., Blanco, R., Calderón-Morales, E., Calvo-Alvarado, J. C., Calvo-Obando, A. J., Chavarría, M. M., Carvajal-Vanegas, D., Jiménez-Rodríguez, C. D., Murillo Chacon, E., Schaffner, C. M., Werden, L. K., Xu, X., & Medvigy, D. (2020). A catastrophic tropical drought kills hydraulically vulnerable tree species. *Global Change Biology*, *26*(5), 3122–3133. https://doi.org/10.1111/gcb.15037

Pugh, T. A. M., Lindeskog, M., Smith, B., Poulter, B., Arneth, A., Haverd, V., & Calle, L. (2019). Role of forest

regrowth in global carbon sink dynamics. *Proceedings of the National Academy of Sciences*, *116*(10), 4382–4387. https://doi.org/10.1073/pnas.1810512116

Restrepo‐Coupe, N., Levine, N. M., Christoffersen, B. O., Albert, L. P., Wu, J., Costa, M. H., Galbraith, D., Imbuzeiro, H., Martins, G., Araujo, A. C. da, Malhi, Y. S., Zeng, X., Moorcroft, P., & Saleska, S. R. (2017). Do dynamic global vegetation models capture the seasonality of carbon fluxes in the Amazon basin? A data-model intercomparison. *Global Change Biology*, *23*(1), 191–208. https://doi.org/10.1111/gcb.13442

Rödenbeck, C., Zaehle, S., Keeling, R., & Heimann, M. (2018). History of El Niño impacts on the global carbon cycle 1957–2017: A quantification from atmospheric CO_2 data. *Philosophical Transactions of the Royal Society B: Biological Sciences*, *373*(1760), 20170303. https://doi.org/10.1098/rstb.2017.0303

Rosan, T. M., Sitch, S., O'Sullivan, M., Basso, L. S., Wilson, C., Silva, C., Gloor, E., Fawcett, D., Heinrich, V., Souza, J. G., Bezerra, F. G. S., von Randow, C., Mercado, L. M., Gatti, L., Wiltshire, A., Friedlingstein, P., Pongratz, J., Schwingshackl, C., Williams, M., … Aragão, L. E. O. C. (2024). Synthesis of the land carbon fluxes of the Amazon region between 2010 and 2020. *Communications Earth & Environment*, *5*(1), 1–15. https://doi.org/10.1038/s43247-024-01205-0

Schimel, D., Stephens, B. B., & Fisher, J. B. (2015). Effect of increasing CO_2 on the terrestrial carbon cycle. *Proceedings of the National Academy of Sciences*, *112*(2), 436–441. https://doi.org/10.1073/pnas.1407302112

Silva Junior, C. H. L., Anderson, L. O., Silva, A. L., Almeida, C. T., Dalagnol, R., Pletsch, M. A. J. S., Penha, T. V., Paloschi, R. A., & Aragão, L. E. O. C. (2019). Fire Responses to the 2010 and 2015/2016 Amazonian Droughts. *Frontiers in Earth Science*, *7*. https://doi.org/10.3389/feart.2019.00097

Silva Junior, C. H. L., Aragão, L. E. O. C., Anderson, L. O., Fonseca, M. G., Shimabukuro, Y. E., Vancutsem, C., Achard, F., Beuchle, R., Numata, I., Silva, C. A., Maeda, E. E., Longo, M., & Saatchi, S. S. (2020). Persistent collapse of biomass in Amazonian forest edges following deforestation leads to unaccounted carbon losses. *Science Advances*, *6*(40), eaaz8360. https://doi.org/10.1126/sciadv.aaz8360

Stocker, B. D., Tumber-Dávila, S. J., Konings, A. G., Anderson, M. C., Hain, C., & Jackson, R. B. (2023). Global patterns of water storage in the rooting zones of vegetation. *Nature Geoscience*, *16*(3), 250–256. https://doi.org/10.1038/s41561-023-01125-2

Trenberth, K. E., Caron, J. M., Stepaniak, D. P., & Worley, S. (2002). Evolution of El Niño–Southern Oscillation and

global atmospheric surface temperatures. *Journal of Geophysical Research: Atmospheres*, *107*(D8), AAC 5-1-AAC 5-17. https://doi.org/10.1029/2000JD000298

van Asperen, H., Jones, S., Lavric, J., Walter, D., Sierra, C., Horna, V., Komiya, S., Botía, S., Warneke, T., Griffith, D., Heimann, M., Andreae, M., & Trumbore, S. (2024). *Long term continuous high-precision greenhouse gas observation at the ATTO fieldsite: An overview*. https://proceedings.science/icdc-2024/papers/long-term-continuous-high-precision-greenhouse-gas-observation-at-the-atto-field?lang=en

van der Laan-Luijkx, I. T., van der Velde, I. R., Krol, M. C., Gatti, L. V., Domingues, L. G., Correia, C. S. C., Miller, J. B., Gloor, M., van Leeuwen, T. T., Kaiser, J. W., Wiedinmyer, C., Basu, S., Clerbaux, C., & Peters, W. (2015). Response of the Amazon carbon balance to the 2010 drought derived with CarbonTracker South America. *Global Biogeochemical Cycles*, *29*(7), 1092–1108. https://doi.org/10.1002/2014GB005082

van der Werf, G. R., Randerson, J. T., Giglio, L., Leeuwen, T. T. van, Chen, Y., Rogers, B. M., Mu, M., Marle, M. J. E. van, Morton, D. C., Collatz, G. J., Yokelson, R. J., & Kasibhatla, P. S. (2017). Global fire emissions estimates during 1997–2016. *Earth System Science Data*, *9*(2), 697–720. https://doi.org/10.5194/essd-9-697-2017

Vickers, D., & Mahrt, L. (1997). Quality Control and Flux Sampling Problems for Tower and Aircraft Data. *Journal of Atmospheric and Oceanic Technology*, *14*(3), 512–526. https://doi.org/10.1175/1520-0426(1997)014<0512:QCAFSP>2.0.CO;2

Wang, J., Zeng, N., Wang, M., Jiang, F., Chevallier, F., Crowell, S., He, W., Johnson, M. S., Liu, J., Liu, Z., Miller, S. M., Philip, S., Wang, H., Wu, M., Ju, W., Feng, S., & Jia, M. (2023). Anomalous Net Biome Exchange Over Amazonian Rainforests Induced by the 2015/16 El Niño: Soil Dryness-Shaped Spatial Pattern but Temperature-dominated Total Flux. *Geophysical Research Letters*, *50*(11), e2023GL103379. https://doi.org/10.1029/2023GL103379

Wigneron, J.-P., Fan, L., Ciais, P., Bastos, A., Brandt, M., Chave, J., Saatchi, S., Baccini, A., & Fensholt, R. (2020). Tropical forests did not recover from the strong 2015–2016 El Niño event. *Science Advances*, *6*(6). https://doi.org/10.1126/sciadv.aay4603

Winderlich, J., Gerbig, C., Kolle, O., & Heimann, M. (2014). Inferences from CO_2 and CH_4 concentration profiles at the Zotino Tall Tower Observatory (ZOTTO) on regional summertime ecosystem fluxes. *Biogeosciences*,

11(7), 2055–2068. https://doi.org/10.5194/bg-11-2055-2014

WWA. (2024). *Climate change, not El Niño, main driver of exceptional drought in highly vulnerable Amazon River Basin – World Weather Attribution*. https://www.worldweatherattribution.org/climate-change-not-el-nino-main-driver-of-exceptional-drought-in-highly-vulnerable-amazon-river-basin/

Yang, H., Ciais, P., Wigneron, J.-P., Chave, J., Cartus, O., Chen, X., Fan, L., Green, J. K., Huang, Y., Joetzjer, E., Kay, H., Makowski, D., Maignan, F., Santoro, M., Tao, S., Liu, L., & Yao, Y. (2022). Climatic and biotic factors influencing regional declines and recovery of tropical forest biomass from the 2015/16 El Niño. *Proceedings of the National Academy of Sciences*, *119*(26), e2101388119. https://doi.org/10.1073/pnas.2101388119

Yang, J., Tian, H., Pan, S., Chen, G., Zhang, B., & Dangal, S. (2018). Amazon drought and forest response: Largely reduced forest photosynthesis but slightly increased canopy greenness during the extreme drought of 2015/2016. *Global Change Biology*, *24*(5), 1919–1934. https://doi.org/10.1111/gcb.14056

AGU Advances

Supporting Information for

Reduced vegetation uptake during the extreme 2023 drought turns the Amazon into a weak carbon source

S. Botía[1], C. Q. Dias-Junior[2], S. Komiya[3], A. M. van der Woude[4], M. Terristi[5,9], R.J. de Kok[4,8], G. Koren[7], H. van Asperen[3], S. P. Jones[3], F.A.F. D'Oliveira[2], U. Weber[9], E. P. Marques-Filho[10], I.M. Cely[11], A. Araujo[12], J. V. Lavric[13], D. Walter[14], X. Li[15], J.P. Wigneron[15], B. D. Stocker[6,21], J. Gonçalves de Souza[16], M. O'Sullivan[16], S. Sitch[16], P. Ciais[17], F. Chevallier[17], W. Li[18], I. Luijkx[4], W. Peters[4,19], C. A. Quesada[20], S. Zaehle[1], S. Trumbore[3], and A. Bastos[5,9]

[1]Biogeochemical Signals Department, Max Planck Institute for Biogeochemistry, Jena, Germany

[2]Departamento de Física, Instituto Federal de Educação, Ciência e Tecnologia do Pará, Belém, Brazil

[3]Biogeochemical Processes Department, Max Planck Institute for Biogeochemistry, Jena, Germany

[4]Wageningen University, Meteorology & Air Quality Dept, Wageningen, The Netherlands

[5]Institute for Earth System Science and Remote Sensing, Leipzig University

[6]Institute of Geography, University of Bern, Hallerstrasse 12, 3012 Bern, Switzerland

[7]Copernicus Institute of Sustainable Development, Utrecht University, Utrecht, The Netherlands

[8]ICOS ERIC, Carbon Portal, Geocentrum II, Sölvegatan 12, SE-22362, Lund, Sweden

[9]Biogeochemical Integration Department, Max Planck Institute for Biogeochemistry, Jena, Germany

[10]Departamento de Física, Universidade Federal da Bahia, Salvador, Brazil

[11]Atmospheric Physics Laboratory, University of São Paulo, São Paulo, Brazil

[12]Embrapa Amazônia Oriental, Belém, Pará, Brazil

[13]Acoem GmbH, Hallbergmoos, Germany

[14]Multiphase Chemistry Department, Max Planck Institute for Chemistry, Mainz, Germany

[15]INRAE, UMR1391 ISPA, 33140 Villenave d'Ornon, France

[16]Faculty of Environment, Science and Economy, University of Exeter, Exeter, UK.

[17]LSCE/IPSL, CEA-CNRS-UVSQ, Université Paris-Saclay, 91191 Gif-sur-Yvette, France

[18]Department of Earth System Science, Ministry of Education Key Laboratory for Earth System Modeling, Institute for Global Change Studies, Tsinghua University, Beijing, China

[19]University of Groningen, Centre for Isotope Research, Nijenborgh 6, Groningen, The Netherlands

[20]Instituto Nacional de Pesquisas da Amazônia (INPA), Manaus, Brazil

[21]Oeschger Centre for Climate Change Research, University of Bern, Bern, Switzerland

Contents of this file

Introduction

The information in this document supports the methods section (Text S1 to S5) of the main text and includes additional Figures (Figures S1 to S17) that help to convey the messages on the main text.

Text S1. Reanalysis Data

We use the ERA5 reanalysis dataset (Hersbach et al., 2020), provided by the European Centre for Medium-Range Weather Forecasts (ECMWF) through the Copernicus Climate Change Service (C3S) Climate Data Store (CDS). This dataset offers a comprehensive reanalysis of global weather conditions from 1950 to the present (Bell et al., 2021), featuring a spatial resolution of approximately 31 km (0.25° x 0.25° grid) and hourly temporal resolution. To characterize the synoptic-scale drivers, monthly mean anomalies were computed for sea surface temperature (SST, K), horizontal wind components (u, v, in m s-1), geopotential height (Z) at 500hPa (m^2 s-2) and the vertical integral of eastward water vapor flux in kilograms per meter per second (kg m^{-1} s^{-1}). These anomalies were calculated relative to the 2000–2023 climatological mean seasonal cycle. Based on ERA5 fields, we further calculated the cumulative water deficit (PCWD) based on the weekly difference between precipitation (P) and potential evapotranspiration (PET) following Stocker et al., (2023). Note that in ERA5, PET is calculated using the Penman-Monteith formulation for a well-watered reference crops. PCWD allows detecting periods when the atmospheric evaporative demand (potential evapotranspiration) exceeds water input from precipitation, and quantifies the cumulative effects of the imbalance between radiation and precipitation until rain terminates the event, i.e. the deficit cumulation. The deficit is reset to zero following sufficient rainfall; i.e., when the weekly water balance compensates the current cumulative water deficit. Where annual total PET generally exceeds annual total P we reset PCWD during the wettest months to avoid unrealistically long PCWD accumulation periods in arid regions. Note that the use of PET generally exceeds actual PCWD in areas where stomatal regulation reduces evapotranspiration. To quantify spatial anomalies in vapor pressure deficit (VPD) and temperature over the biogeographic Amazon, we used the ERA5-Land dataset (Muñoz-Sabater et al., 2021)

retrieved from the Copernicus Climate Change Service, (2022). We downloaded the dataset at hourly resolution, with 0.1 x 0.1 degree spatial resolution. As VPD is not directly provided by ERA5, we derived it using 2m air temperature and relative humidity at hourly resolution. The anomalies in VPD and temperature were also relative to the period from 2000 to 2023. The shape file containing the area corresponding to the biogeographic Amazon, used in the climate analyses and throughout this paper, can be downloaded here: https://edmond.mpg.de/privateurl.xhtml?token=a4af161f-1b77-4611-aa01-7de9203639b8.

Text S2. Bottom-up Model Simulations

We used simulations from four terrestrial biosphere models forced with historical climate from ERA5 reanalysis in near-real time. The contributing models were the Simple Biosphere model Version 4 (SiB4, Haynes et al., 2019), ORCHIDEE-MICT (Guimberteau et al., 2018; Krinner et al., 2005) , O-CN (hereafter referred to as OCN, Zaehle et al., 2010) and JULES (Clark et al., 2011). All models simulate water, energy, carbon allocation and exchange, vegetation growth, and soil carbon changes driven by a common set of forcing data, but they differ on the number of plant functional types that they represent and the processes included. The model simulations were conducted at 0.5 x 0.5 degree spatial resolution and were done using changing climate forcing at 3-hourly (JULES), 6-hourly (ORCHIDEE), and daily (OCN) temporal resolution from 1960 to 2023 and annual CO_2, following a spin-up with recycled 1960s climate and 1960 CO_2 levels to equilibrate carbon pools. Both the spin-up and the transient simulations used a fixed land-cover map based on the Land-Use Harmonization dataset for global carbon budgets (LUH-GCB, Chini et al., 2021) in the year 2010. The fixed land-cover aims to reduce variability introduced by land-cover changes (Bastos et al., 2020), given that the main interest in this study is to evaluate climate impacts. The choice of 2010 ensures a land-cover distribution close to the present state, but we note that this can lead to inconsistencies in the absolute fluxes estimated by the bottom-up models, when compared to inversions and in-situ observations. The simulations by SiB4 were done at 3-hourly temporal resolution for the period 1980-2023 and used a land-cover distribution based on MODIS data between 2001-2003 (Lawrence & Chase, 2007). For practical reasons we will refer to the four bottom-up models as DGVMs. Note that from all the models we obtained Net Ecosystem Exchange (NEE, see section 2.6) by using the simulated Gross Primary Productivity (GPP) and Total Ecosystem Respiration (TER). We do not include the Fire emissions simulated in the DGVMs and

thus we obtain the Net Biome Exchange (NBE) from the DGVMs using the fire emissions from remote-sensing-based products, see Figure 1 for more details.

Text S3. Top-down OCO2-Inversion (OCO2-Inv)

We used a global high resolution (1 x 1 degree) atmospheric inversion driven by the OCO-2 satellite atmospheric CO_2 concentration data from the Copernicus Atmosphere Monitoring Service (CAMS, https://atmosphere.copernicus.eu). CAMS delivers global estimates of weekly greenhouse gas fluxes with a typical 4-month latency. The product used here is an intermediate version between versions FT23r3 and FT24r1. It differs from version FT24r1 only by its regular resolution of 0.7 degree in latitude and 1.4 degree in longitude and follows the usual production and quality-control process of the CAMS products. It covers the OCO-2 period from 2015 to December 2023, and its mean fluxes and anomalies are close to the median of 14 inversions used in previous assessments (Friedlingstein et al., 2023). The underlying transport model was nudged towards horizontal winds from the ERA5 reanalysis. The inferred fluxes were estimated in each horizontal grid point of the transport model with a temporal resolution of 8 days, separately for day-time and night-time. The prior values of the fluxes combine estimates of (i) gridded monthly fossil fuel and cement emissions (GCP-GridFED version 2023.1, Jones et al., 2021) extended to year 2023 following Chevallier et al., (2020) using the emission changes reported by https://carbonmonitor.org/, together with anomalies in retrievals of NO_2 columns from the Tropospheric Monitoring Instrument (TROPOMI, van Geffen et al., (2019), (ii) monthly ocean fluxes (Chau, Chevallier, et al., 2024; Chau, Gehlen, et al., 2024), 3-hourly (when available) or monthly biomass burning emissions (GFED 4.1s) described in van der Werf et al., (2017) and climatological 3-hourly biosphere-atmosphere fluxes taken as the 1981-2020 mean of a simulation of the ORCHIDEE model, version 2.2, revision 7262 (ORCHIDEE, Krinner et al., (2005)). The variational inversion accounts for spatial and temporal correlations of the prior errors, resulting in a total 1-sigma uncertainty for the prior fluxes over a full year of 3.0 $PgC \cdot year^{-1}$ for the land pixels and of 0.2 $PgC \cdot year^{-1}$ for the marine pixels. Over land, the correlations decrease exponentially with a length of 500 km. To make the inverse estimates comparable with the DGVMs we have subtracted the lateral fluxes from the NBE estimates using the data available here: https://meta.icos-cp.eu/objects/FHbD8OTgCb7Tlvs99lUDApO0, last accessed 28, May, 2024.

Text S4. Remote sensing datasets

Sun-induced fluorescence (SIF) is a proxy for photosynthesis rate (Frankenberg et al., 2011) and can therefore be used as an approximation for gross primary productivity (GPP) by vegetation. SIF (L1 product) is taken from the OCO-2 satellite (Kurosu et al., 2022, c.f. Parazoo et al., 2019), hereafter OCO2-SIF. We use the daily SIF at 740 nm, which is calculated based on the retrievals at 757 nm and 771 nm. We use only full years from 2014 to 2023 and select all retrievals that have passed the quality control (quality flag < 2) within the biogeographic Amazon. In addition, we used Sentinel-5p TROPOMI SIF L3 data (Guanter et al., 2021) for the years 2018-2023. Furthermore, we have included another GPP proxy, the Near-Infrared Reflectance of vegetation (NIRv) (Badgley et al., 2017), which has been used previously to quantify the impact of drought on photosynthesis (Smith et al., 2020; van der Woude et al., 2023). Here, we calculated NIRv from MODIS surface reflectance with Bi-Directional Reflectance Distribution Function (BRDF) correction, from retrieval algorithm v6.1 (Schaaf & Wang, 2021). Following Badgley et al. (2017), we used an empirical correction for removing the effect of soil reflectance.

Aboveground biomass (AGB) changes were estimated from L-band Vegetation Optical Depth (L-VOD) data computed from observations of the SMOS (Soil Moisture and Ocean Salinity) passive microwave satellite using the SMOS-IC version 2 (V2) algorithm (Wigneron et al., 2021, 2024). As most spaceborne sensors have a limited capability to quantify high carbon density in the Amazon forest, the SMOS L-VOD AGB dataset, which does not present obvious saturation in dense tropical forest areas, is now a major satellite-based dataset for monitoring inter-annual changes of AGB (Brandt et al., 2018; Fan et al., 2023; Qin et al., 2021; Wigneron et al., 2024; Yang et al., 2023). Here, we calculated the annual global L-VOD AGB using the following steps. First, we only chose the ascending daily L-VOD observations (acquired at 6 am), which are less affected by diurnal changes in the vegetation moisture. Then, yearly median L-VOD values were estimated for each grid cell and converted to carbon density using previously published biomass map as references for regressions between annual median of L-VOD (2011) and AGB maps. No single AGB benchmark map can be considered completely reliable, and all AGB maps contain uncertainties and biases. To reduce dependence on only one map, we calculated 34 sets of L-VOD AGB products for each year based on the calibrations of L-VOD with several biomass reference maps, including four global maps (Dubayah et al., 2022; Saatchi et al., 2011; Santoro et al., 2021; Spawn et al., 2020) and two pan-tropical maps (Avitabile et al., 2016; Baccini et al., 2012). Instead

of creating a single global spatial calibration function as in previous studies, where outliers can affect the fitting parameters, we conducted separate calibrations for three regions: the tropics (30° S–30° N), the Northern Hemisphere (30° N–90° N), and the Southern Hemisphere (90° S–30° S), as detailed in Yang et al. (2023). We then averaged these 34 L-VOD AGB products to obtain the final annual AGB maps during 2010 and 2023. The minima and maxima were also calculated to provide estimates of the uncertainty associated with the derived AGB estimates, which are related to systematic errors in the biomass benchmark maps. In a detailed analysis, the uncertainties associated with the L-VOD–derived AGB estimates and the relative uncertainties associated with changes in the carbon stocks over the tropics have been estimated to be in the order of 20 to 25% (Fan et al., 2019). The L-VOD data product has a spatial resolution of ~25 km covering the period from January 12, 2010 to the present. Daily observations affected by radio frequency interference, which is very limited in the Amazon basin, were removed as described in Wigneron et al., (2021).

Direct fire counts from MODIS were obtained from the Fire Information for Resource Management System (FIRMS) dataset (Earth Science Data Systems, 2020) and aggregated to the biogeographic Amazon mask. We selected all MODIS fire counts from the Terra and Aqua sensors which had a confidence level above 60%. Fire emission estimates are based on the Global Fire Assimilation System (GFAS) (Kaiser et al., 2012) and the Global Fire Emissions Database (GFED4s) (van der Werf et al., 2017). With the fire counts and the fire emissions we analyze the seasonal dynamics for all the years from 2003 until 2023. In addition, we aggregate fire emissions of both products (GFAS and GFED4s) over the biogeographic Amazon and report the average between the two for the period between 2003 and 2023. Additionally, we have also used Equivalent Water Height anomalies from the Gravity Recovery and Climate Experiment, specifically the CSR GRACE/GRACE-FO RL0.63 Mascon solution (GRACE-FO CSR) available at: https://grace.jpl.nasa.gov/data-analysis-tool/ covering the period from 2004 to 2023.

Text S5. ATTO data, eddy fluxes and mole fraction data

The mole fraction CO_2 data from 2014 to 2021 are calibrated on the World Meteorological Organization (WMO) CO_2 X2007 scale using 1-point calibration and specifically the 80 m level used here follows the details in Botía et al., (2022). We

have adjusted the scale from X2007 to X2019 of the 2014-2021 data using the recommendation available at: https://gml.noaa.gov/ccl/scale_conversion.html, last accessed December 12, 2024. For the period between 2022 to 2023, CO_2 mole fractions were measured by a new analyzer (Picarro Inc. model G2401), and calibrated by a 3-point calibration (van Asperen et al., 2024). Using the CO_2 mole fractions, we obtained a regional signal (ΔCO_2) by subtracting a background concentration from the measurements. The background is calculated using the Stochastic Time-Inverted Lagrangian Transport (STILT) model (Lin et al., 2003), in which a 100-particle ensemble is released at the ATTO location and 10-day back-trajectories are produced. Using the mean ending position (lat/lon) of the trajectory ensemble we obtain the corresponding CO_2 background as a function of latitude and the CO_2 record from two NOAA stations, Ragged Point Barbados (RPB, 13.1650, -59.432) and Ascension Island (ASC, -7.9667, -14.4) (Lan et al., 2024). With this, we obtain a background concentration associated with each hourly measurement.

To calculate half-hourly turbulent EC-CO_2 fluxes, Alteddy software was applied for processing EC raw datasets sampled at 10 Hz in January to July 2014. For the other period (i.e., July 2014 to 2023), EddyPro software was used for the EC raw data processing. Both software de-spiked and filtered EC raw time-series data following Vickers & Mahrt, (1997). The Alteddy and EddyPro software used the Foken et al., (2005) and Mauder & Foken (2004) approaches, for data quality flags on half-hourly turbulent EC-CO_2 fluxes. We defined good data using the quality flags 1-3 using the Foken et al., (2005) method and flags 0 and 1 when using the Mauder and Foken (2004) method. We also filtered half-hourly turbulent EC-CO_2 fluxes for the favorable wind direction ([0°: +180°] sector) and removed anomalous half-hourly turbulent EC-CO_2 fluxes with absolute flux values above 60 µmol m^{-2} sec^{-1} (i.e., above + 60 µmol m^{-2} sec^{-1} or below - 60 µmol m^{-2} sec^{-1}), most likely due to human or instrumental error, based on the 10-year record. The filtered high-quality and half-hourly turbulent EC-CO_2 fluxes were used for further data analysis: net ecosystem exchange (EC-NEE) calculation, gap-filling and EC-NEE partitioning. The EC-NEE can be calculated as, $NEE = F_{stor} + F_{eddy} + F_{adv}$. Following Winderlich et al., (2014), we have neglected the advection flux (F_{adv}) and added the turbulent flux (F_{eddy}) and the storage flux (F_{stor}) to obtain EC-NEE. To obtain the storage flux term, we applied the methodology described in Winderlich et al., (2014). The EC-NEE partitioning follows the methodology in Botía et al., (2022). The footprint of the EC-NEE, which is located at 80m, is less than 100 km^2. In addition, we use 11 years of

ATTO measurements (from 2013 to 2023), of several meteorological variables at different heights across the canopy, from 4 m (within the canopy) to 80 m (~40 m above the canopy top). The variables are: air temperature, precipitation, soil moisture, soil temperature, and relative humidity. Rainfall (Rain gauge TB4, Hydrological Services Pty. Ltd., Australia) was measured at 81 m. Air Temperature was measured by a Termo-higrometer CS215, Rotronic Measurement UK Solutions. For soil water content we used a Water content reflectometer CS615, Campbell Scientific Inc., USA, and for soil temperature a Thermistor 108, Campbell Scientific Inc., USA.

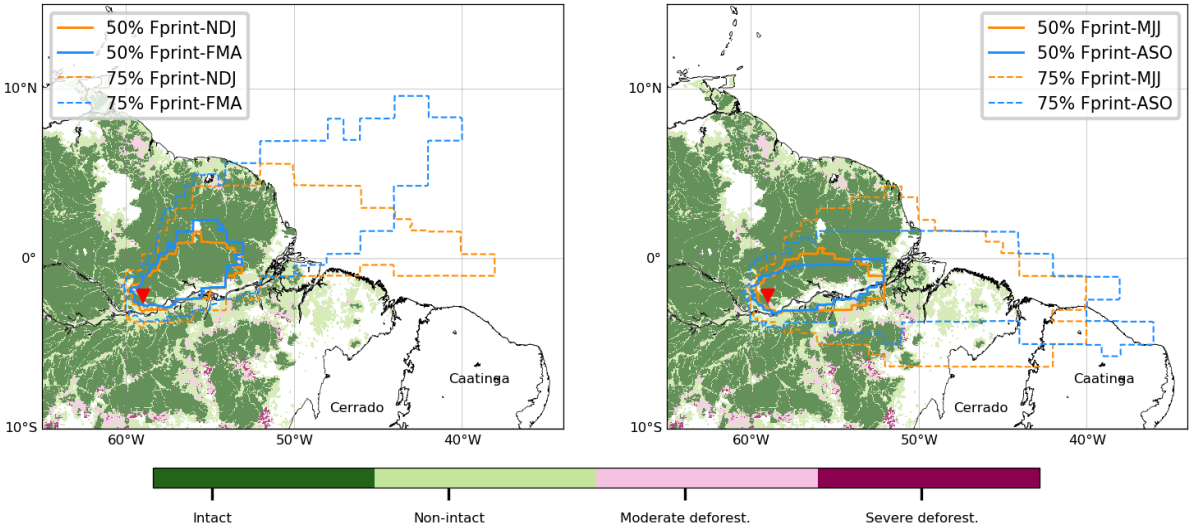

Figure S1. Seasonally time-varying concentration footprint for the ATTO site. The figure was taken from our previous study describing the footprint using the STILT model (Botía et al., 2022).

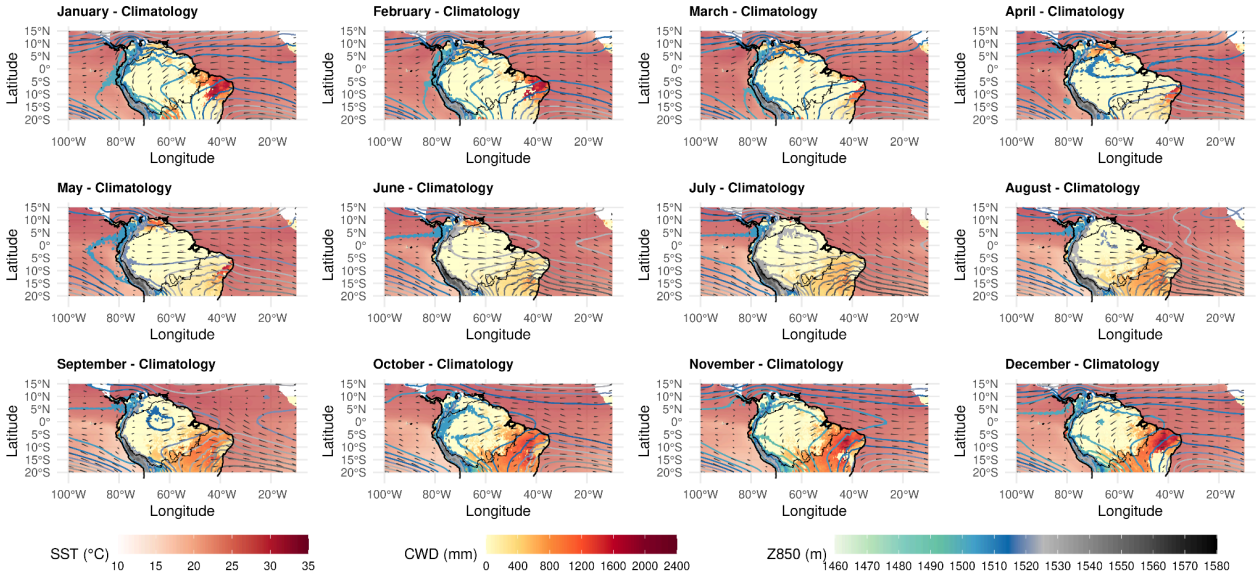

Figure S2. Regional climatology of PCWD, geopotential height at 850hPa, wind fields at 850 hPa and SST (°C).

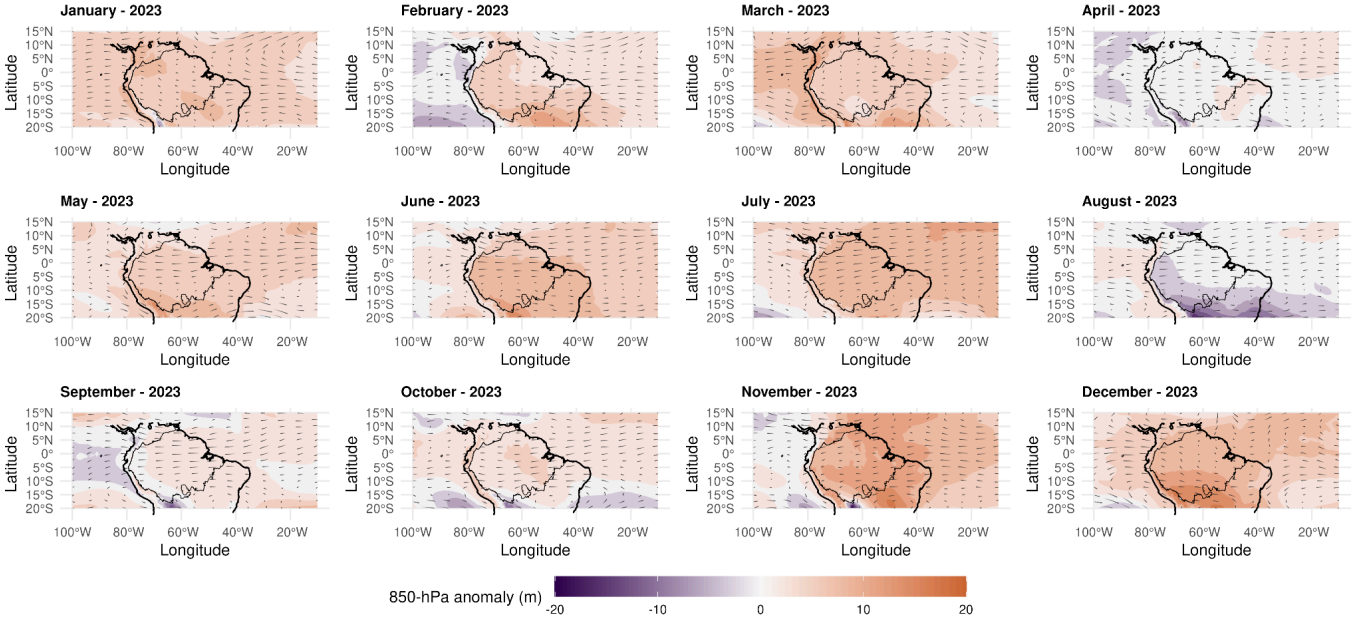

Figure S3. Monthly geopotential height anomalies at 850hPa in reference to baseline (2000-2023), monthly wind fields at 850 hPa.

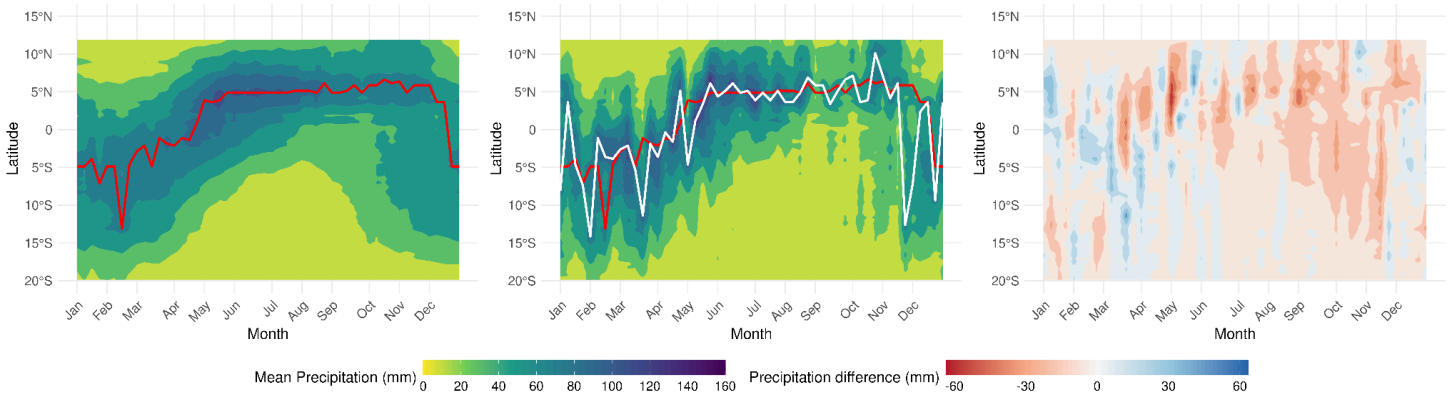

Figure S4. Hovmöller plot showing the latitudinal position of the Intertropical Convergence Zone (ITCZ) between 81°W and 56°E for the climatology (left plot) and year 2023 (middle plot). The x-axis represents time (months), and the y-axis shows latitude from 20°S to 10°N. Colors indicate mean weekly precipitation (mm), with warmer colors (blue to purple) representing higher precipitation and cooler colors (yellow to green) representing lower precipitation. The red line traces the latitude of the weekly maxima from climatology and the white line, from 2023. This visualization enables the identification of anomalies in the 2023 ITCZ position and intensity relative to the multi-decadal mean. Note any deviations of the 2023 precipitation patterns from the precipitation bands, the climatological contours, and the red maximum curve, particularly any northward shifts or delayed southward migrations in the latter half of the year. The difference plot (right plot) highlights these anomalies more clearly by showing the deviation in precipitation (mm) in 2023 compared to the climatological average, with positive values (blue) indicating wetter-than-normal conditions and negative values (red) indicating drier-than-normal conditions.

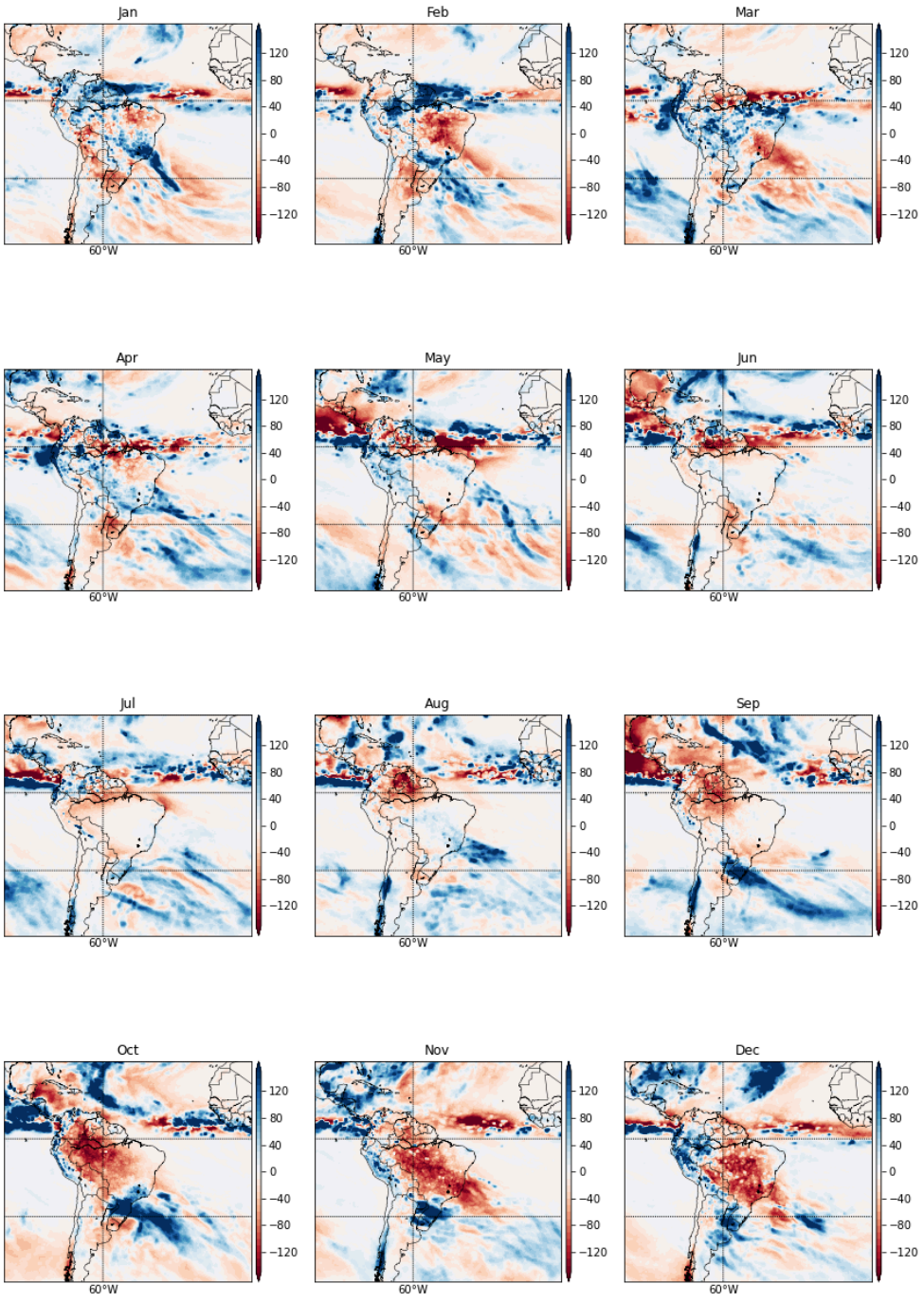

Figure S5. Seasonal development of precipitation anomalies (units in mm) for 2023 based on ERA5.

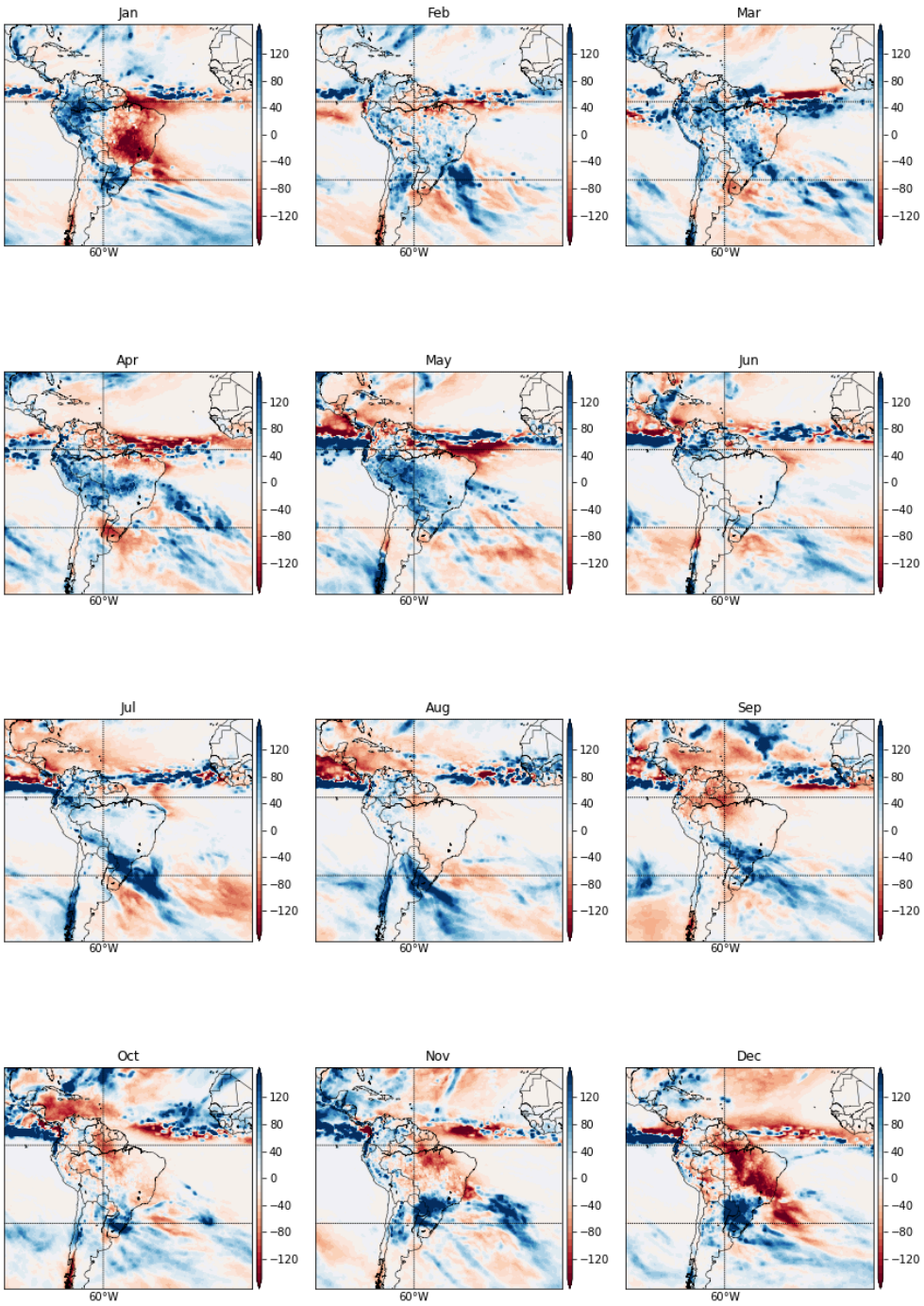

Figure S6. Seasonal development of precipitation anomalies (units in mm) for 2015 based on ERA5.

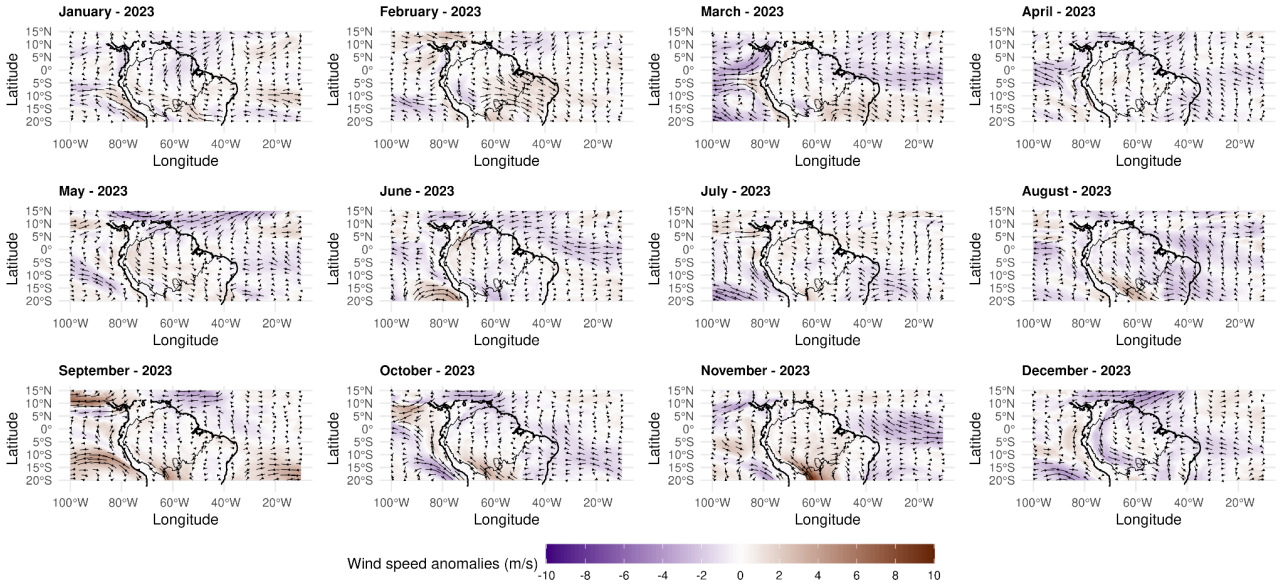

Figure S7. Monthly wind speed (m/s) and direction anomalies (baseline 2000-2023) at 850 hPa.

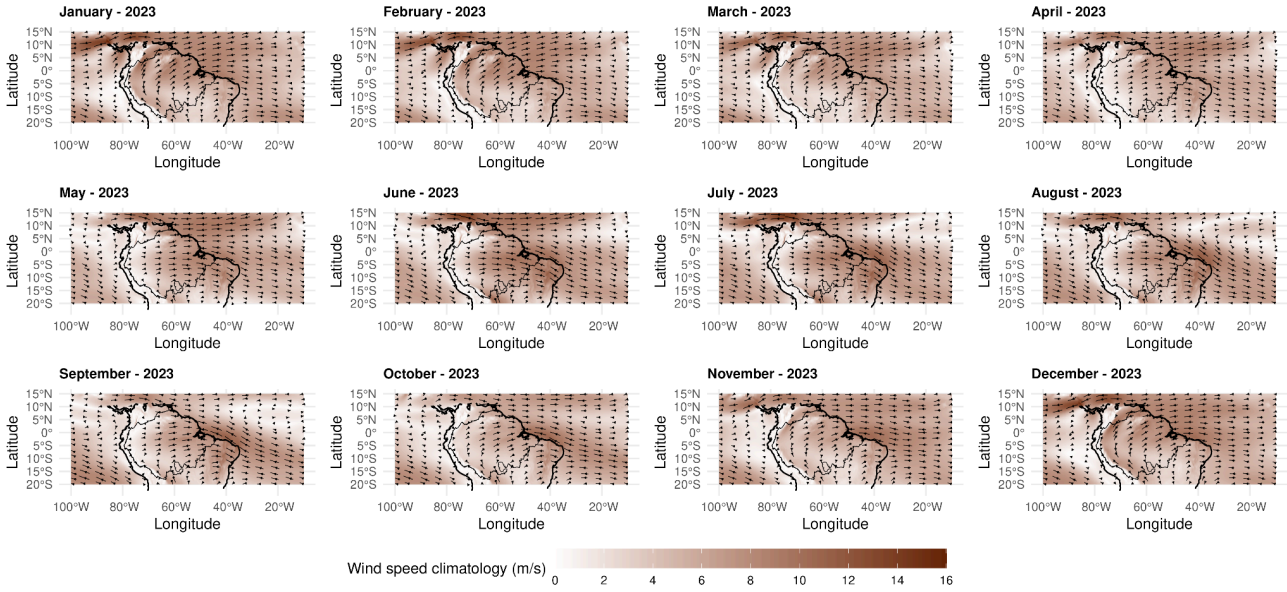

Figure S8. Monthly wind speed (m/s) and direction climatology (2000-2023) at 850 hPa.

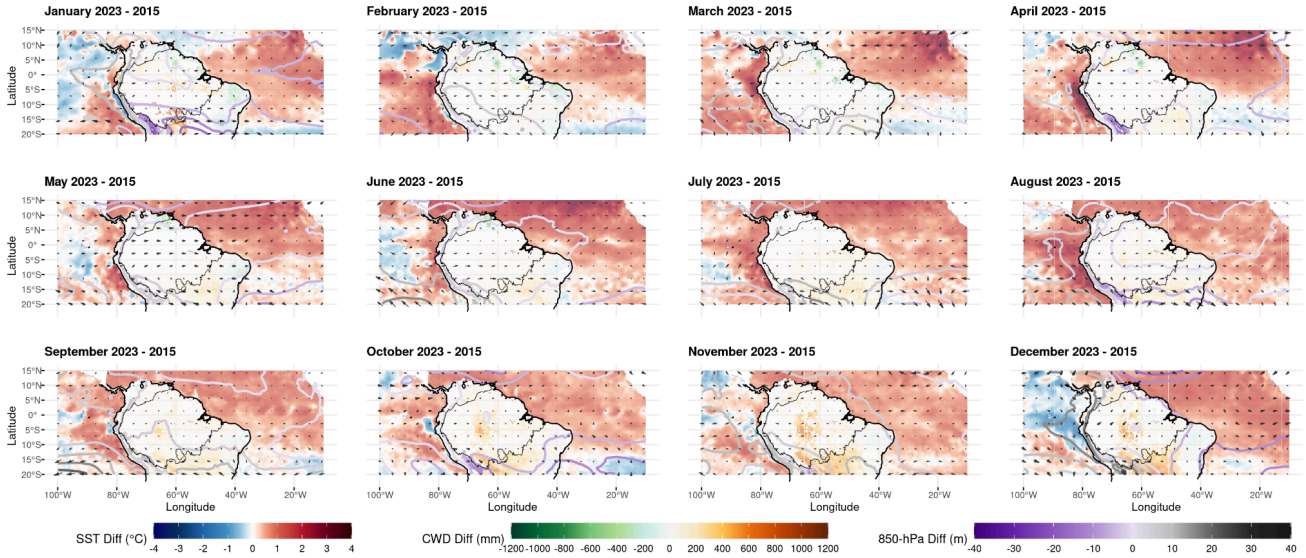

Figure S9. Difference in regional climate patterns during El Niño years: 2023 vs 2015 – PCWD, 500hPa Geopotential height, wind vectors, and SST anomalies. The color bar indicates the magnitude of the difference between 2023 and 2015 fields. Contour of the Amazon region in black.

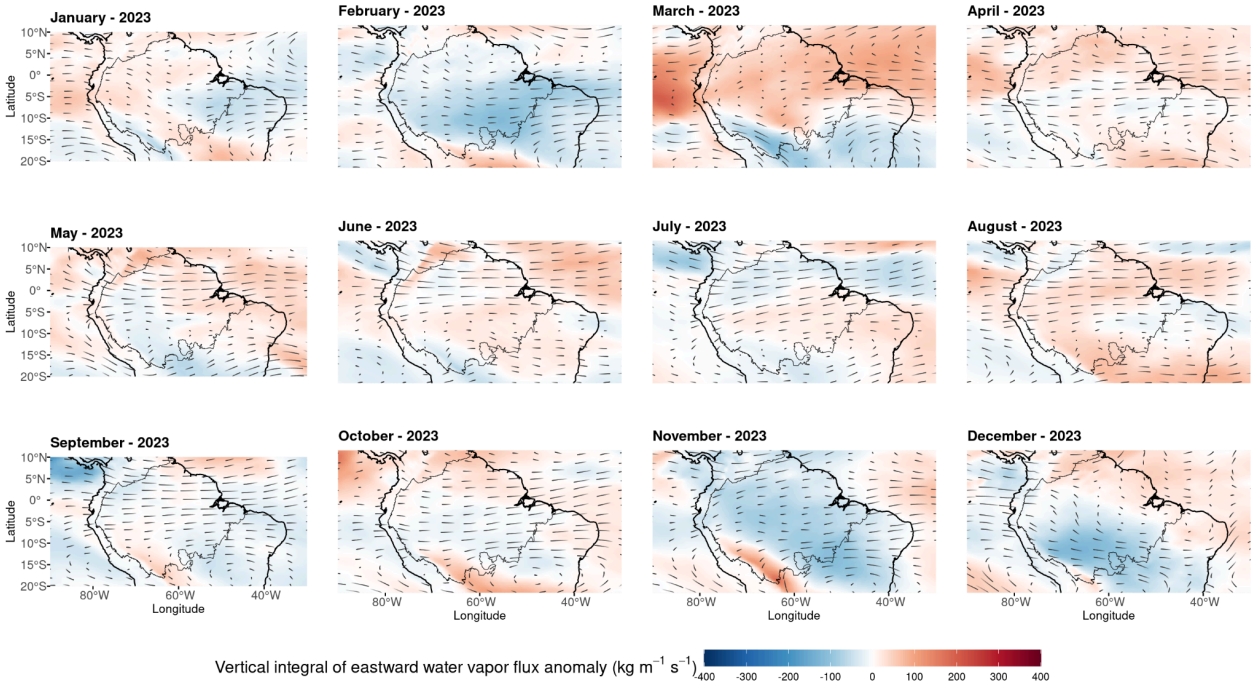

Figure S10. Monthly vertical integral of eastward water vapor flux anomalies (kg m^{-1} s^{-1}) for 2023 over South America (90°W-30°W, 20°S-10°N). Streamlines indicate monthly wind patterns. The anomalies represent the deviation from the

climatological mean (2000-2023) of eastward moisture transport through the atmospheric column. Negative anomalies (blue) indicate stronger westward transport (more moisture transport from the Atlantic to the Amazon), while positive anomalies (red) indicate stronger eastward transport (less moisture transport from the Atlantic to the Amazon).

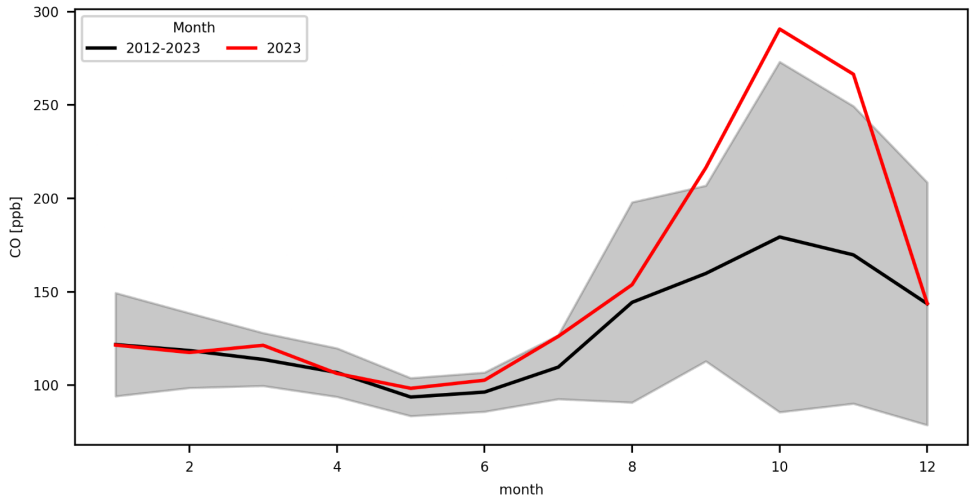

Figure S11. Mean seasonal cycle (averaged over 2012-2023) of CO at ATTO (-2.1441, -58.99) with a shaded area showing the standard deviation for each month. In red, the seasonal evolution of 2023 is shown.

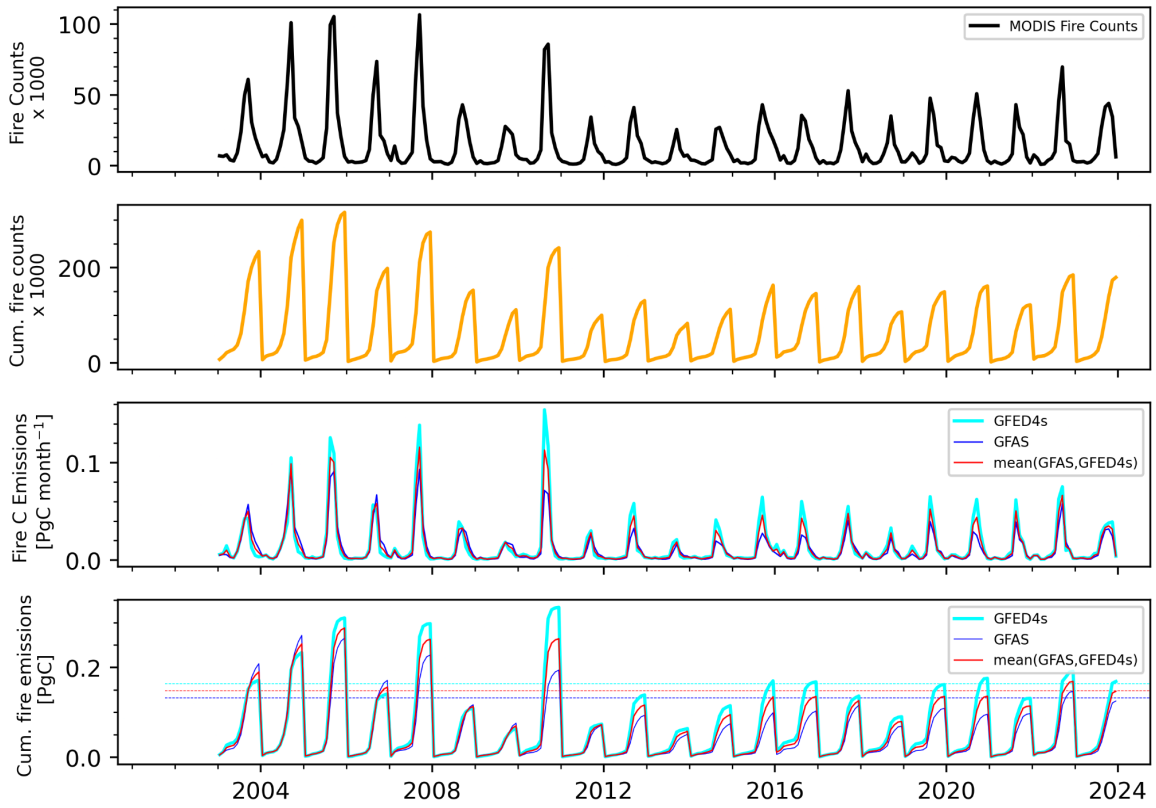

Figure S12. Monthly fire counts and cumulative fire counts (two upper panels) for the biogeographic Amazon. Monthly fire emissions and cumulative fire emissions from GFED4s, GFAS and the mean between the two products also for the biogeographic Amazon (lower two panels). The dashed lines denote the long term mean of the annual fire emissions from each product and their mean.

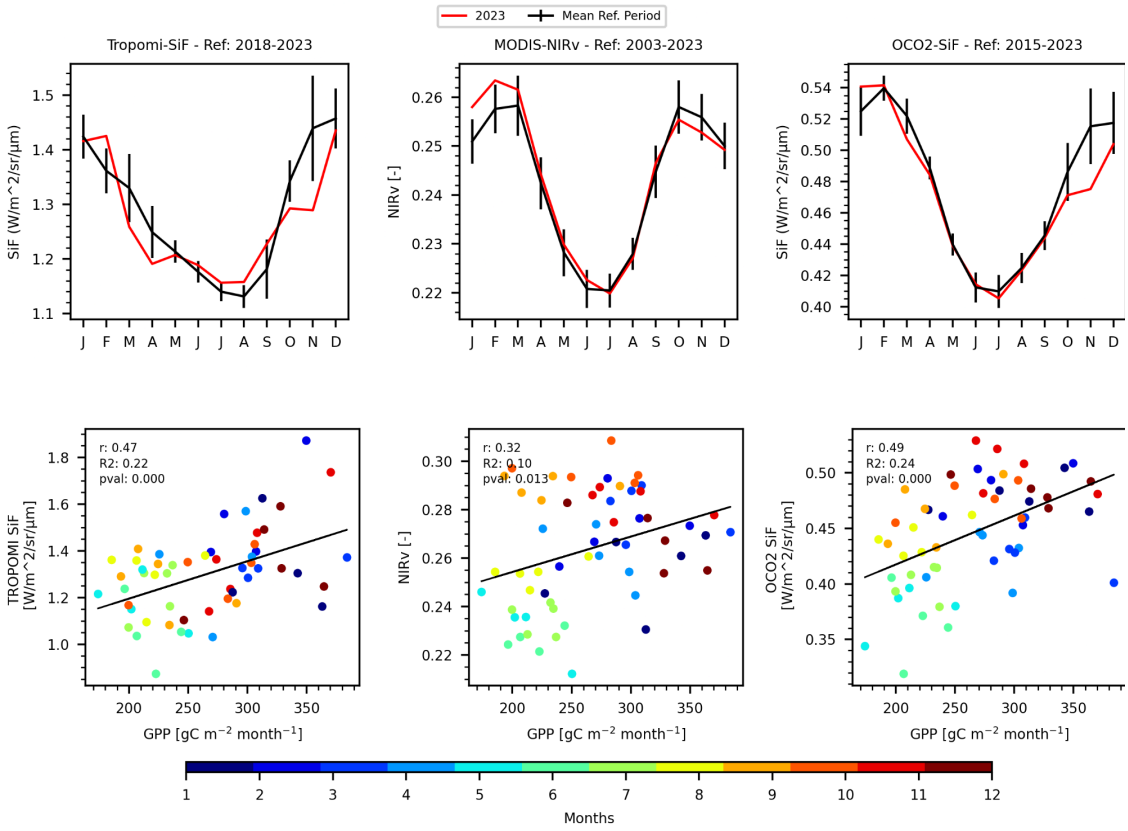

Figure S13. Seasonal development of GPP proxies (SiF and NIRv) for the biogeographic Amazon and their evaluation at ATTO. The first row shows the average seasonality and the 2023 development for each GPP proxy for the biogeographic Amazon. The second row presents the evaluation against the local EC-GPP using the pixel in which ATTO is located. Given that the GPP proxies have different time coverage we limited the comparison against EC-GPP to the 2018-2023 period, following the TROPOMI data availability and thus n=72.

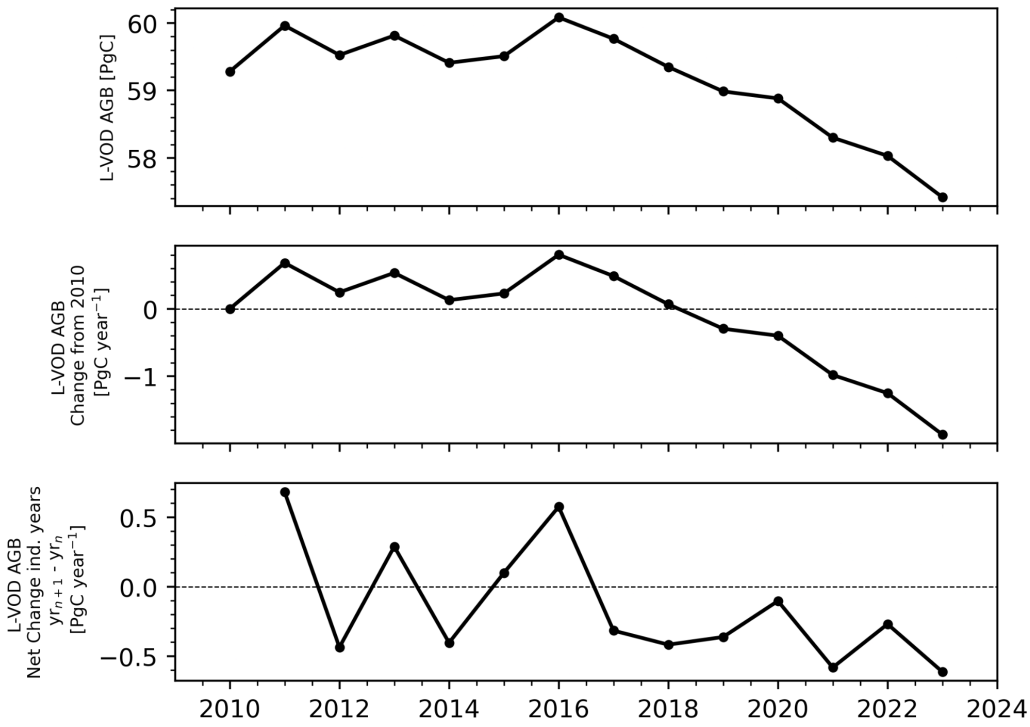

Figure S14. AGC stocks (upper panel), AGC change relative to 2010 (middle panel) and yearly change (lower panel) for the Biogeographic Amazon.

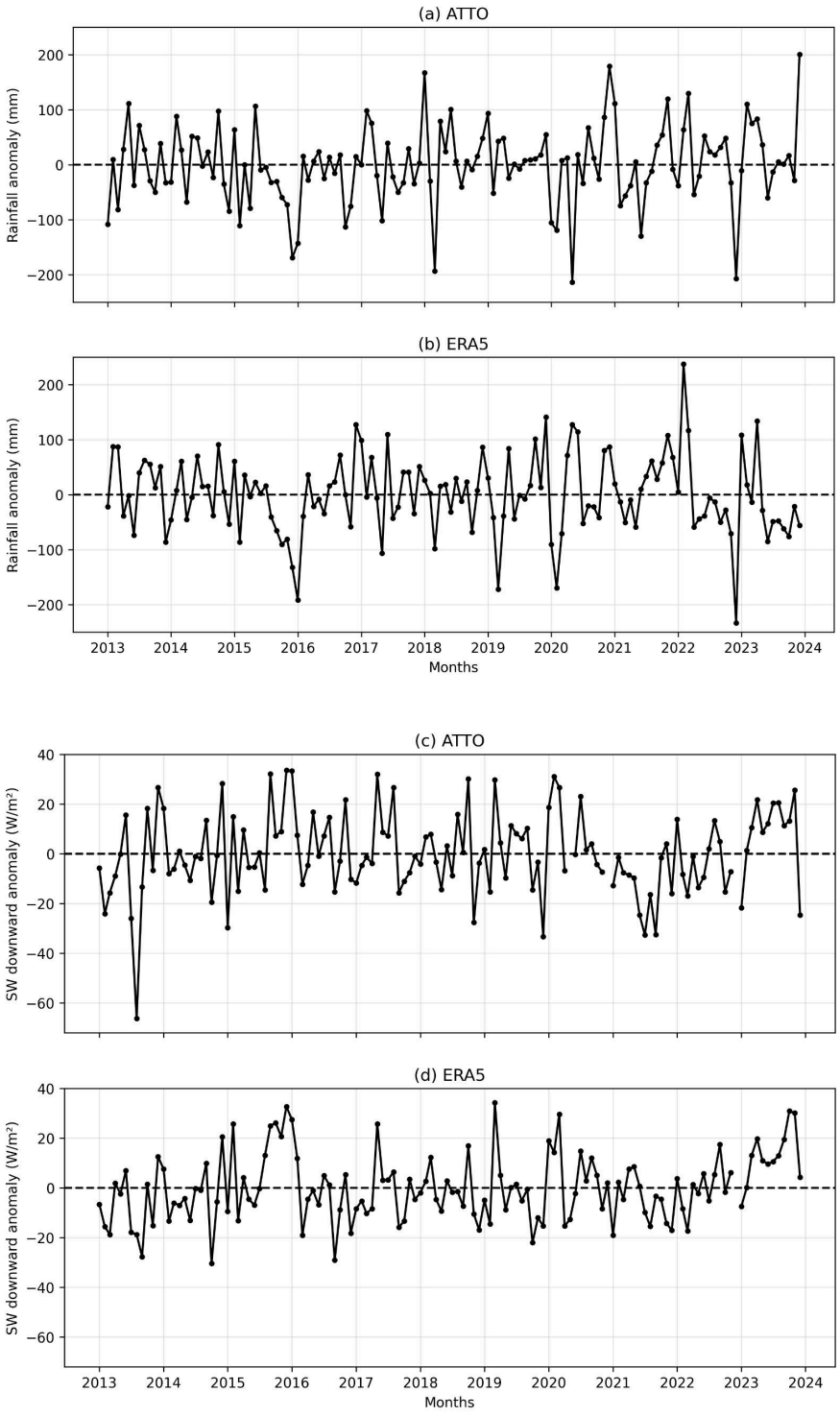

Figure S15. Precipitation (a,b) and Shortwave radiation (c,d) anomalies at ATTO and in the ERA5 grid cell extracted at the ATTO location.

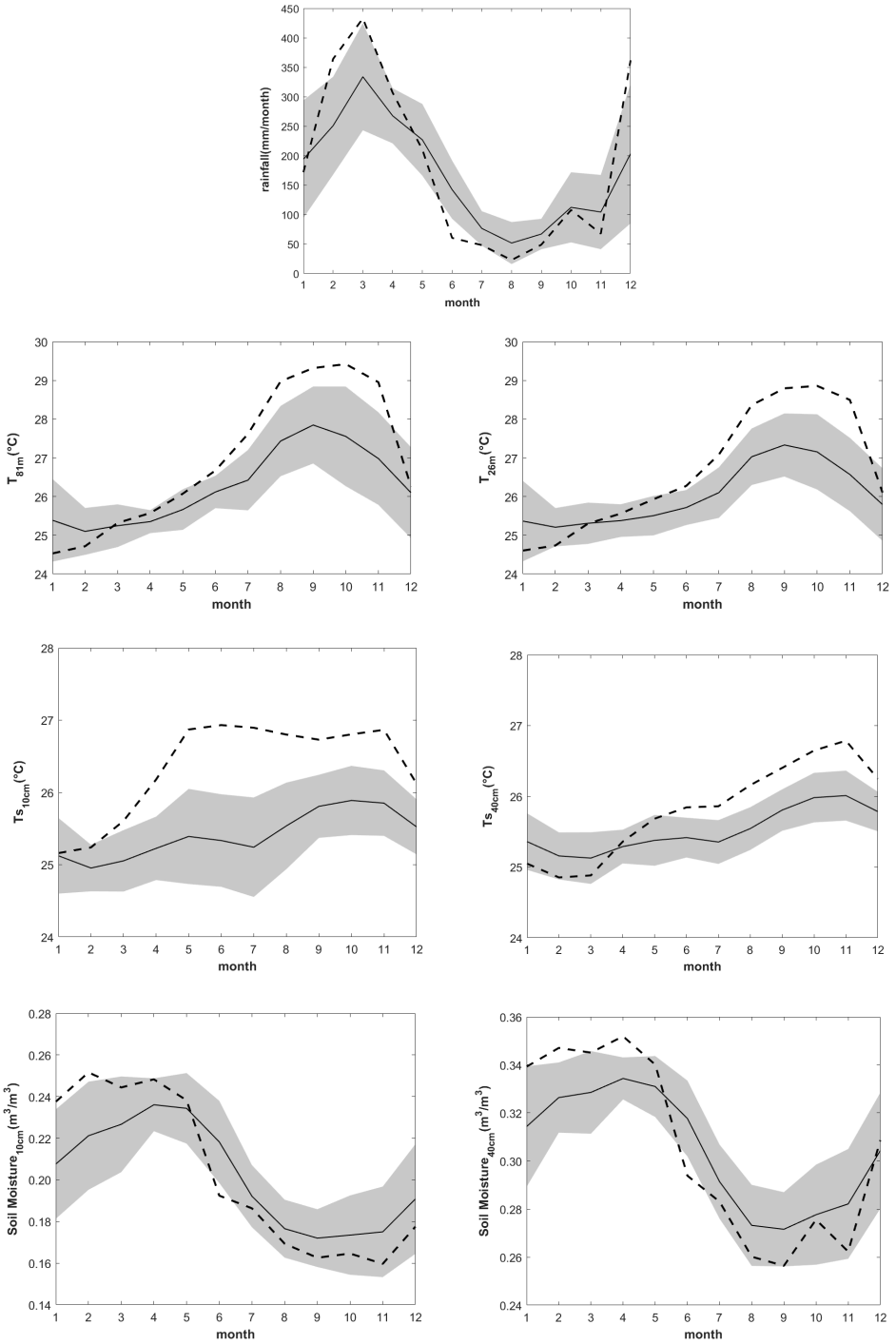

Figure S16. Seasonality of environmental variables at ATTO. The solid line is the mean over 2013-2023 and the dashed line is the seasonal development in 2023.

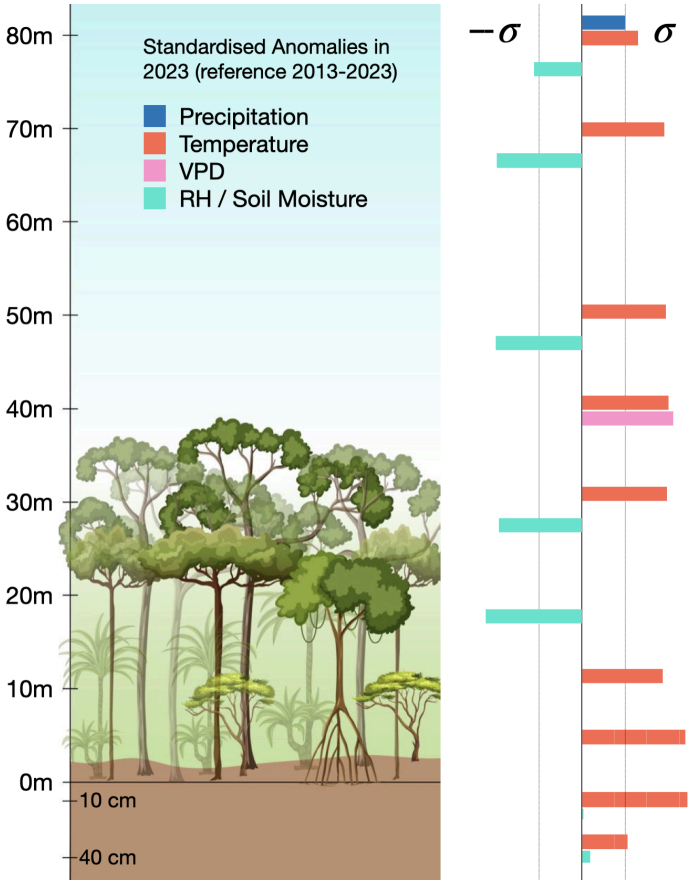

Figure S17. Vertical profile of annual anomaly in environmental variables in the ATTO site. The height is scaled with respect to the canopy height, but not for the soil depths. The bars show the 2023 standardized anomaly of each environmental variable along the vertical profile when available. The vertical lines indicate the -1σ to 1σ range.

References

Avitabile, V., Herold, M., Heuvelink, G. B. M., Lewis, S. L., Phillips, O. L., Asner, G. P., Armston, J., Ashton, P. S., Banin, L., Bayol, N., Berry, N. J., Boeckx, P., de Jong, B. H. J., DeVries, B., Girardin, C. A. J., Kearsley, E., Lindsell, J. A., Lopez-Gonzalez, G., Lucas, R., … Willcock, S. (2016). An integrated pan-tropical biomass map using multiple reference datasets. *Global Change Biology*, *22*(4), 1406–1420. https://doi.org/10.1111/gcb.13139

Baccini, A., Goetz, S. J., Walker, W. S., Laporte, N. T., Sun, M., Sulla-Menashe, D., Hackler, J., Beck, P. S. A., Dubayah, R., Friedl, M. A., Samanta, S., & Houghton, R. A. (2012). Estimated carbon dioxide emissions from tropical deforestation improved by carbon-density maps. *Nature Climate Change*, *2*(3), Article 3. https://doi.org/10.1038/nclimate1354

Badgley, G., Field, C. B., & Berry, J. A. (2017). Canopy near-infrared reflectance and terrestrial photosynthesis. *Science Advances*, *3*(3), e1602244. https://doi.org/10.1126/sciadv.1602244

Bastos, A., Ciais, P., Friedlingstein, P., Sitch, S., Pongratz, J., Fan, L., Wigneron, J., Weber, U., Reichstein, M., Fu, Z., & others. (2020). Direct and seasonal legacy effects of the 2018 heat wave and drought on European ecosystem productivity. *Science Advances*, *6*(24), eaba2724.

Bell, B., Hersbach, H., Simmons, A., Berrisford, P., Dahlgren, P., Horányi, A., Muñoz-Sabater, J., Nicolas, J., Radu, R., Schepers, D., Soci, C., Villaume, S., Bidlot, J.-R., Haimberger, L., Woollen, J., Buontempo, C., & Thépaut, J.-N. (2021). The ERA5 global reanalysis: Preliminary extension to 1950. *Quarterly*

Journal of the Royal Meteorological Society, *147*(741), 4186–4227. https://doi.org/10.1002/qj.4174

Botía, S., Komiya, S., Marshall, J., Koch, T., Gałkowski, M., Lavric, J., Gomes-Alves, E., Walter, D., Fisch, G., Pinho, D. M., Nelson, B. W., Martins, G., Luijkx, I. T., Koren, G., Florentie, L., Carioca de Araújo, A., Sá, M., Andreae, M. O., Heimann, M., … Gerbig, C. (2022). The CO2 record at the Amazon Tall Tower Observatory: A new opportunity to study processes on seasonal and inter-annual scales. *Global Change Biology*, *28*(2), 588–611. https://doi.org/10.1111/gcb.15905

Brandt, M., Wigneron, J.-P., Chave, J., Tagesson, T., Penuelas, J., Ciais, P., Rasmussen, K., Tian, F., Mbow, C., Al-Yaari, A., Rodriguez-Fernandez, N., Schurgers, G., Zhang, W., Chang, J., Kerr, Y., Verger, A., Tucker, C., Mialon, A., Rasmussen, L. V., … Fensholt, R. (2018). Satellite passive microwaves reveal recent climate-induced carbon losses in African drylands. *Nature Ecology & Evolution*, *2*(5), 827–835. https://doi.org/10.1038/s41559-018-0530-6

Chau, T.-T.-T., Chevallier, F., & Gehlen, M. (2024). Global Analysis of Surface Ocean CO2 Fugacity and Air-Sea Fluxes With Low Latency. *Geophysical Research Letters*, *51*(8), e2023GL106670. https://doi.org/10.1029/2023GL106670

Chau, T.-T.-T., Gehlen, M., Metzl, N., & Chevallier, F. (2024). CMEMS-LSCE: A global, 0.25°, monthly reconstruction of the surface ocean carbonate system. *Earth System Science Data*, *16*(1), 121–160. https://doi.org/10.5194/essd-16-121-2024

Chevallier, F., Zheng, B., Broquet, G., Ciais, P., Liu, Z., Davis, S. J., Deng, Z., Wang, Y., Bréon, F.-M., & O'Dell, C. W. (2020). Local Anomalies in the Column-Averaged

Dry Air Mole Fractions of Carbon Dioxide Across the Globe During the First Months of the Coronavirus Recession. *Geophysical Research Letters*, *47*(22), e2020GL090244. https://doi.org/10.1029/2020GL090244

Chini, L., Hurtt, G., Sahajpal, R., Frolking, S., Klein Goldewijk, K., Sitch, S., Ganzenmüller, R., Ma, L., Ott, L., Pongratz, J., & Poulter, B. (2021). Land-use harmonization datasets for annual global carbon budgets. *Earth System Science Data*, *13*(8), 4175–4189. https://doi.org/10.5194/essd-13-4175-2021

Clark, D., Mercado, L., Sitch, S., Jones, C., Gedney, N., Best, M., Pryor, M., Rooney, G., Essery, R., Blyth, E., & others. (2011). The Joint UK Land Environment Simulator (JULES), model description–Part 2: Carbon fluxes and vegetation dynamics. *Geoscientific Model Development*, *4*(3), 701–722.

Copernicus Climate Change Service. (2022). *ERA5-Land hourly data from 1950 to present. Copernicus Climate Change Service (C3S) Climate Data Store (CDS)*. 10.24381/cds.e2161bac

Dubayah, R. O., Armston, J., Healey, S. P., Yang, Z., Patterson, P. L., Saarela, S., Stahl, G., Duncanson, L., & Kellner, J. R. (2022). GEDI L4B Gridded Aboveground Biomass Density, Version 2. *ORNL DAAC*. https://doi.org/10.3334/ORNLDAAC/2017

Earth Science Data Systems, N. (2020). *MODIS Collection 6 Hotspot / Active Fire Detections MCD14ML distributed from NASA FIRMS* [Dataset]. Earth Science Data Systems, NASA. https://doi.org/Fire Information for Resource Management System

Fan, L., Wigneron, J.-P., Ciais, P., Chave, J., Brandt, M., Fensholt, R., Saatchi, S. S.,

Bastos, A., Al-Yaari, A., Hufkens, K., Qin, Y., Xiao, X., Chen, C., Myneni, R. B., Fernandez-Moran, R., Mialon, A., Rodriguez-Fernandez, N. J., Kerr, Y., Tian, F., & Peñuelas, J. (2019). Satellite-observed pantropical carbon dynamics. *Nature Plants*, *5*(9), 944–951. https://doi.org/10.1038/s41477-019-0478-9

Fan, L., Wigneron, J.-P., Ciais, P., Chave, J., Brandt, M., Sitch, S., Yue, C., Bastos, A., Li, X., Qin, Y., Yuan, W., Schepaschenko, D., Mukhortova, L., Li, X., Liu, X., Wang, M., Frappart, F., Xiao, X., Chen, J., … Fensholt, R. (2023). Siberian carbon sink reduced by forest disturbances. *Nature Geoscience*, *16*(1), 56–62. https://doi.org/10.1038/s41561-022-01087-x

Foken, T., Göockede, M., Mauder, M., Mahrt, L., Amiro, B., & Munger, W. (2005). Post-Field Data Quality Control. In X. Lee, W. Massman, & B. Law (Eds.), *Handbook of Micrometeorology: A Guide for Surface Flux Measurement and Analysis* (pp. 181–208). Springer Netherlands. https://doi.org/10.1007/1-4020-2265-4_9

Frankenberg, C., Fisher, J. B., Worden, J., Badgley, G., Saatchi, S. S., Lee, J.-E., Toon, G. C., Butz, A., Jung, M., Kuze, A., & Yokota, T. (2011). New global observations of the terrestrial carbon cycle from GOSAT: Patterns of plant fluorescence with gross primary productivity. *Geophysical Research Letters*, *38*(17). https://doi.org/10.1029/2011GL048738

Friedlingstein, P., O'Sullivan, M., Jones, M. W., Andrew, R. M., Bakker, D. C. E., Hauck, J., Landschützer, P., Le Quéré, C., Luijkx, I. T., Peters, G. P., Peters, W., Pongratz, J., Schwingshackl, C., Sitch, S., Canadell, J. G., Ciais, P., Jackson, R. B., Alin, S. R., Anthoni, P., … Zheng, B. (2023). Global Carbon Budget 2023. *Earth System*

Science Data, *15*(12), 5301–5369. https://doi.org/10.5194/essd-15-5301-2023

Guanter, L., Bacour, C., Schneider, A., Aben, I., van Kempen, T. A., Maignan, F., Retscher, C., Köhler, P., Frankenberg, C., Joiner, J., & Zhang, Y. (2021). The TROPOSIF global sun-induced fluorescence dataset from the Sentinel-5P TROPOMI mission. *Earth System Science Data*, *13*(11), 5423–5440. https://doi.org/10.5194/essd-13-5423-2021

Guimberteau, M., Zhu, D., Maignan, F., Huang, Y., Yue, C., Dantec-Nédélec, S., Ottlé, C., Jornet-Puig, A., Bastos, A., Laurent, P., Goll, D., Bowring, S., Chang, J., Guenet, B., Tifafi, M., Peng, S., Krinner, G., Ducharne, A., Wang, F., … Ciais, P. (2018). ORCHIDEE-MICT (v8.4.1), a land surface model for the high latitudes: Model description and validation. *Geosci. Model Dev.*, *11*(1), 121–163.

Haynes, K. D., Baker, I. T., Denning, A. S., Stöckli, R., Schaefer, K., Lokupitiya, E. Y., & Haynes, J. M. (2019). Representing Grasslands Using Dynamic Prognostic Phenology Based on Biological Growth Stages: 1. Implementation in the Simple Biosphere Model (SiB4). *Journal of Advances in Modeling Earth Systems*, *11*(12), 4423–4439. https://doi.org/10.1029/2018MS001540

Hersbach, H., Bell, B., Berrisford, P., Hirahara, S., Horányi, A., Muñoz-Sabater, J., Nicolas, J., Peubey, C., Radu, R., Schepers, D., Simmons, A., Soci, C., Abdalla, S., Abellan, X., Balsamo, G., Bechtold, P., Biavati, G., Bidlot, J., Bonavita, M., … Thépaut, J.-N. (2020). The ERA5 global reanalysis. *Quarterly Journal of the Royal Meteorological Society*, *146*(730), 1999–2049. https://doi.org/10.1002/qj.3803

Jones, M. W., Andrew, R. M., Peters, G. P., Janssens-Maenhout, G., De-Gol, A. J., Ciais,

P., Patra, P. K., Chevallier, F., & Le Quéré, C. (2021). Gridded fossil CO2 emissions and related O2 combustion consistent with national inventories 1959–2018. *Scientific Data*, *8*(1), 2. https://doi.org/10.1038/s41597-020-00779-6

Kaiser, J. W., Heil, A., Andreae, M. O., Benedetti, A., Chubarova, N., Jones, L., Morcrette, J.-J., Razinger, M., Schultz, M. G., Suttie, M., & van der Werf, G. R. (2012). Biomass burning emissions estimated with a global fire assimilation system based on observed fire radiative power. *Biogeosciences*, *9*(1), 527–554. https://doi.org/10.5194/bg-9-527-2012

Krinner, G., Viovy, N., de Noblet-Ducoudré, N., Ogée, J., Polcher, J., Friedlingstein, P., Ciais, P., Sitch, S., & Prentice, I. C. (2005). A dynamic global vegetation model for studies of the coupled atmosphere-biosphere system. *Global Biogeochem. Cycles*, *19*(1), GB1015-.

Lan, X., Mund, J. W., Crotwell, A. M., Thoning, K. W., Moglia, E., Madronich, M., Baugh, K., Petron, G., Crotwell, M. J., Neff, D., Wolter, S., Mefford, T., & DeVogel, S. (2024). *Atmospheric Carbon Dioxide Dry Air Mole Fractions from the NOAA GML Carbon Cycle Cooperative Global Air Sampling Network, 1968-2023* (Version 2024-07-30) [Dataset]. https://doi.org/10.15138/wkgj-f215

Lawrence, P. J., & Chase, T. N. (2007). Representing a new MODIS consistent land surface in the Community Land Model (CLM 3.0). *Journal of Geophysical Research: Biogeosciences*, *112*(G1), G01023. https://doi.org/10.1029/2006JG000168

Mauder, M., & Foken, T. (2004). *Documentation and Instruction Manual of the Eddy Covariance Software Package TK2*.

Muñoz-Sabater, J., Dutra, E., Agustí-Panareda, A., Albergel, C., Arduini, G., Balsamo, G., Boussetta, S., Choulga, M., Harrigan, S., Hersbach, H., Martens, B., Miralles, D. G., Piles, M., Rodríguez-Fernández, N. J., Zsoter, E., Buontempo, C., & Thépaut, J.-N. (2021). ERA5-Land: A state-of-the-art global reanalysis dataset for land applications. *Earth System Science Data*, *13*(9), 4349–4383. https://doi.org/10.5194/essd-13-4349-2021

Qin, Y., Xiao, X., Wigneron, J.-P., Ciais, P., Brandt, M., Fan, L., Li, X., Crowell, S., Wu, X., Doughty, R., Zhang, Y., Liu, F., Sitch, S., & Moore, B. (2021). Carbon loss from forest degradation exceeds that from deforestation in the Brazilian Amazon. *Nature Climate Change*, *11*(5), 442–448. https://doi.org/10.1038/s41558-021-01026-5

Saatchi, S. S., Harris, N. L., Brown, S., Lefsky, M., Mitchard, E. T. A., Salas, W., Zutta, B. R., Buermann, W., Lewis, S. L., Hagen, S., Petrova, S., White, L., Silman, M., & Morel, A. (2011). Benchmark map of forest carbon stocks in tropical regions across three continents. *Proceedings of the National Academy of Sciences*, *108*(24), 9899–9904. https://doi.org/10.1073/pnas.1019576108

Santoro, M., Cartus, O., Carvalhais, N., Rozendaal, D. M. A., Avitabile, V., Araza, A., de Bruin, S., Herold, M., Quegan, S., Rodríguez-Veiga, P., Balzter, H., Carreiras, J., Schepaschenko, D., Korets, M., Shimada, M., Itoh, T., Moreno Martínez, Á., Cavlovic, J., Cazzolla Gatti, R., … Willcock, S. (2021). The global forest above-ground biomass pool for 2010 estimated from high-resolution satellite observations. *Earth System Science Data*, *13*(8), 3927–3950. https://doi.org/10.5194/essd-13-3927-2021

Schaaf, C., & Wang, Z. (2021). *MODIS/Terra+Aqua BRDF/Albedo Nadir BRDF-Adjusted Ref Daily L3 Global 0.05Deg CMG V061* [Dataset]. NASA EOSDIS Land Processes Distributed Active Archive Center. https://doi.org/10.5067/MODIS/MCD43C4.061

Smith, N. E., Kooijmans, L. M. J., Koren, G., van Schaik, E., van der Woude, A. M., Wanders, N., Ramonet, M., Xueref-Remy, I., Siebicke, L., Manca, G., Brümmer, C., Baker, I. T., Haynes, K. D., Luijkx, I. T., & Peters, W. (2020). Spring enhancement and summer reduction in carbon uptake during the 2018 drought in northwestern Europe. *Philosophical Transactions of the Royal Society B: Biological Sciences*, *375*(1810), 20190509. https://doi.org/10.1098/rstb.2019.0509

Spawn, S. A., Sullivan, C. C., Lark, T. J., & Gibbs, H. K. (2020). Harmonized global maps of above and belowground biomass carbon density in the year 2010. *Scientific Data*, *7*(1), 112. https://doi.org/10.1038/s41597-020-0444-4

Stocker, B. D., Tumber-Dávila, S. J., Konings, A. G., Anderson, M. C., Hain, C., & Jackson, R. B. (2023). Global patterns of water storage in the rooting zones of vegetation. *Nature Geoscience*, *16*(3), 250–256. https://doi.org/10.1038/s41561-023-01125-2

van Asperen, H., Jones, S., Lavric, J., Walter, D., Sierra, C., Horna, V., Komiya, S., Botía, S., Warneke, T., Griffith, D., Heimann, M., Andreae, M., & Trumbore, S. (2024). *Long term continuous high-precision greenhouse gas observation at the ATTO fieldsite: An overview*. https://proceedings.science/icdc-2024/papers/long-term-continuous-high-precision-greenhouse-gas-observation-at-the-atto-field?lang=en

van der Werf, G. R., Randerson, J. T., Giglio, L., Leeuwen, T. T. van, Chen, Y., Rogers, B. M., Mu, M., Marle, M. J. E. van, Morton, D. C., Collatz, G. J., Yokelson, R. J., & Kasibhatla, P. S. (2017). Global fire emissions estimates during 1997–2016. *Earth System Science Data*, *9*(2), 697–720. https://doi.org/10.5194/essd-9-697-2017

van der Woude, A. M., Peters, W., Joetzjer, E., Lafont, S., Koren, G., Ciais, P., Ramonet, M., Xu, Y., Bastos, A., Botía, S., Sitch, S., de Kok, R., Kneuer, T., Kubistin, D., Jacotot, A., Loubet, B., Herig-Coimbra, P.-H., Loustau, D., & Luijkx, I. T. (2023). Temperature extremes of 2022 reduced carbon uptake by forests in Europe. *Nature Communications*, *14*(1), 6218. https://doi.org/10.1038/s41467-023-41851-0

van Geffen, J. H. G. M., Eskes, H. J., Boersma, K. F., & Veefkind, J. P. (2019). *TROPOMI ATBD of the total and tropospheric NO2 data products*. https://sentinel.esa.int/documents/247904/2476257/Sentinel-5P-TROPOMI-ATBD-NO2-data-products.pdf

Vickers, D., & Mahrt, L. (1997). Quality Control and Flux Sampling Problems for Tower and Aircraft Data. *Journal of Atmospheric and Oceanic Technology*, *14*(3), 512–526. https://doi.org/10.1175/1520-0426(1997)014<0512:QCAFSP>2.0.CO;2

Wigneron, J.-P., Ciais, P., Li, X., Brandt, M., Canadell, J. G., Tian, F., Wang, H., Bastos, A., Fan, L., Gatica, G., Kashyap, R., Liu, X., Sitch, S., Tao, S., Xiao, X., Yang, H., Espinoza Villar, J. C., Frappart, F., Li, W., … Fensholt, R. (2024). Global carbon balance of the forest: Satellite-based L-VOD results over the last decade. *Frontiers in Remote Sensing*, *5*. https://doi.org/10.3389/frsen.2024.1338618

Wigneron, J.-P., Li, X., Frappart, F., Fan, L., Al-Yaari, A., De Lannoy, G., Liu, X., Wang, M., Le Masson, E., & Moisy, C. (2021). SMOS-IC data record of soil moisture and L-VOD: Historical development, applications and perspectives. *Remote Sensing of Environment*, *254*, 112238. https://doi.org/10.1016/j.rse.2020.112238

Winderlich, J., Gerbig, C., Kolle, O., & Heimann, M. (2014). Inferences from CO_2 and CH_4 concentration profiles at the Zotino Tall Tower Observatory (ZOTTO) on regional summertime ecosystem fluxes. *Biogeosciences*, *11*(7), 2055–2068. https://doi.org/10.5194/bg-11-2055-2014

Yang, H., Ciais, P., Frappart, F., Li, X., Brandt, M., Fensholt, R., Fan, L., Saatchi, S., Besnard, S., Deng, Z., Bowring, S., & Wigneron, J.-P. (2023). Global increase in biomass carbon stock dominated by growth of northern young forests over past decade. *Nature Geoscience*, *16*(10), 886–892. https://doi.org/10.1038/s41561-023-01274-4

Zaehle, S., Friend, A. D., Friedlingstein, P., Dentener, F., Peylin, P., & Schulz, M. (2010). Carbon and nitrogen cycle dynamics in the O-CN land surface model: 2. Role of the nitrogen cycle in the historical terrestrial carbon balance. *Global Biogeochem. Cycles*, *24*(1), GB1006-.